# REDOX ACTIVE TYROSINE RESIDUES IN BIOMIMETIC BETA HAIRPINS

A Dissertation
Presented to
The Academic Faculty

by

Robin S. Sibert

In Partial Fulfillment
of the Requirements for the Degree
Doctor of Philosophy in the
School of Chemistry and Biochemistry

Georgia Institute of Technology
August 2009

# REDOX ACTIVE TYROSINE RESIDUES IN

# BIOMIMETIC BETA HAIRPINS

Approved by:


Dr. Bridgette Barry, Advisor
School of Chemistry and Biochemistry
*Georgia Institute of Technology*

Dr. Jake Soper
School of Chemistry and Biochemistry
*Georgia Institute of Technology*

Dr. David Collard
School of Chemistry and Biochemistry
*Georgia Institute of Technology*

Dr. Ingeborg Schmidt-Krey
School of Biology
*Georgia Institute of Technology*

Dr. Mira Josowicz
School of Chemistry and Biochemistry
*Georgia Institute of Technology*



Date Approved: July 3rd, 2009

To my sister, Alicia. More than anything, I want you to understand how God uses our perseverance to accomplish His amazing works within us. I look forward to seeing the fruit of your endurance. I love you!

# ACKNOWLEDGEMENTS

I would like to thank my parents who have always been there to cheer me on and help me aim high in my educational endeavors. I thank them also for all of their love and support. I thank my brothers and sisters at the Greater Atlanta Church of Christ. I appreciate every encouraging word and prayer that they have offered over the past three years. I especially thank Dyneka Russell and Anne Magloire for being wonderful friends, confidants and study partners. I thank Dr. Bridgette Barry her support. I have become a better scientist as a result of her guidance. I also wish to thank the former and current members of the Barry Lab: Dr. Shana Bender, Dr. Jun Chen, Dr. Ian Cooper, Tina Dreaden, David Jensen, James Keough, Adam Offenbacher, and Brandon Polander for their valuable input.

# TABLE OF CONTENTS

# LIST OF TABLES

# LIST OF FIGURES

# LIST OF SYMBOLS

| | |
|---|---|
| $\Delta \delta H_{\alpha}$ | alpha proton chemical shift |
| $P_{680}^{+}$ | primary electron donor of photosystem II |
| $Y_D$ | tyrosine D |
| $Y_Z$ | tyrosine Z |
| $T_m$ | melting temperature |

## LIST OF ABBREVIATIONS

| | |
|---|---|
| Ala or A | alanine |
| Asn or N | asparagine |
| Asp or D | aspartic acid |
| Cha | cyclohexylalanine |
| Gly or G | glycine |
| His or H | histidine |
| Ile or I | isoleucine |
| Phe or F | phenylalanine |
| Pro or P | proline |
| Thr or T | threonine |
| Trp or W | tryptophan |
| Tyr or Y | tyrosine |
| Val or V | valine |
| CD | circular dichroism |
| EPR | electron paramagnetic resonance |

| | |
|---|---|
| FT-IR | Fourier transform-infrared |
| NMR | nuclear magnetic resonance |
| UV | ultra violet |
| PCET | proton coupled electron transfer |

# SUMMARY

Biomimetic peptides are autonomously folding secondary structural units designed to serve as models for examining processes that occur in proteins. Although de novo biomimetic peptides are not simply abbreviated versions of proteins already found in nature, designing biomimetic peptides does require an understanding of how native proteins are formed and stabilized. The discovery of autonomously folding fragments of ribonuclease A and tendamistat pioneered the use of biomimetic peptides for determining how the polypeptide sequence stabilizes formation of alpha helices and beta hairpins in aqueous and organic solutions. A set of rules for constructing stable alpha helices have now been established. There is no exact set of rules for designing beta hairpins; however, some factors that must be considered are the identity of the residues in the turn and non-covalent interactions between amino acid side chains. For example, glycine, proline, aspargine, and aspartic acid are favored in turns. Non-covalent interactions that stabilize hairpin formation include salt bridges, pi-stacked aromatic interactions, cation-pi interactions, and hydrophobic interactions. The optimal strand length for beta hairpins depends on the numbers of stabilizing non-covalent interactions and high hairpin propensity amino acids in the specific peptide being designed. Until now, de novo hairpins have not previously been used to examine biological processes aside from protein folding. This thesis uses de novo designed biomimetic peptides as tractable models to examine how non-covalent interactions control the redox properties of tyrosine in enzymes.

Photosystem II provides an example of how non-covalent interactions may alter the redox properties of tyrosine. Photosystem II contains two redox active tyrosine residues, Tyr 161 in the D1 polypeptide and Tyr 160 in the D2 polypeptide. Both Tyr 161 and Tyr 160 contain hydrogen bonds to nearby histidines, yet the two tyrosines are functionally distinct. Tyr 161 mediates electron transfer between the primary donor, $P_{680}^{+}$. Tyr 160 is involved in assembly of the manganese cluster. Moreover, Tyr 160 and Tyr 161 have different midpoint potentials and their tyrosyl radicals have different lifetimes. The 2.9 Å crystal structure of photosystem II reveals that a pi-cation interaction between Tyr 160 and neighboring arginine residue (Arg 272CP47) may contribute to the difference in redox properties of Tyr 160 and Tyr 161.

We have incorporated tyrosine into five de novo designed biomimetic beta hairpin peptides: peptide A, peptide C, peptide D, peptide E, and peptide F. The amino acid content of the peptides was systematically altered to determine how non-covalent interactions with amino acids modulate the redox properties of tyrosine in enzymes. In peptide A, tyrosine is involved in an aromatic interaction with histidine, a hydrogen bond with arginine, and a pi-cation interaction with a second arginine. These non-covalent interactions were varied by single or double amino acid substitution in peptides C through F, and the concomitant alterations in the redox properties of tyrosine were analyzed by EPR spectroscopy, electrochemical titration, and optical titration.

Electrochemical titration of peptide A revealed that oxidation of tyrosine is coupled with protonation of histidine. Substitution of histidine by cyclohexylalanine (peptide C) or by valine (peptide D) eliminated this PCET reaction. Electrochemical titration of peptide A also showed that the aromatic interaction between tyrosine and

histidine is associated with a 50 mV decrease in the redox potential of tyrosine. However, removal of the hydrogen bond with arginine (peptide F) or the pi-cation interaction (peptide E) reversed this decrease in redox potential.

Optical titrations were used to predict the pK of tyrosine in peptides A through F. The pKs of tyrosine in peptides A, C, D, and F were indistinguishable. Removal of the Tyr 5-Arg 16 hydrogen bond (Peptide E) decreased the pK of tyrosine from 9.3 to 8.3 and caused small changes in the EPR spectrum of peptide E at pH 5.0.

These data demonstrate that the proton transfer to histidine, the hydrogen bond to arginine, and the pi-cation interaction create a peptide environment that lowers the midpoint potential of tyrosine. Moreover, these interactions contribute equally to control the midpoint potential. The data also show that hydrogen bonding is not the sole determinant of the midpoint potential of tyrosine. Finally, the data suggest that the Tyr 160D2-Arg 272CP47 pi-cation interaction contributes to the differences in redox properties between Tyr 160 and Tyr 161 of photosystem II.

# CHAPTER 1

# INTRODUCTION

## 1.1 Hierarchy of Protein Formation

In nature, proteins perform functions ranging from enzymatic catalysis to creating channels by which charged particles enter or exit cells. Often, the function of a protein can be determined by examining its structure. The structure of native proteins consists of a hierarchical organization of primary, secondary, tertiary, and quaternary structure.[1,2] Figure 1.1 shows an example of the four levels involved in native protein formation. Primary structure is the amino acid sequence of the protein's polypeptide chains.[2] The amide linkages that join amino acids in the primary structure are called peptide bonds; they create the polypeptide backbone.[2] Secondary structure forms when the backbone C=O and N-H groups hydrogen bond with one another, giving rise to specific folding patterns, such as helices, pleated sheets, and turns.[2] In helices, the backbone is twisted so that hydrogen bonding occurs between C=O and N-H groups within a single polypeptide strand, while pleated sheets form when two or more polypeptide strands hydrogen bond.[2] Amino acid side chain interactions help stabilize secondary structures as they form.[2] Interaction of different secondary structural elements leads to the formation of tertiary structure.[2] If the protein contains multiple polypeptide chains, those chains can associate via non-covalent interactions to give the quaternary structure of the protein.[2]

## 1.2 Secondary Structures in Proteins

The two most common forms of secondary structural motifs found in native proteins are alpha helices and beta sheets.[2] The torsion angles, psi (Ψ) and phi (Φ), of the polypeptide backbone specify alpha helix and beta sheet conformations.[2] Psi is the dihedral angle affected by rotation around $C_\alpha$-NH bond. Phi is the dihedral angle affected by rotation about the $C_\alpha$-C'O bond. In alpha helices, Ψ is $-47^o$ and Φ is $-57^o$.[1] In addition to characteristic psi and phi angles, alpha helices also contain 3.6 residues per turn and have a distance (pitch) of 5.4 angstroms between turns.[2] The backbone hydrogen bonding pattern of alpha helices is such that the C=O group of the *n*th amino acid residue points toward the N-H group of the *n*+4 residue.[2] The amino acid side chains point outward from the helical axis. In beta sheets, psi and phi vary depending on whether the strands in the sheet are parallel or anti-parallel. Anti-parallel beta sheets have Ψ and Φ angles of $135^o$ and $-139^o$, respectively.[1] Parallel beta sheets have Ψ and Φ angles of $113^o$ and $-119^o$, respectively.[1] The hydrogen bonding pattern in beta sheets is called a two-residue repeat. As a result of this pattern, the beta sheet has a hydrogen bonded face and a non-hydrogen bonded face. The side chains of the component amino acids extend outward from the backbone toward the hydrogen bonded or non-hydrogen bonded face in an alternating pattern.

## 1.3 Considerations for Designing Beta Hairpins

### *1.3.1 Turn Sequence*

Beta hairpins consist of two anti-parallel beta strands connected by a short loop sequence.[3] Beta turns are composed of up to four residues (i through i+4, with the loop region corresponding to residues i+1 and i+2) and are classified by their Ψ and Φ dihedral angles (Figure 1.2 and 1.3).[3] Table 1.1 shows dihedral angles for nine possible beta turn conformations. Beta hairpins are named as hairpins X:Y, where X is the number of residues in the loop and Y is the number of residues in the turn that do not occur in the strand.[3,4] For example, a beta hairpin with a loop containing three residues and one hydrogen bond closing the loop would have five residues in the turn that are not considered to be a part of the strand. This beta hairpin would be classified as a hairpin 3:5 (Figure 1.4A). The smallest beta turn that can lead to beta hairpin formation contains a two-residue loop closed by two hydrogen bonds, to give four total residues in the turn.[3,5] This type of beta hairpin is called a hairpin 2:2 (Figure 1.4B).[3,5]

**Table 1.1** Phi and psi dihedral angles of residues i+1 and i+2 in beta turns

| Turn Type | $\Phi_{i+1}$ | $\Psi_{i+1}$ | $\Phi_{i+2}$ | $\Psi_{i+2}$ |
|---|---|---|---|---|
| I | -60 | -30 | -90 | 0 |
| I' | 60 | 30 | 90 | 0 |
| II | -60 | 120 | 80 | 0 |
| II' | 60 | -120 | -80 | 0 |
| IV | -61 | 10 | -53 | 17 |
| VIa1 | -60 | 120 | -90 | 0 |
| VIa2 | -120 | 120 | -60 | 0 |
| VIb | -135 | 135 | -75 | 160 |
| VIII | -60 | -30 | -120 | 120 |

Statistical analysis of beta hairpins in native proteins by Sibanda and Thornton revealed that beta hairpins usually contain type I' and type II' turns.[6] The high occurrence of type I' and type II' turns in beta hairpins was attributed to the compatibility between the natural right handed twists of the turns and the natural twist of beta sheets formed by anti-parallel strands.[6] This explanation was confirmed experimentally by Haque and Gelman by examining the NMR spectra of 16-mer peptides containing $_{D}$-Pro or $_{L}$-Pro at the i+1 turn position and $_{D}$-Ala or $_{L}$-Ala at the i+2 turn position.[7]

The turn sequence defines the overall conformation of the beta hairpin. Figure 1.5 shows the peptide sequences examined by De Alba using NMR spectroscopy.[8] Residues 15-23 of native tedamistat forms a β-hairpin 2:2 with a type I Trp-Arg turn. Substitution of Ser 12, Trp 18, Arg 19, and Tyr 20 with Asn 17, Pro 18, Asp 19 and Gly 20 leads to formation of a β-hairpin 3:5. Moreover, in native tendamistat, Tyr 15, Gln 16, and Ser 17 are facing Gln 22, Ser 21, and Tyr 20, respectively. In the mutant peptide, Tyr 15, Gln 16, and Asn 17 are facing Ala 23, Gln 22, and Ser 21, respectively. In other designed peptides examined by De Alba [9], single amino acid substitutions also altered the β-hairpin strand register.

Two-residue loop sequences are most attractive for designing beta hairpins. Two strategies for constructing beta hairpins involve incorporation of either a $_{D}$-Pro-Gly turn[10] or an $_{L}$-Asn-Gly turn, as observed by NMR spectroscopy.[11] In Figure 1.6, the vertical axis shows the change in $C_{\alpha}H$ chemical shift values for each amino acid when the designed peptides are compared with the random coil peptides. A change in the $C_{\alpha}H$ chemical shift value of 0.1 ppm or greater for consecutive amino acids suggests beta sheet formation. In peptides containing the $_{D}$-Pro-Gly turn or the $_{L}$-Asn-Gly turn, the $C_{\alpha}H$

signals shift downfield by 0.1 ppm or more, as expected for polypeptide sequences that adopt beta sheets in solution. The $C_\alpha H$ downfield shifts of the $_D$-Pro-Gly peptide were larger than those yielded by the $_L$-Asn-Gly peptide, indicating that the $_D$-Pro-Gly turn is a stronger beta hairpin promoter than the $_L$-Asn-Gly turn in the peptides examined. No clear trend was observed in the chemical shift index for the peptide containing an $_L$-Pro-Gly turn. Therefore, these results, reported by Stanger and Gelman also indicate that the conformation of the amino acids in the turn sequence affects beta hairpin formation. Although Stanger and Gelman reported that the $_D$-Pro-Gly turn promoted a more stable beta hairpin in their peptides, the $_L$-Asn-Gly loop sequence is found more often in type I' turns in crystalline proteins than the $_D$-Pro-Gly loop sequence.[12] Several other studies have successfully designed folded beta hairpins using the $_L$-Asn-Gly turn.[11,13-15] In fact, the efficacy of the $_L$-Asn-Gly turn was proven in an experiment comparing a 16-mer beta hairpin (KKYTVSINGKKITVSI) with its truncated 11-mer counterpart (SINGKKITVSI) (Figure 1.7).[13] Figure 1.8 shows the two-dimensional (NOESY) NMR spectrum of SINGKKITVSI. NOESY NMR spectroscopy is useful for analyzing long distance interactions between protons in peptides and proteins. In Figure 1.8 the signals located symmetrically off of the diagonal line are called cross-peaks and show the proton chemical shifts resulting from the through-space interactions of amino acid side chains. Two-dimensional NMR cross-peaks between S6 and K11, I7 and K10, and I7 and N8 showed that the 11-mer still adopted a beta hairpin conformation in solution, despite not having any of the stabilizing hydrophobic interactions that were present in the 16-mer (Figure 1.8).

*1.3.2 Side Chain-Side Chain Interactions*

The amino acid side chains in beta hairpins can have through space, long-distance non-covalent interactions with one another. Once beta turn nucleation occurs, these side-chain interactions help stabilize the beta hairpin conformation. Griffiths-Jones and co-workers demonstrated this point by performing a pH titration and mutation studies on the 16-residue beta hairpin peptide, KKYTVSINGKKITVSI.[11] In their work, changing the pH of the peptide solution from 5.5 to 2.2 decreased the value of $\Delta\delta C_{\alpha H}$ ($\Delta\delta C_{\alpha H}$ is defined as the difference in the proton chemical shift values for a given amino acid in a random coil sequence and in a beta sheet) for all 16 residues in the peptide (Figure 1.9). Apparently, lowering the pH led to protonation of the C-terminal carboxylate group and subsequent removal of a salt bridge between the $C_{\alpha COO}$- of I16 and the $C_{\alpha NH3}^{+}$ of K1, causing destabilization of the hairpin structure. In the same peptide, Y3A and V5A mutations were used to test the effects of removing hydrophobic interactions from the sequence. No beta hairpin structure could be detected via NMR spectroscopy of the mutated peptides.

The energetic contributions of different types of side-chain interactions have been reported. Waters and Tatko compared the contribution of a pi-stacked aromatic interaction with the contributions of a hydrophobic interaction, and a mixed aromatic/hydrophobic interaction in designed peptides Ac-$RX_1VOVNGKGIX_2Q$-$NH_2$.[16] X1 and X2 are Phe and Phe, Phe and Cha, Cha and Phe, or Cha and Cha. Phe denotes phenylalanine and Cha denotes cyclohexylalanine. Sequences containing the Phe-Phe aromatic interaction or the Cha-Cha hydrophobic interaction had similar $\Delta H^{o}$ values of about -4 kcal/mol relative to random coil peptides. Sequences containing the mixed

aromatic/hydrophobic interactions (Phe-Cha or Cha-Phe) were less stable, with $\Delta H^o$ values of -2.3 kcal/mol and -3.2 kcal/mol. Therefore, it was concluded that attractive interactions between pi-stacked aromatic residues or hydrophobic residues promote beta hairpin formation.[16] However, pi-stacked aromatic interactions impart specificity on the polypeptide sequence. These results were later corroborated by Kiehna and Waters in different peptides (FRTVFVPGOFITQF, ERTVFVPGOFITQK, and ARTVFVPGOFITQA) for which $\Delta G^o$ was calculated to be -0.2 to -0.3 kcal/mol (0.8-1.3 kJ/mol).[17]

Ciani and co-workers used 16-mer hairpins containing zero, one, or two side chain salt bridges to quantify the energetic contribution of salt bridges to beta hairpin formation.[18] Their work showed that the presence of one salt bridge stabilizes the beta hairpin by about 1.2-1.3 kJ/mol. Two salt bridges stabilize the hairpin by 3.6 kJ/mol. The fact that the actual energetic contribution of two salt bridges is greater than the sum of the energetic contributions of the individual salt bridges indicates that the two salt bridges cooperatively stabilize the beta hairpin. Ramirez-Alvarado also showed that inclusion of a Lys-Glu salt bridge in the designed hairpin BH8 led to a more stable hairpin structure than when Lys and Glu were substituted with Ala residues.[14]

*1.3.3 Beta sheet forming tendencies of the amino acids*

The beta sheet forming tendencies of the 20 naturally occurring amino acids was determined by Smith, Withka, and Regan by measuring $T_m$ and $\Delta\Delta G$ of model proteins derived from the B1 domain of staphylococcal IgG binding protein G.[19] B1 contains four anti-parallel beta strands that are diagonally crossed by a single alpha helix. In native B1,

Thr 53 is solvent-exposed and its side chain extends from the face of the sheet that is opposite the helix. Therefore, Thr 53 was substituted with each of the 20 amino acids. Thr 53 is in close contact with Ile 6 and Thr 44; thus, Ile 6 and Thr 44 were mutated to Ala to limit interactions between guest amino acids at position 53 and neighboring side chains of the host protein. Their results showed that substitution of Val, Ile, Thr, Phe, Tyr, or Trp at position 53 yielded model proteins with the highest melting temperatures ($T_m$) and the lowest $\Delta\Delta G$ values. Substitution of Ala, Asp, Gly, or Pro yielded model proteins with the lowest $T_m$ values and highest $\Delta\Delta G$ values. So, Val, Ile, Thr, Phe, Tyr, and Trp are the best beta sheet forming amino acids, while Ala, Asp, Gly, and Pro are the worst beta sheet forming amino acids. Table 1.2 shows that Smith's calculations correlate well with results reported in a similar study performed by Kim and Berg [20] and with statistical surveys performed by Chou and Fasman.[21,22]

**Table 1.2** Summary of beta Sheet propensity data[36]

| Guest Residue | $T_m$ (°C) | ΔΔG (kcal/mol) | $P_\beta$ | $\Delta\Delta G_{(Kim\ \&\ Berg)}$ (kcal/mol) |
|---|---|---|---|---|
| Tyr | 69.22 | -1.63 | 1.31 | -0.50 |
| Thr | 68.67 | -1.36 | 1.33 | -0.48 |
| Ile | 67.78 | -1.25 | 1.57 | -0.56 |
| Phe | 67.68 | -1.08 | 1.23 | -0.55 |
| Trp | 65.73 | -1.04 | 1.24 | -0.48 |
| Val | 65.47 | -0.94 | 1.64 | -0.53 |
| Ser | 64.80 | -0.87 | 0.94 | -0.39 |
| Met | 64.26 | -0.90 | 1.01 | -0.46 |
| Cys | 63.99 | -0.78 | 1.07 | -0.47 |
| Leu | 62.47 | -0.45 | 1.17 | -0.48 |
| Arg | 61.41 | -0.40 | 0.94 | -0.44 |
| Asn | 61.88 | -0.52 | 0.66 | -0.38 |
| His | 60.96 | -0.37 | 0.83 | -0.46 |
| Gln | 60.90 | -0.38 | 1.00 | -0.40 |
| Lys | 60.65 | -0.35 | 0.73 | -0.41 |
| Glu | 58.81 | -0.23 | 0.51 | -0.41 |
| Ala | 57.05 | 0 | 0.79 | -0.35 |
| Asp | 50.91 | 0.85 | 0.66 | -0.41 |
| Gly | 45.95 | 1.21 | 0.87 | 0 |
| Pro | <10 | ND | 0.62 | 0.23 |

### 1.4 PSII and the Need for Model Peptides to Exam the Redox Properties of Tyrosine

In green plants and cyanobacteria, photosystem II (PSII) uses energy derived from sunlight to catalyze the oxidation of water and the reduction of plastoquinone. Tyrosine 161 of the D1 polypeptide in PSII facilitates this process by oxidizing the manganese cluster and reducing the primary donor $P680^{+}$. A second tyrosine residue, Tyr 160 of the D2 polypeptide is not required for catalytic activity[23], but may be required for assembly of the manganese cluster.[23,24] In addition to performing different functions, Tyr161D1 and Tyr160D2 also have different redox properties.[25-31] Tyr161D1 has a midpoint potential of 1 V[28] and a lifetime on the microsecond to millisecond timescale.[26,27,29] Tyr160D2 has a midpoint potential of 760 mV[25] and a lifetime on the minutes to hours timescale.[30,31] Although efforts have been made to determine how the redox properties of tyrosine and its derivative compounds are regulated, the origin of the differences between Tyr161D1 and Tyr160D2 is still unclear.

One explanation for the differences between Try161D1 and Tyr160D2 is that their redox properties are controlled by interactions with nearby amino acids. The 2.9 Å crystal structure shows that Tyr161D1 hydrogen bonds with His190D1 and is 5.08 Å from a salt bridge formed by Asp170D1 and Arg357CP43.[32] In the D2 polypeptide, Tyr160D2 also forms a hydrogen bond with a histidine residue (His189D2) and is 6.95 Å from an Arg180D2-Asp333D2 salt bridge.[32] However, the D2 polypeptide contains two additional arginine residues, Arg294D2 and Arg272CP47.[32] Arg272CP47 is 7.81 Å from Tyr160D2 and is positioned for a pi-cation interaction with this redox active tyrosine.[32] This putative pi-cation interaction may be responsible for the differences in redox properties observed when Tyr160D2 and Tyr161D1 are compared. Pi-cation interactions

are expected to contribute ~13 mV to the decrease in midpoint potential observed for Tyr160D2.[33]

In the studies presented here, we examine how the protein sequence controls the redox properties of tyrosine by incorporating a single tyrosine residue into small biomimetic beta hairpins. The beta hairpins were designed using the concepts discussed in section 1.3. These beta hairpins serve as tractable models in which the non-covalent interactions with tyrosine are systematically altered so that the subsequent effect on the proton affinity of tyrosine, and the midpoint potential and spin density distribution of the tyrosyl radical can be determined. The necessity of such biomimetic beta hairpins is understood by considering the complexity of photosystem II. Photosystem II is a 356 kD enzyme.[32] PSII consists of 13 intrinsic protein subunits, 3 extrinsic protein subunits, 2 antenna proteins (CP43 and CP47), and 2 reaction center proteins (D1 and D2). In addition to these 20 protein subunits, PS II also contains 35 chlorophyll molecules, 25 lipids, 12 carotenoids, 1oxygen evolving complex, 1 heme b, 1 heme c, 1 non-heme iron, 3 plastoquinones, and 2 pheophytins.[32]

In order to unambiguously determine how interactions with vicinal amino acids influence the redox properties of tyrosine, the interactions of interest must be isolated from all other protein components and enzymatic cofactors. This has been accomplished for the hydrogen bonding interaction by synthesizing phenol derivatives that contain pendant bases.[34] However, in that study, the bases were covalently attached to the phenol compound so that any alteration in the midpoint potential might also be attributed to an inductive effect. In another study, the effect of the pi-cation interaction on the midpoint potential was predicted using helical maquettes.[35] But in that study theoretical evidence

for pi-cation induced alterations in the midpoint potential of tyrosine was presented with no supporting experimental evidence. The beta hairpins used in the studies presented here provide a system in which the influence of hydrogen bonding, pi-cation interactions, and aromatic interactions on the midpoint potential can be examined without the restriction of a covalent attachment. Moreover, these studies present experimental evidence that such interactions lower the midpoint potential of tyrosine.

## 1.5 Figures

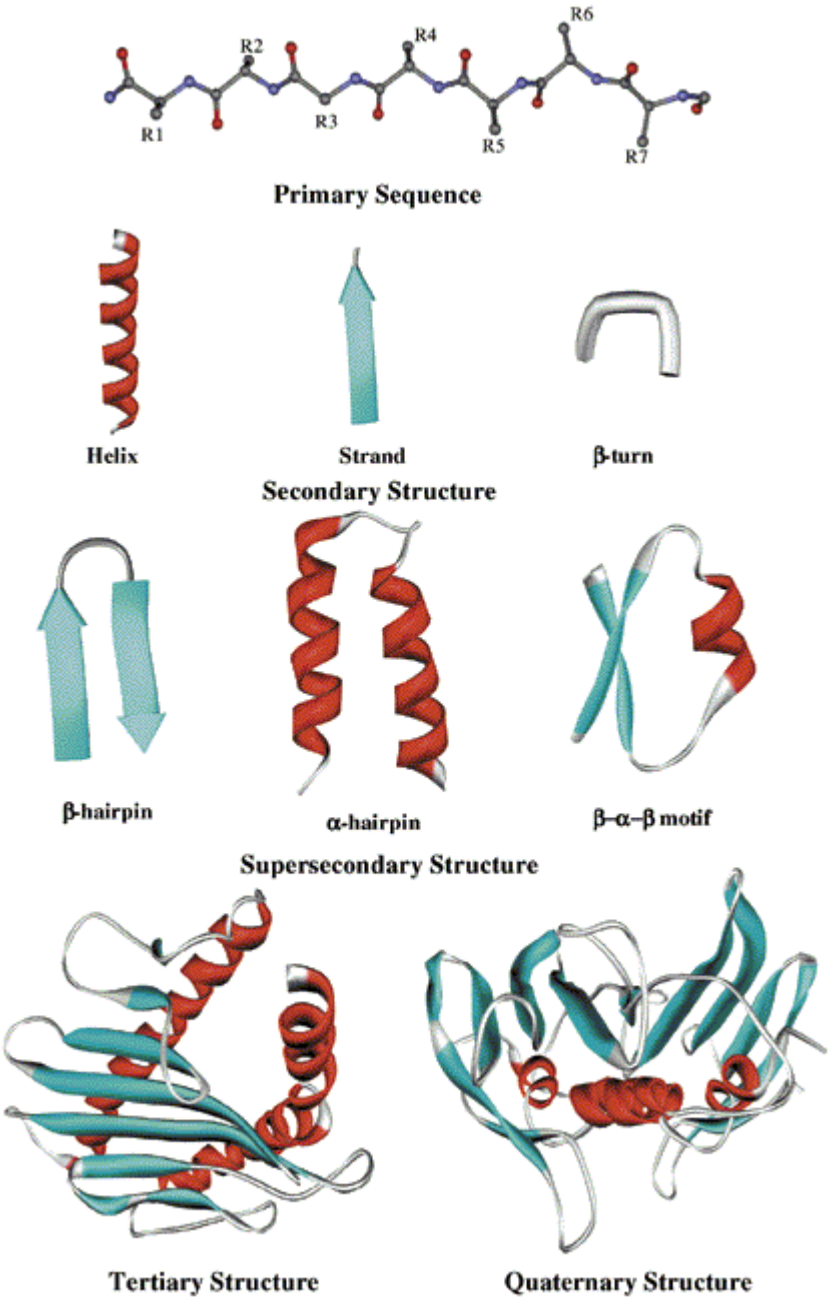


**Figure 1.1** Hierarchical organization of protein structure. This figure was reproduced with permission from Venkatraman et al (1999).[20]

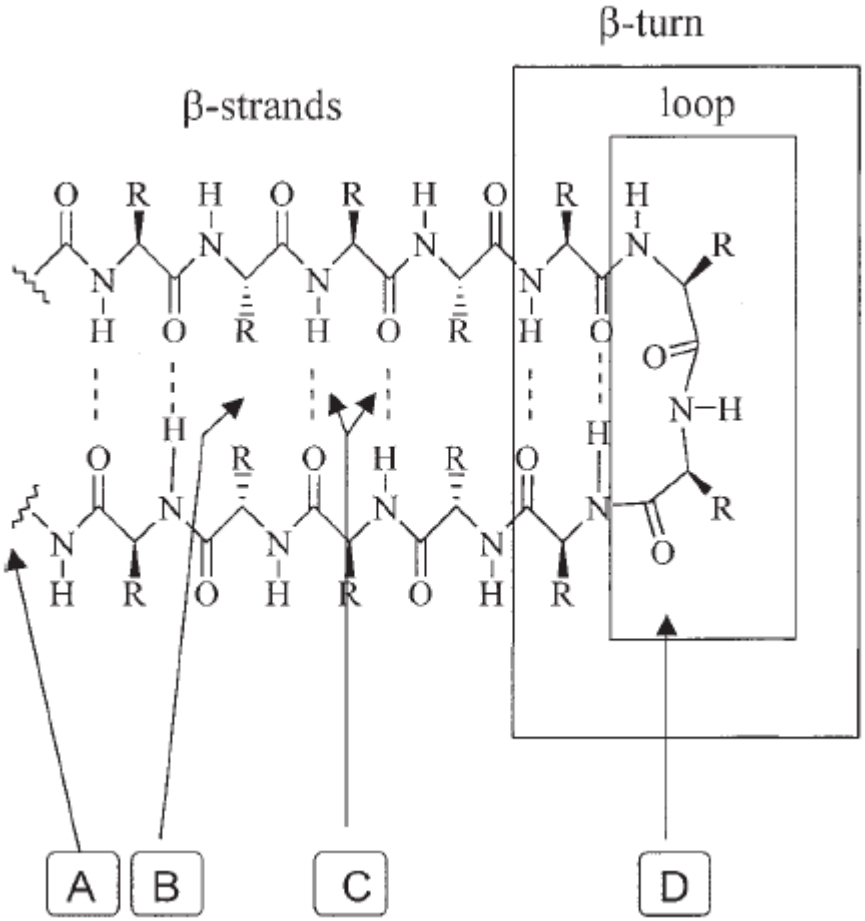


**Figure 1.2** Structural elements of a beta hairpin. The beta hairpin consists of two β-strands connected by a four-residue β-turn. Elements that contribute the beta hairpin structure are (A) the strand length (B) side-chain interactions (C) backbone hydrogen bonding (D) the sequence and conformation of the turn (E) the identity of the residues in the loop. This figure was reproduced with permission from Stotz and Topp (2004). [3]

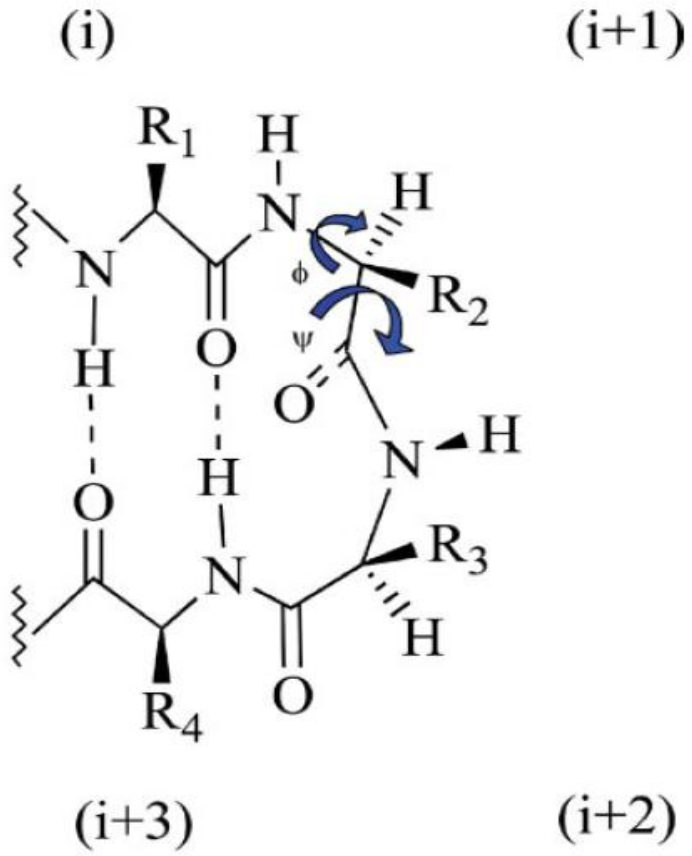


| Turn Type | ϕ(i+1) | ψ(i+1) | ϕ(i+2) | ψ(i+2) |
|---|---|---|---|---|
| I | -60 | -30 | -90 | 0 |
| I' | 60 | 30 | 90 | 0 |
| II | -60 | 120 | 80 | 0 |
| II' | 60 | -120 | -80 | 0 |

**Figure 1.3** Schematic of a β-turn. The arrows in the structure indicate Φ and Ψ dihedral angles at the i+1 position. The table shows Φ and Ψ values for the i+1 and i+2 positions in type I, type I', type II, and type II' beta turns. This figure was reproduced with permission from Stotz and Topp (2004). [3]

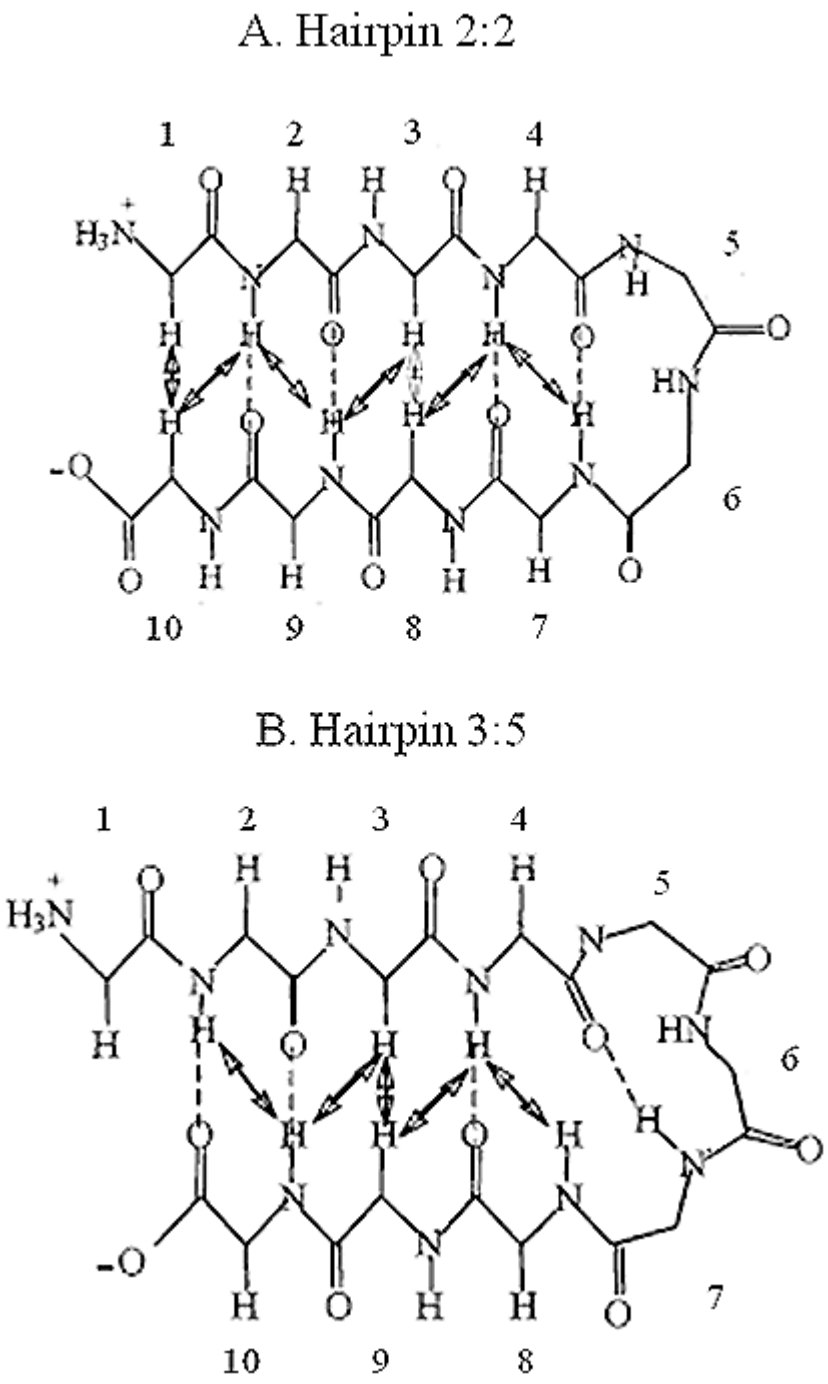


**Figure 1.4** Comparison of a hairpin 2:2 and a hairpin 3:5. This figure was adapted with permission from De Alba et al.[21]

A. Tendamistat, Hairpin 2:2, Type I Turn

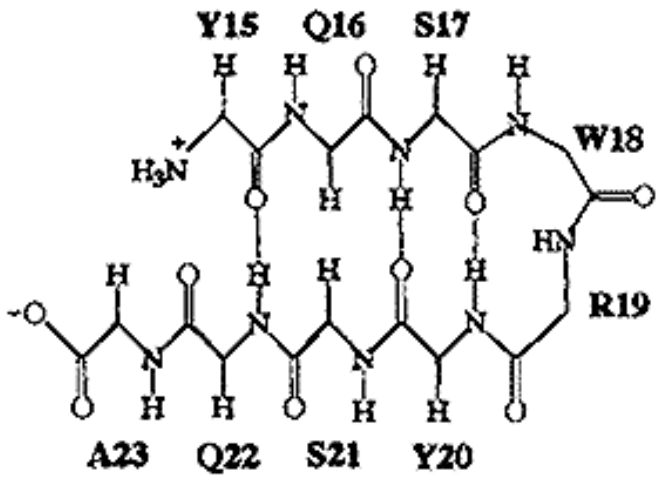


B. Mutant, Hairpin 3:5, Type I + G1 Bulge Turn

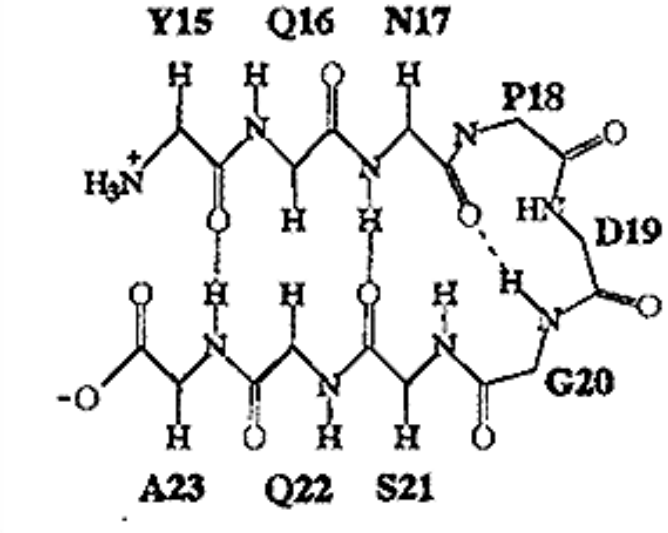


**Figure 1.5** Effect of mutations in the turn sequence on the beta hairpin conformation of tendamistat residues 15-23. In native tendamistat (A), the turn is composed of S17, W18, R19, and Y20. In the mutant (B), S17, W18, R19, and Y20 are replaced with N17, P19, D19, and G20. This figure was adapted with permission from De Alba et al (1997).[8]

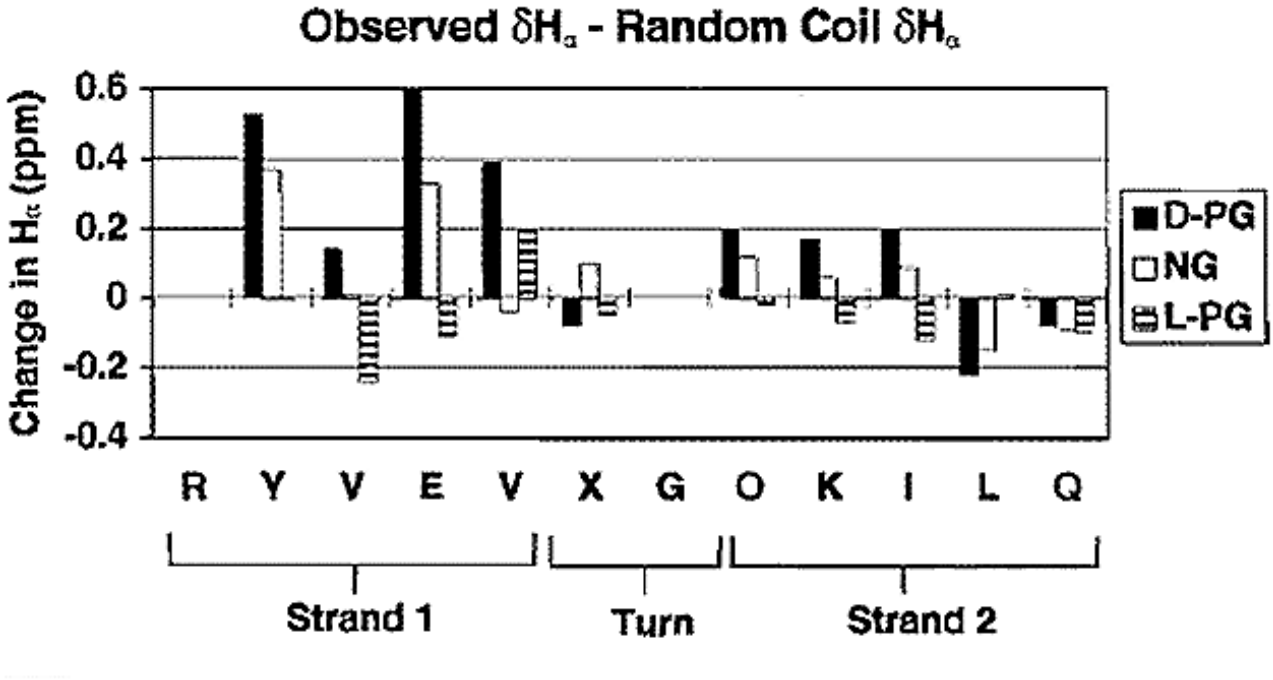


**Figure 1.6** Comparison of $C_{\alpha H}$ chemical shift values for RYVEVXGOKILQ. X = $_{D}$-Pro, $_{L}$-Arg, or $_{L}$-Pro. Reproduced with permission from Stanger and Gellman (2008).[10]

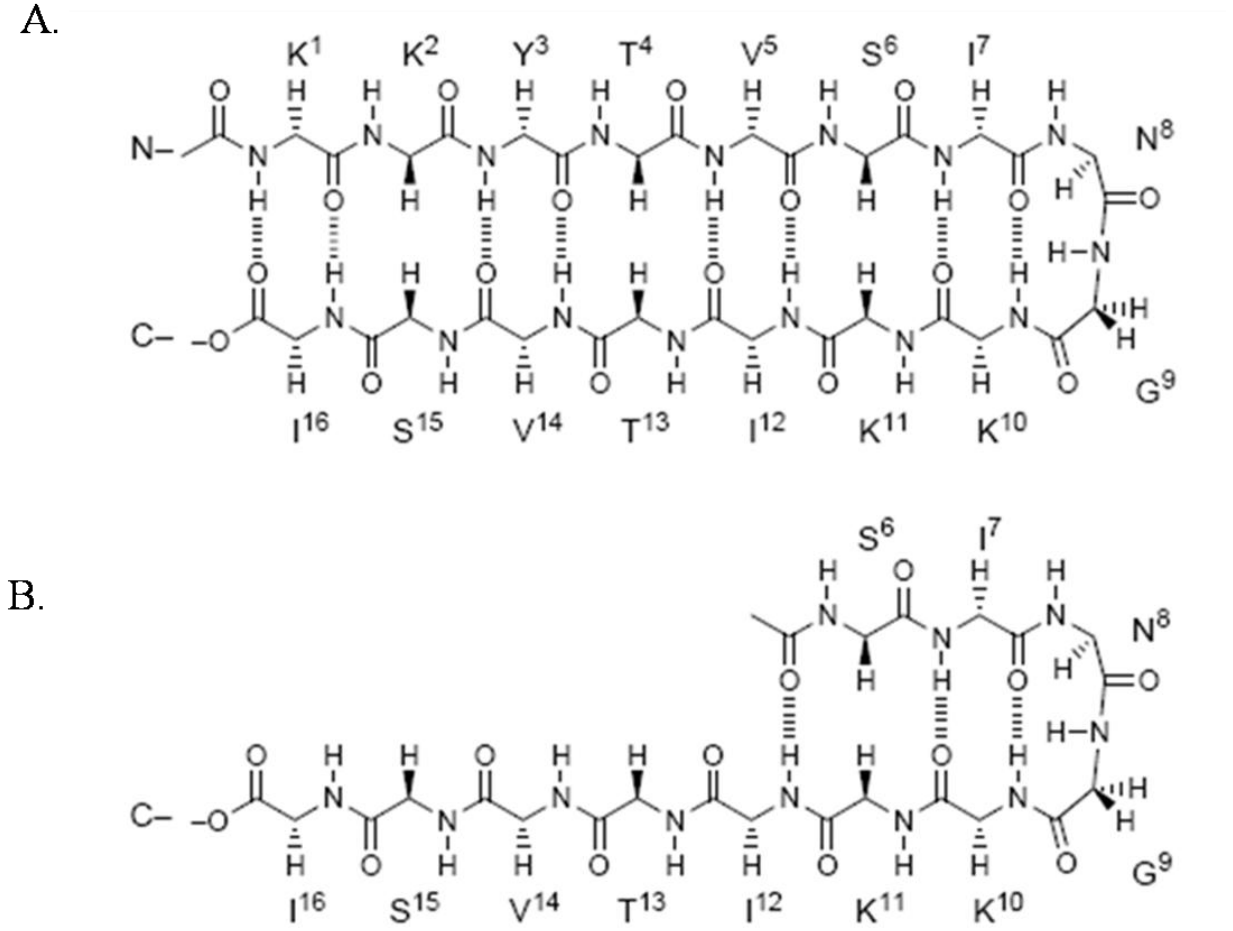


**Figure 1.7** Conformation of KKYTVSINGKKITVSI (A.) and SINGKKITVSI (B.). In the truncated hairpin, hydrophobic interactions between Y3 and V14, T4 and T13, and V5 and I12 have been removed. This figure was adapted with permission from Griffiths-Jones et al (1998) [13]

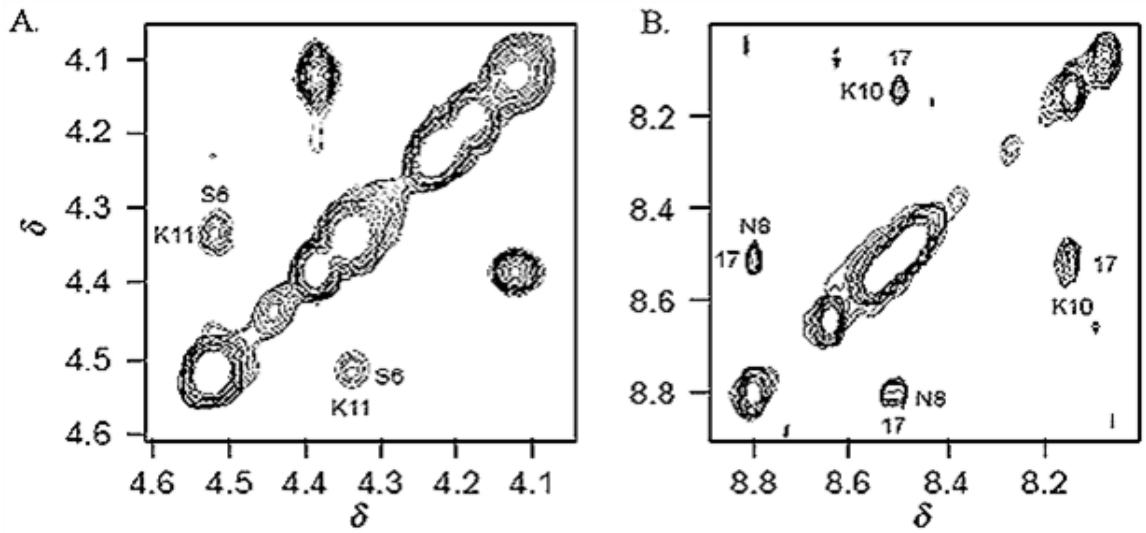


**Figure 1.8** Two-dimensional (NOESY) NMR spectrum of SINGKKITVSI. Signals along the diagonal are the chemical shift values of protons in the composite amino acids from the one-dimensional spectrum. The symmetric off-diagonal signals arise from through-space interactions between protons on the composite amino acids. The alpha proton region is shown in A. The amide proton region is shown in B. This figure was reproduced with permission from Griffiths-Jones et al (1998).[13]

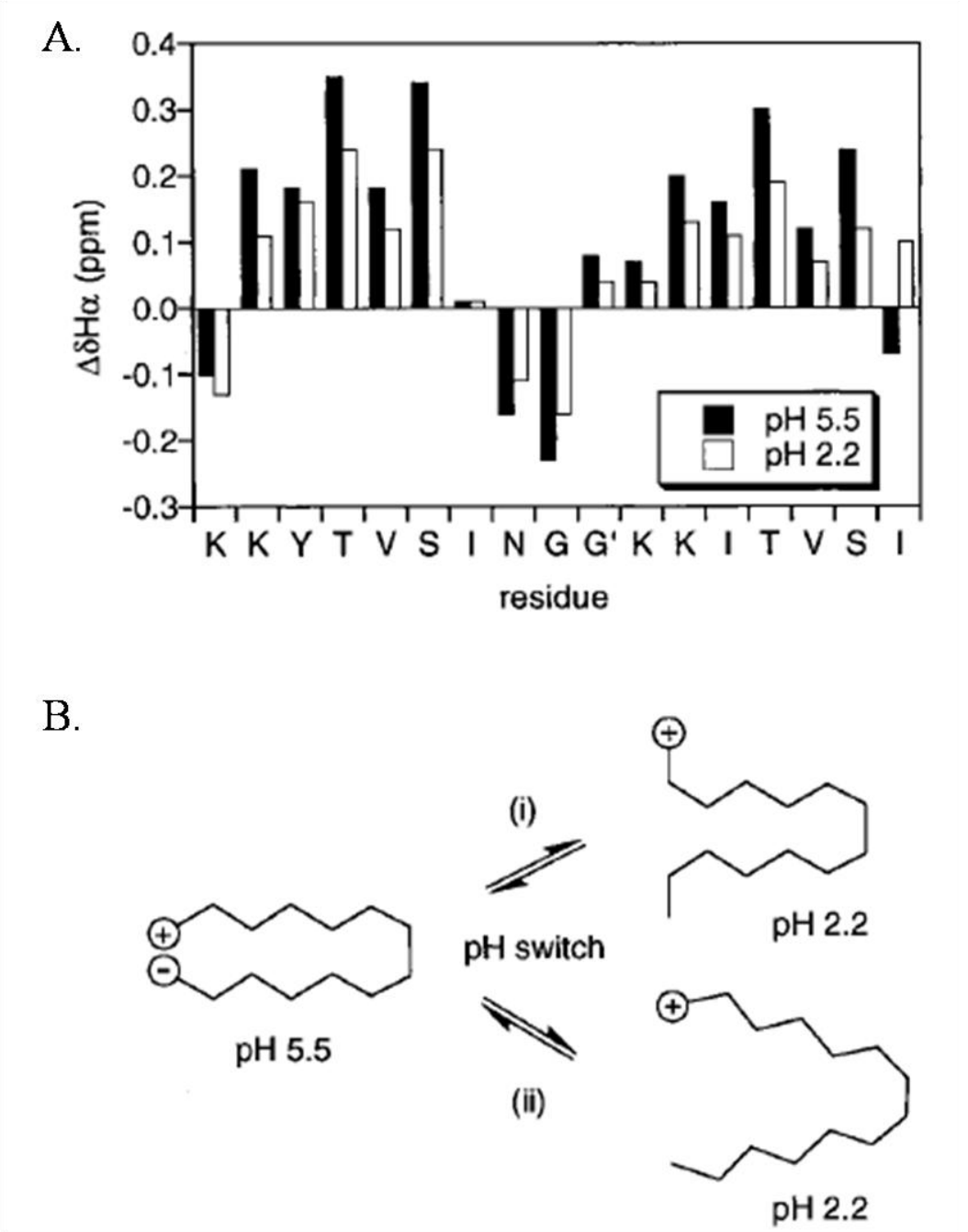


**Figure 1.9** Effect of pH on the conformation of beta hairpin KKYTVSINGG'KKITVSI. The NMR $C_{\alpha}H$ chemical shift index is shown in **A.** Decreasing the pH from 5.5 to 2.2 reduces the beta sheet population of the peptide. The proposed effects of decreasing the pH from 5.5 to 2.2 on the beta hairpin structure are shown in **B.** Lowering the pH disrupts a terminal salt bridge between and may lead to (i) fraying of the hairpin at the C- and N-termini or (ii) co-operative unfolding of the entire hairpin. This figure was reproduced with permission from Griffiths-Jones et al (1999).[11]

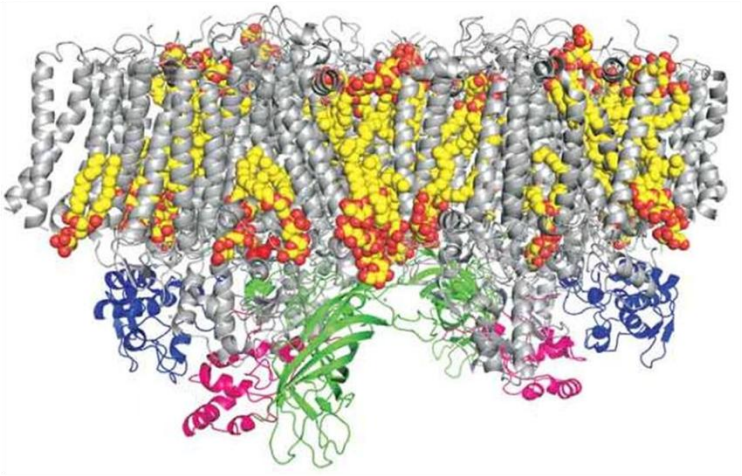

- Mass = 356 kD
- 20 protein subunits
  - 13 intrinsic proteins
  - 3 extrinsic proteins
  - Antenna proteins (CP43 and CP47)
  - Reaction center proteins (D1 and D2)
- 35 chlorophylls
- 25 lipids
- 12 carotenoids
- 1 OEC
- 1 heme b
- 1 heme c
- 1 non-heme Fe
- 3 plastoquinones
- 2 pheophytins

**Figure 1.10.** Structure and complexity of photosystem II. The bullets give details concerning the mass and number of protein subunits and cofactors in photosystem II. The structure was obtained with permission from Guskov et al.[32]

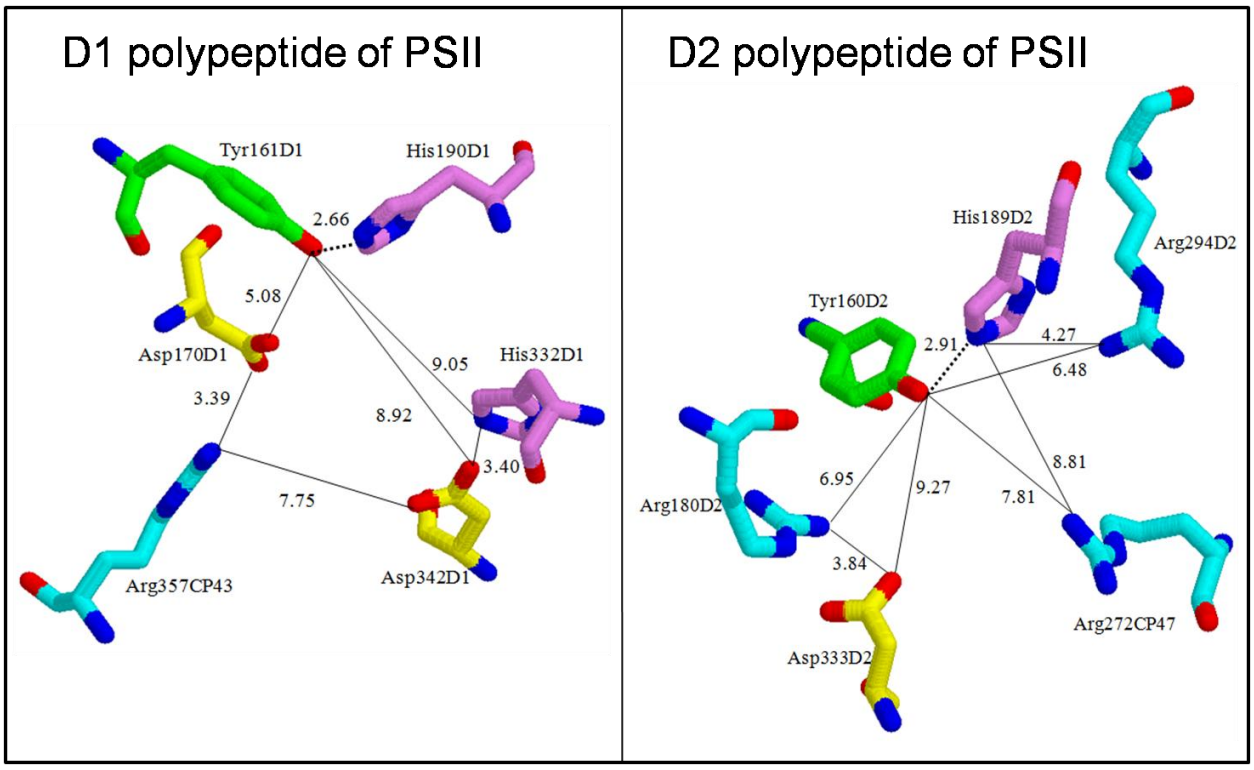


**Figure 1.11.** Environment of the redox active tyrosines (Tyr161D1 and Tyr160D2) in the D1 and D2 polypeptides of PSII (PDB ID 3BZ1[32]). The solid lines indicate distances between tyrosine and neighboring amino acids, and the dotted lines represent hydrogen bonds. The RasMol molecular visualization tool was used to depict histidine (violet), arginine (cyan), and aspartic acid (yellow) residues within 10.0 Å of the tyrosine (green).

## 1.6 References


1. Venkatraman, J.; Shankaramma, S.; Balaram, P. *Chemical Reviews* **2001**, *101*, 3131-3151.

2. Voet, D.; Voet, J.; 2nd ed.; John Wiley and Sons, Inc.: New York, 1995, p 105-213.

3. Stotz, C. E.; Topp, E. M. *Journal of Pharmaceutical Sciences* **2004**, *93*, 2881-2894.

4. Sibanda, B.; Blundell, T.; Thornton, J. *Journal of Molecular Biology* **1989**, *206*, 759-777.

5. Sibanda, B.; Blundell, T.; Thornton, J. *Journal of Molecular Biology* **1989**, *206*, 759-777.

6. Sibanda, B.; Thornton, J. *Nature* **1985**, *316*, 170-176.

7. Haque, T. S.; Little, J. C.; Gellman, S. *Journal of the American Chemical Society* **1994**, *116*, 4105-4106.

8. De Alba, E.; Jimenez, M.; Rico, M. *Journal of the American Chemical Society* **1997**, *119*, 175-183.

9. De Alba, E.; Rico, M.; Jimenez, M. A. *Protein Science* **1997**, *6*, 2548-2560.

10. Stanger, H. E.; Gellman, S. H. *Journal of the American Chemical Society* **1998**, *120*, 4236-4237.

11. Griffiths-Jones, S. R.; Maynard, A., J.; Searle, M. S. *Journal of Molecular Biology* **1999**, *292*, 1051-1069.

12. Hutchinson, G. E.; Thornton, J. M. *Protein Science* **1994**, *3*, 2207-2216.

13. Griffiths-Jones, S. R.; Maynard, A. J.; Sharman, G. J. *Chemical Communications* **1998**, 789-790.

14. Ramirez-Alvarado, M.; Blanco, F. J.; Serrano, L. *Protein Science* **2001**, *10*, 1381-1392.

15. Tatko, C. D.; Waters, M. L. *Journal of the American Chemical Society* **2004**, *126*, 2028-2034.

16. Tatko, C. D.; Waters, M. L. *Journal of the American Chemical Society* **2002**, *124*, 9372-9373.

17. Kiehna, S. E.; Waters, M. L. *Protein Science* **2003**, *12*, 2657-2667.

18. Ciani, B.; Jourdan, M.; Searle, M. S. *Journal of the American Chemical Society* **2003**, *125*, 9038-9047.

19. Smith, C. K.; Withka, J. M.; Regan, L. *Biochemistry* **1994**, *33*, 5510-5517.

20. Kim, C.; Berg, J. *Nature* **1993**, *362*, 267-270.

21. Chou, P.; Fasman, G. *Biochemistry* **1974**, *13*, 211-222.

22. Chou, P.; Fasman, G. *Advances in Enzymology and Related Areas in Molecular Biology* **1978**, *47*, 45-148.

23. Rutherford, A. W.; Boussac, A.; Faller, P. *Biochimica et Biophysica Acta* **2004**, *1655*, 222-230.

24. Ananyev, G.; Sakiyan, I.; Diner, B. A.; Dismukes, G. *Biochemistry* **2002**, *41*, 974-980.

25. Boussac, A.; Etienne, A. L. *Biochimica et Biophysica Acta* **1984**, *766*, 576-581.

26. Dekker, J. P.; Gorkom, H. J. V.; Brok, M.; Ouwehand, L. *Biochimica et Biophysica Acta* **1984**, *764*, 301-309.

27. Hoganson, C. W.; Babcock, G. T. *Biochemistry* **1988**, *27*, 5848-5855.

28. Metz, J. G.; Nixon, P. J.; Rögner, M.; Brudvig, G. W.; Diner, B. A. *Biochemistry* **1989**, *28*, 6960-6969.

29. Rappaport, F.; Blanchard-Desce, M.; Lavergne, J. *Biochimica et Biophysica Acta* **1994**, *1184*, 178-192.

30. Styring, S.; Rutherford, A. W. *Biochemistry* **1987**, *26*, 2401-2405.

31. Vass, I.; Styring, S. *Biochemistry* **1991**, *30*, 830-839.

32. Guskov, A.; Kern, J.; Gabdulkhakov, A.; Boser, M.; Zouni, A.; Saenger, W. *Nature Structural and Molecular Biology* **2009**, *19*, 334-342.

33. Tatko, C. D.; Waters, M. L. *Protein Science* **2004**, *12*, 2443-2452.

34. Rhile, I. J.; Markle, T. F.; Nagao, H.; G, D. A.; Lam, O. P.; Lockwood, M. A.; Rotter, K.; Mayer, J. *Journal of the American Chemical Society* **2006**, *128*, 6075-6088.

35. Tommos, C. S.; Skalicky, J. J.; Pilloud, D. L.; Wand, J.; Dutton, L. *Biochemistry* **1999**, *38*, 9495-9507.

36. Chou, P.; Fasman, G. *Advances in Enzymology and Related Areas in Molecular Biology* **1978**, *47*, 45-148.

# CHAPTER 2

# PROTON COUPLED ELECTRON TRANSFER IN A BIOMIMETIC PEPTIDE AS A MODEL FOR ENZYME REGULATORY MECHANISMS

## 2.1 Abstract

Proton-coupled electron-transfer reactions are central to enzymatic mechanism in many proteins. In several enzymes, essential electron-transfer reactions involve oxidation and reduction of tyrosine side chains. For these redox-active tyrosines, proton transfer couples with electron transfer, because the phenolic pK of the tyrosine is altered by changes in the tyrosine redox state. To develop an experimentally tractable peptide system in which the effect of proton and electron coupling can be investigated, we have designed a novel amino acid sequence that contains one tyrosine residue. The tyrosine can be oxidized by ultraviolet photolysis or electrochemical methods and has a potential cross-strand interaction with a histidine residue. NMR spectroscopy shows that the peptide forms a $\beta$-hairpin with several interstrand dipolar contacts between the histidine and tyrosine side chains. The effect of the cross-strand interaction was probed by electron paramagnetic resonance and electrochemistry. The data are consistent with an increase in histidine pK when the tyrosine is oxidized; the effect of this thermodynamic coupling is to increase tyrosyl radical yield at low pH. The coupling mechanism is attributed to an interstrand Tyr-His interaction, which stabilizes the tyrosyl radical. A similar interaction between histidine and tyrosine in enzymes provides a regulatory mechanism for enzymatic electron-transfer reactions.

## 2.2 Introduction

Redox-active tyrosine residues mediate long-distance electron transfer reactions in several enzymes.[1] For example, in photosystem II (PSII), Tyr 161 of the D1 polypeptide (TyrZ) participates in water oxidation by reducing the primary donor $P_{680}^{+}$ and by oxidizing the manganese cluster.[2] Tyr 160 in the D2 polypeptide (TyrD) is also redox-active but is not required for water oxidation {reviewed in ref 3}. In addition to TyrZ in PSII, tyrosyl radicals are essential for catalytic activity of prostaglandin H synthase,[4] ribonucleotide reductase (RNR),[5] and galactose oxidase.[6] Elucidation of the environmental factors, which influence the structure and function of the radical, will provide insights into the control of the activity in these enzymes. EPR studies of isotopically labeled tyrosinate have revealed that tyrosine oxidation occurs from the aromatic ring, generating a neutral radical with spin density located on the 1′, 3′, and 5′ carbon atoms and on the phenolic oxygen.[7,8] Additionally, rotation around the $C_1'$-$C_\alpha$ bond alters the EPR line shape.[7,8] In dipeptides, pentapeptides, and PSII, evidence for spin density delocalization to the amide group has been obtained {see ref 9 and references therein}. Oxidation of a protonated tyrosine at neutral pH values is coupled with the deprotonation of the phenolic oxygen.[10] This coupling of electron and proton transfer is due to a dramatic decrease in the pK of the phenolic oxygen in the radical state.[10] Therefore, changes in the pK of the proton-accepting group can alter the free energy of the oxidation/reduction reaction.[11] In direct coupling reactions, the proton and electron movement may be simultaneous, sequential, or nonsynchronous.[12]

According to Marcus theory, one of the factors influencing the electron-transfer rate is the oxidation potential of the redox-active cofactor.[13] Previous work has reported

a shift in tyrosine redox potential in designed helical proteins that contain tyrosine residues.[14,15] In one study, the observed increase was attributed to the non-polar environment and to shielding of the aromatic side chain from potential proton acceptors.[14] More specific intermolecular interactions with hydrogen bonded and charged groups are also expected to shift the midpoint potential.[11] The effect of non-covalent interactions on the potential of redox-active cofactors, such as hemes, iron sulfur clusters, and other metal centers, has been systematically explored in peptide models or maquettes {for examples, see refs 16-24}. Also, peptide bond formation may change the midpoint potential of a redox active amino acid residue, if spin density delocalization occurs to the peptide bond.[9] To develop a peptide system in which the effect of specific intermolecular and covalent interactions on tyrosyl radical can be probed, we designed an 18 amino acid sequence (Figure 2.1A, Peptide A), which we predicted would fold into a *β*-hairpin polypeptide {for previous examples of designed *β*-hairpin peptides, see refs 25,26}. This peptide exhibits an interstrand proton-coupled electron-transfer reaction between a histidine and the redox-active tyrosine. Our data suggest that thermodynamic coupling between electron and proton transfer decreases the midpoint potential of the redox-active tyrosine at low pH values.

## 2.3 Materials and Methods

*2.3.1 Samples.* Peptide A, IMDRYRVRNGDRIHIRLR, and peptide C, IMDRYRVRNGDRI[Cha]IRLR, in which a cyclohexylalanine (Cha) is substituted for a histidine, were synthesized by Sigma Genosys (The Woodlands, Texas). The peptides

were purified to 95% homogeneity by the manufacturer. Mass spectrometry was used to verify the sequence, and the purity was determined by analysis of the reversed phase HPLC chromatogram.

*2.3.2 NMR Spectroscopy.* The NMR samples had a concentration of 1mM in 90% $^{1}H_2O$/10% $^{2}H_2O$ and were buffered with 10 mM sodium phosphate, pH 5.0. NMR spectra were recorded using a Varian Unity spectrometer operating at 600 MHz at a temperature of 25 °C. An inverse detection triple-resonance probe was used. Resonance assignments were performed using two-dimensional $^{1}H/^{1}H$ TOCSY (75 ms mixing times) and $^{1}H/^{1}H$ ROESY (100, 200, 350 ms mixing time) experiments.[27] Water suppression was achieved using the WATERGATE technique.[28] Spectra were collected with 256 complex data points in the $t_1$ dimension and 1024 in the $t_2$ dimension. TOCSY spectra were acquired using a DIPSI-2 pulse sequence.[29,30] The spectral widths were 8 kHz on both the $t_1$ and $t_2$ dimensions. The DQF-COSY spectrum[31,32] was acquired on the 800 MHz Varian Unity spectrometer using 512 complex data points in the $t_1$ dimension and 2048 in the $t_2$ dimension. The DQF-COSY data were apodized with a 90° shifted sine bell in both dimensions prior to zero filling to 2048 _ 4096 data matrices to obtain the maximum digital resolution for coupling constant measurements. Proton chemical shifts were referenced to internal 3-(trimethylsilyl) propionic acid (TSPA). NMR spectra were processed using NMRPipe[33] and analyzed using SPARKY.[34] 2D spectra were processed with a sine bell window function shifted by 90°. The data were zero filled to twice their size before Fourier transformation. In the ROESY spectrum obtained with a mixing time of 300 ms, ROE cross-peaks were integrated and used for the structure calculations. The ROE volumes were calibrated using the average ROE volume from resolved aromatic

vicinal protons of Tyr 5. The ROE volumes were classified as strong, medium, and weak, corresponding to distance restraints of 1.9-2.7 Å, 1.9-3.3 Å, and 1.9-5.0 Å, respectively.[35] Structure calculations were performed using XPLOR-NIH,[36,37] starting from extended structures and using random simulated annealing calculations.[38] An initial high-temperature phase consisting of 6000 restrained molecular dynamics steps of 0.5 fs each was performed at a temperature of 1000 K. During this stage, all of the force constants were kept fixed. Subsequently, a molecular dynamics cooling phase comprised of 3000 steps of 0.5 fs each was employed, with the temperature decreasing from 1000 to 100 K during this interval. To refine the generated conformers, a second simulated annealing was carried out starting at 2000 K, including the full van der Waals potential. The temperature was decreased from 2000 to 0 K. During the high-temperature steps, the dihedral angles were constrained using a harmonic potential with a force constant of 200 kcal/mol. A final minimization of 500 steps was performed using the Conjugated Gradients Method. A total of 147 ROEs (78 inter- and 69 intra-residue) was used in the calculations. All the ROEs were unambiguously assigned, and since stereo-specific assignments could not be made pseudo atoms were employed using the center of mass approach. The backbones of all the structures generated give an identical fold with RMSDs on the average backbones within 0.5 Å. A total of 50 structures were generated by the simulated annealing protocol. 20 structures were then accepted for further analysis. The conformers generated were accepted on the basis of the lowest ROE violations. The analysis was carried out using the "accept.inp" routine included in the XPLOR software package. The 20 structures showed no violations of ROE constraints higher than 0.5 Å, bond angles higher than 5°, and bond lengths higher than 0.05 Å. The covalent geometry

of the conformers generated was analyzed using PROCHECK_NMR.[39] For one-dimensional NMR studies at pH 11, samples were prepared to a concentration of 4 mM in 90% $^{1}H_2O$:10% $^{2}H_2O$ at pH 11 using 10 mM borate buffer. The pH was adjusted with NaOH. The spectra were collected on a 500 MHz Bruker spectrometer at 25$^{o}$C, using 128 scans and 64 K data points. Water suppression was achieved using the WATERGATE technique. The data were processed using Mestre-C v.23 and IgorPro software.

*2.3.3 FT-IR Spectroscopy.* Solutions of 50 mM peptide A, buffered with 10 mM borate-NaOH, pH 11, were used. Absorbance spectra (Figure 2.7) were collected at room temperature on a Magna 550 spectrometer (Nicolet, Madison, WI), equipped with a MCT detector. The detector was cooled at least 30 minutes prior to data collection. The sample holder was a Hansen cryostat (RG Hansen & Associates, Santa Barbara, CA). The spectrometer was purged with nitrogen gas throughout data acquisition in order to minimize water vapor. Spectral were as follows: resolution, 4 cm-1; mirror velocity, 1.57 cm/s; apodization function, Happ-Genzel; levels of zero filling, one. Data were collected for 200 sec and on two different samples. Buffer contributions were subtracted interactively, and the resulting spectrum reflects hydrogen bonding to the amide bonds of peptide A.

*2.3.4 UV Spectroscopy and pK Determination*. pH titrations were conducted to measure the pK of the tyrosine in peptide A and in tyrosine solutions. Changes in tyrosine protonation were monitored by measuring the absorbance at 270 (TyrOH) nm and dividing by the sum of the absorbance at 270 (TyrOH) and 295 (TyrO-) nm.[14] A Hitachi U-3000 UV-visible spectrophotometer and 1 cm path length cuvettes were employed. The tyrosine or peptide concentration was 50 $\mu$M, and 10 mM MES-NaOH (pH 4.0-5.5),

10 mM HEPES-NaOH (pH 6.0-8.0), 10 mM boric acid-NaOH (8.5-10.5), or 10 mM CAPS-NaOH (pH 11.0-11.5) were employed as buffers. Experiments were performed on two different samples and then averaged. Experiments performed with a different choice of buffering agent gave the same result.

*2.3.5 EPR Spectroscopy*. The tyrosine or peptide A concentration was 1.0 mM, and either 10 mM sodium phosphate-NaOH (pH 5) or 10 mM boric acid-NaOH (pH 11) was used as a buffer. EPR spectra were collected on a Bruker EMX spectrometer (Billerica, MA). Spectra were recorded at 103 K through the use of a Wilmad (Buena, NJ) flowthrough dewar. The radical was generated with a 266 nm photolysis pulse using methods previously described.[9] After baseline correction, spectra were integrated twice using Igor Pro software (Wavemetrics, Lake Oswego, OR). Experiments were performed on two different samples and averaged.

*2.3.6 Electrochemistry*. Tyrosine (0.01 mM), peptide A (0.05-0.1 mM), and peptide C (0.1 mM) samples were prepared in buffered solutions that contained 0.2 M KCl and 10 mM sodium acetate-NaOH (pH 4.0-5.5), 10 mM sodium phosphate (pH 6.0-7.8), 10 mM boric acid-NaOH (8.0-9.5), or 10 mM CAPS-NaOH (pH 10.0-11.8). Square wave voltammetry measurements were performed on a computer controlled CH Instruments, Inc. (Austin, TX) electrochemical workstation. The experiments were conducted in a three-electrode cell, equipped with a 3 mm diameter glassy carbon working electrode from Bioanalytical Systems, Inc. (West Lafayette, IN), a platinum foil counter electrode, and a reference electrode, Ag/AgCl in 1 M KCl, $E$ = 0.22 V (NHE). In order to eliminate junction potential between the reference electrode and the test solution an electrolytic junction filled with 1 M $KNO_3$ was used. The sample was purged with nitrogen gas

during data collection. Oxidation was initiated with a holding time of 2 s at 0.1 V and then scanned up to 1.1 V. Data were collected in increments of $\Delta E$ = 0.004 V. The square wave frequency, *f*, was 5 Hz, and the amplitude, *A*, of the applied pulse was 0.025 V (scan rate $v = f * A$ = 125 mV/s). The parameters were optimized in relation to the maximum value of peak current and peak width (half peak potential). The data were fit to a baseline manually, and the centroid was used to derive

the peak potential. Experiments were performed on two to four samples and averaged, and experiments conducted with different buffers gave similar results. A standard, hexaamine ruthenium(III) chloride (Strem Chemicals, Newburyport, MA) at 2.5 mM in 1 N KCl, was run on each day of data acquisition. The averaged value for this standard was -0.18± 0.01 V. Experiments performed with a different choice of buffering agent gave the same result. The pH dependence of the peak potential was analyzed using Igor Pro software. The data for tyrosine and peptide C were fit with the following equation: $E_m = E^* - 0.06 \log[\{10^{-pKox} + 10^{-pH}\}/\{10^{-pKred} + 10^{-pH}\}]$, which describes the influence of a single ionizable group on the midpoint potential of a single electron-transfer reaction.[40,41] In this equation, $E^*$ is the extrapolated midpoint potential at pH 0, and $pK_{ox}$ and $pK_{red}$ are the pK values of the tyrosine side chain in the oxidized (tyrosyl radical) and reduced forms, respectively. In trial fits, $E^*$ and $pK_{red}$ were estimated from the data and then varied so as to minimize the chi-square value. In the resulting best fit to both the tyrosine and the peptide C data, $pK_{ox}$ was equal to 0 (see ref 10) and $pK_{red}$ was equal to 10.0 (see optical titration data, Figure 2.3). $E^*$ was equal to 1.33 V for tyrosine and 1.28 V for peptide C. For peptide C, equations including the protonation of more than one titratable group gave a less reliable fit to the data, as assessed by the chi-square value.

For peptide A, data, describing the pH dependence of the peak potential, were fit with the following equation, $E_m$ ) $E^*$ - 0.06 log [[({$10^{-pH}$}$^3$ + {$10^{-pH}$}$^2$ * {$10^{-pKox1}$}) + ({$10^{-pH}$} * {$10^{-pKox1}$} * {$10^{-pKox2}$}) + ({$10^{-pKox1}$} * ($10^{-pKox2}$) * {$10^{-pKox3}$})]/[({$10^{-pH}$}$^3$ + {$10^{-pH}$}$^2$ * {$10^{-pKred1}$}) + ({$10^{-pH}$} * {$10^{-pKred1}$} * {$10^{-pKred2}$}) + ({$10^{-pKred1}$} * ($10^{-pKred2}$) * {$10^{-pKred3}$})]], which describes the influence of three titratable groups on the midpoint potential of a one-electrontransfer reaction.[40,41] Initial values of the pK values were estimated from observed inflection points in the data, and the initial value of $E^*$ was estimated by extrapolation. $E^*$ and the pK values were then varied to optimize the chi-square value. In the final fit, the three values of p$K_{ox}$ were equal to 0 (p$K_{ox1}$, assigned to tyrosine), 8.0 (p$K_{ox2}$, assigned to histidine), and 4.5 (p$K_{ox3}$, assigned to aspartic acid). The three values of p$K_{red}$ were equal to 10.0 (p$K_{red1}$, assigned to tyrosine), 7.0 (p$K_{red2}$, assigned to histidine), and 4.0 (p$K_{red3}$, assigned to aspartic acid). In the final fit, $E^*$ was equal to 1.09 V. Inclusion of only one or two titratable groups in the equation gave a less reliable fit to the data, as assessed by the chi-squared value.

*2.3.7 Calculations.* Electronic structure calculations were performed on gas-phase models of tyrosine and a tyrosyl radical with the Kohn-Sham density-functional theory (DFT) using the hybrid exchange functional of Becke[42,43] and the Lee, Yang, and Parr correlation functional44 (B3LYP). All electronic structure calculations were performed with the GAUSSIAN03 suite of programs.[45] The singlet tyrosine was modeled by an anionic tyrosine (with a proton on the phenolic oxygen) in the A conformation, as previously defined.[46] The tyrosyl radical was modeled by an anionic tyrosyl (with a deprotonated phenolic oxygen) in the A conformation.[46] The molecules are anionic due to the negative charge on the carboxylate group. These gas-phase model structures have

been quite successful in previous studies of tyrosine and tyrosyl vibrational spectra.[46] Geometries were obtained using the 6-31++G(d,p) basis set,[47] as in ref 46. Integrals involving the exchange-correlation potential used the default numerical integration mesh with a maximum of 75 radial shells and 302 angular quadrature points per shell pruned to approximately 7000 points per atom.[48] Geometry optimizations were done in redundant internal coordinates with the default convergence criteria.[49] Maps of the electrostatic potential were created from B3LYP/6-311++G(3df,2p) single-point calculations.[47] The electrostatic potential was mapped onto an isodensity contour at 0.001 au using the gOpenMol suite of programs.[50]

**2.4 Results and Discussion**

Peptide A, IMDRYRVRNGDRIHIRLR (Figure 2.1A), was designed with an amino acid composition that promotes $\beta$-sheet formation,[51] an Asn-Gly type I' turn sequence,[52] two salt bridges,[53] and a Tyr-His aromatic interaction.[54] As a control, another peptide (peptide C) was synthesized in which His 14 was replaced with cyclohexylalanine (Cha). NMR spectroscopy was used to determine the structure of peptide A at pH 5.0. Representative data and a complete list of all observed ROE values are presented in Figures 2.2 and 2.3. As predicted, the peptide forms a well-ordered $\beta$-hairpin (Figure 2.1B). The chemical shift index of $H_\alpha$ reported in Figure 2.3B displays only positive deviations from the random coil values. Excluding the terminal residues, an average of 10 ROEs per residues were detected, resulting in a well-ordered backbone structure with an ~0.5 Å RMSD (Figure 2.3C). A plot summarizing the backbone ROEs and $^3J_{HN\text{-}HR}$ is reported in Figure 2.3A. The average minimized structure (Figure 2.1C) obtained from the simulated

annealing calculations shows that the two aromatic residues Tyr 5 and His 14 are co-facially aligned. The interstrand ROEs between these residues are highlighted in Figure 2.2, showing that the distances between the protons of His 14 and Tyr 5 are less than 5 Å. This offset, stacked orientation is typical of $\pi$-$\pi$ interactions in proteins.[55] Tyr 5 is also located within ~5 Å of Arg 16 and Asp 3. The average, minimized structure suggests that Arg 16 forms a salt bridge with the cross-strand Asp 3 (Figure 2.1C) and that Arg 16 forms a hydrogen bond to the Tyr 5 phenolic oxygen through the arginine $\varepsilon$-NH group (Figure 2.1C).

The effect of these intermolecular interactions on the pK of the tyrosine side chain in peptide A was investigated. This experiment was performed by monitoring the deprotonation of the tyrosine side chain through optical spectroscopy. There was no significant shift of the pK when tyrosine solutions were compared to peptide A (Figure 2.4). This can be rationalized by reference to the averaged and minimized peptide NMR structure (Figure 2.1C), which shows that the arginine, which is hydrogen bonded to the tyrosine, is also involved in a salt bridge with aspartate. The effect of this arginine-aspartate interaction is to neutralize the charge on the arginine side chain.

Tyrosine can be oxidized photochemically by 266 nm UV photolysis, and the resulting neutral radical can be detected and quantitated by EPR spectroscopy (Figure 2.5). Microwave power saturation curves for tyrosine and peptide A samples were measured at both pH 5 and pH 11. These experiments showed that the $P_{1/2}$ values for the tyrosyl radical in the tyrosine and peptide samples were significantly altered, when the two samples are compared. For peptide A, the values were 1.8 mW at pH 11 and 1.6 mW at pH 5.0. For tyrosine, the values were 0.5 mW at pH 11 and 0.7 mW at pH 5.

Accordingly, EPR experiments were conducted at 0.2 mW, at which no significant saturation or power broadening would be expected in either sample. The difference in $P_{1/2}$, when the tyrosine and peptide A samples are compared, provides support for the conclusion that the peptide tyrosyl radical is involved in an interstrand, non-covalent interaction at both pH values and is not in an exclusively aqueous environment.

Under non-saturating microwave power conditions at 0.2 mW, the EPR spectra recorded in tyrosine (Figure 2.5B and D) and peptide A (Figure 2.5A and C) samples showed small differences in line shape, which mainly corresponded to broadening of the peptide A EPR line shape. Observed differences in the EPR signals (Figure 2.5) are consistent with a difference in the distribution of side chain conformers in the peptide or with a redistribution of spin density, which could be caused by hydrogen bonding between the arginine side chain and the tyrosyl radical.[7,9] The origin of this effect is interesting and can be pursued by eventual isotopic labeling of the tyrosyl radical in peptide A and by EPR simulations. A contribution to the EPR spectrum from an oxidized histidine side chain is unlikely due to the reported redox potentials of histidine and tyrosine.[56,57]

The EPR spectra were doubly integrated in order to quantitate the amount of signal. The 266 nm optical properties of the samples at 103 K were similar. The results show that, at pH 11, the yield of the neutral radical was indistinguishable in peptide A and tyrosine (Figure 2.5A and B, Table 2.1). However, there was a significant increase in radical yield in the peptide at pH 5.0, relative to tyrosine were solutions (Figure 2.5C and D, Table 2.1). These EPR results could be consistent with a change in the redox potential of the tyrosine side chain at low pH, if there is no difference in non-radiative decay rate.

**Table 2.1.** Electrochemical and EPR studies of peptide A and tyrosine samples

| Sample | pH | Voltammetry Peak Potential (V)[a] | EPR Radical Yield[b] |
|---|---|---|---|
| Peptide A | 5.0 | 0.97 ± 0.01 | 97 ± 12 |
| Tyrosine | 5.0 | 1.02 ± 0.01 | 65 ± 9 |
| Peptide A | 11.0 | 0.69 ± 0.01 | 119 ± 15 |
| Tyrosine | 11.0 | 0.70 ± 0.01 | 112 ± 10 |

[a]Peak potential versus NHE.

[b]Relative yield derived by double integration of the tyrosyl radical EPR spectrum under non-saturating conditions.

Upon photo-ionization of tyrosine at room temperature, the solvated electron can be detected optically, so the eventual electron acceptor in both samples is likely to be solvent {reviewed in ref 1}. The issue of the non-radiative decay rate can be pursued in future experiments.

At pH 11, the one-dimensional NMR spectrum shows no collapse of the $H_\alpha$ region, indicating that the peptide is folded (Figure 2.6). At pH 11, complete structural determination for peptide A was not attempted because of rapid exchange of the amide protons. However, the one-dimensional spectrum shows chemical shift dispersion in the $H_\alpha$ region. Chemical shift dispersion is characteristic of folded proteins.[2] FT-IR measurements at a concentration of 50 mM also provide evidence for $\beta$-strand content at pH 11 (Figure 2.7).

To test the idea that there is a change in tyrosine redox potential in peptide A, square wave voltammetry was employed {see refs 14,57}. Representative voltammograms for tyrosine and peptide A are presented in Figure 2.8. The tyrosine oxidation reaction has been shown to be irreversible in voltammetric experiments, but in

previous work, the observed peak potentials can be corrected to give redox potentials.[57] In our experiments, there was no significant (<2%) effect of scan rate and concentration on the measured potentials for peptide A,[14] suggesting that any correction factor is negligible. In previous work on a tyrosine-containing designed peptide, the correction was reported as 0.02 V.[14] Because we are not deriving any thermodynamic quantities in our analysis of the electrochemical data, we report the uncorrected peak potentials. For tyrosine, data had to be recorded at a low concentration to avoid increased data scatter due to a putative sample-electrode interaction.

The potential for tyrosine at pH 7 was in good agreement with results in ref 57 after correction for NHE (+0.22V), when the same concentration was used.[58] In Figure 2.9, the peak potential of tyrosine was determined as a function of pH at pH values between 4 and 12. For tyrosine solutions, the results (Figure 2.9, open triangles) show that, as expected, the potential increases linearly with decreasing pH under the pK (10.0) of the tyrosine phenolic oxygen. The observed, absolute value of the slope between pH 4 and 10 is 63 mV/pH unit. This slope is in reasonable agreement with the expected slope (59 mV/pH unit) for an electron-transfer process in which both a proton and an electron are transferred at 25 °C.[57] The data were fit (Figure 2.9, open triangles, dashed line) with a modified Nernst equation, in which it is assumed that a single proton-transfer reaction, in this case, the protonation of the tyrosine side chain, influences the potential.[40,41] However, the pH dependence of the peak potential (Figure 2.9, squares) for tyrosine-containing peptide A reveals a more complex reaction process. Peptide A data were fit best with a model in which three ionizable groups, attributed to aspartic acid, histidine, and tyrosine, influence the potential (solid line). In particular, two pK values of 7.0 and

8.0 are evident as inflection points (Figure 2.9, arrows) in the data.[41] These pK values are attributed to the cross-strand histidine (His 14), which has dipolar contacts with the tyrosine side chain (Tyr 5) (Figure 1B and C). This conclusion is supported by studies of peptide C, a peptide A variant in which cyclohexylalanine is substituted for His 14 and in which these turning points are not observed (Figure 2.9, circles, dot-dashed line). From the slope change at each inflection point, the value of 7.0 is assigned to the pK of His 14 in the reduced state and the value of 8.0 is assigned to the pK of His 14 in the oxidized state {see ref 41 and references therein}. In peptide A (solid line), pK values of 0 (oxidized state) and 10 (reduced state) were attributed to Tyr 5, and pK values of 4.5 (oxidized state) and 4.0 (reduced state) were attributed to Asp 3. A pK of 7.0 is typical of the histidine side chain in proteins. As observed in Figure 2.9 and the associated fit, when the tyrosine side chain in peptide A is oxidized, the pK of the histidine increases by ~1 pH unit. Therefore, in the pH range from 7.0 to 8.0, the histidine side chain protonates when the tyrosine side chain is oxidized, and the oxidation reaction between pH 7.0 and 8.0 results in the net transfer of a proton from the tyrosine to the histidine. In the ranges from pH 8.0-10.0 and 4.5-6.9 (Figure 2.9), the absolute values of linear slopes derived from the data are 51 ± 9 mV/pH unit and 53 ± 3 mV/pH unit, respectively. As stated above, these values are consistent with the expected one proton-one electron reaction. The change in slope (to 27 ± 6 mV/pH unit) in the pH range between 7.0 and 8.0 may be due to the close overlap of the histidine pK values. As observed in Table 2.1, the consequence of this proton-coupled electron-transfer reaction is to favor tyrosyl radical formation at low pH. If one considers thermodynamic linkage of the oxidation and reduction reactions, the expected alteration in midpoint potential for a one unit pK change

is a decrease of 59 mV at 25 °C {$nF\Delta Em = RT \ln(K_{ox}/K_{red})$}.[11,41] When tyrosine and peptide A are compared, a 0.050 V decrease in peak potential in peptide A is observed at pH 5 (Table 2.1). Moreover, the cyclohexylalanine variant shows a confirmatory increase in peak potential at low pH, when compared to peptide A (Figure 2.9, circles). Taken together, these data suggest that histidine protonation and tyrosine oxidation are thermodynamically linked in peptide A.

## 2.5 Summary

Our results show that peptide bond formation and proton transfer involving histidine can alter the redox potential of tyrosine, even when the histidine and tyrosine are not directly hydrogen bonded. To understand the basis of this interaction, electrostatic maps were calculated[46] for tyrosine (Figure 2.10A) and for the tyrosyl radical (Figure 2.10B). As observed in Figure 2.10, oxidation of tyrosine is associated with an increase in negative charge on the phenolic oxygen, which may stabilize the positive charge on the histidine side chain. In turn, the protonated imidazole group will stabilize the tyrosyl radical, relative to tyrosine. Thus, our results suggest a novel method by which the protein environment can alter tyrosyl radical function and control electron-transfer rates.

**2.6 Acknowledgments.**

The authors thank Prof. Jake Soper for helpful comments on the manuscript, Dr. Les Gelbaum for assistance with the one-dimensional NMR measurements, and NIH GM43273 (B.A.B.), NIH GM 64742 (G.V.), and NSF CHE 0452045 (M.J.) for research support.

## 2.7 Figures

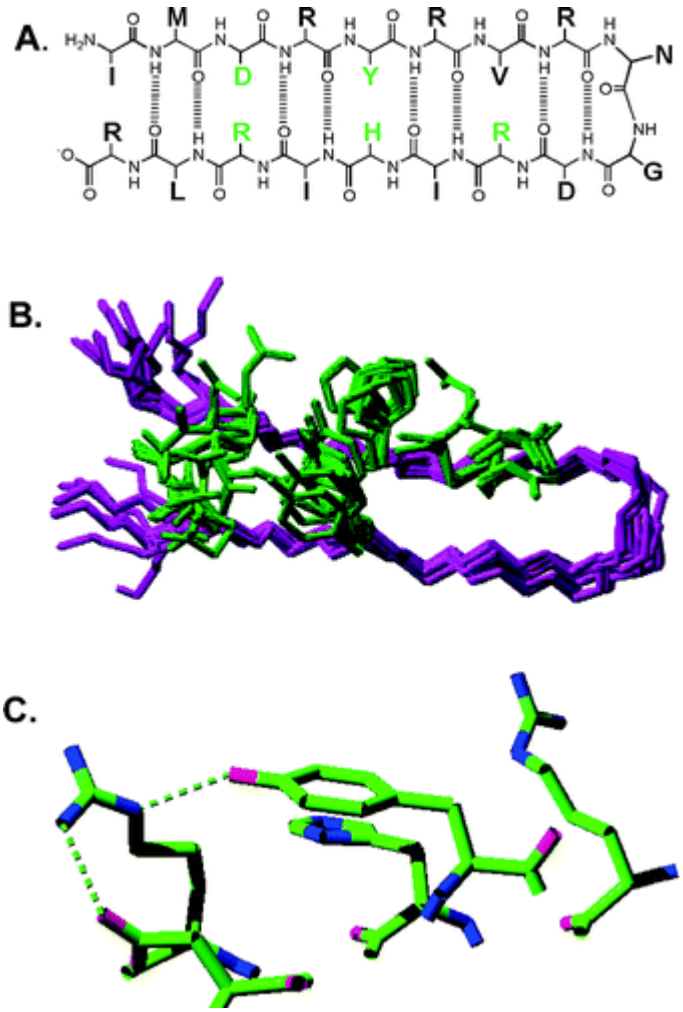


**Figure 2.1.** Structures of peptide A, IMDRYRVRNGDRIHIRLR. **A.**The primary sequence, predicted hydrogen bonds, and predicted cross-strand interactions with tyrosine (green) are shown. **B.** The overlap of the 20 lowest energy structures, as derived from 2-D NMR spectroscopy at pH 5.0, is presented. Only five amino acid side chains (see part A, green) are shown. **C.** Interactions with the tyrosine, Y5, in the averaged, minimized NMR structure are shown. Hydrogen atoms are omitted, and hydrogen bonds are shown as dotted lines.

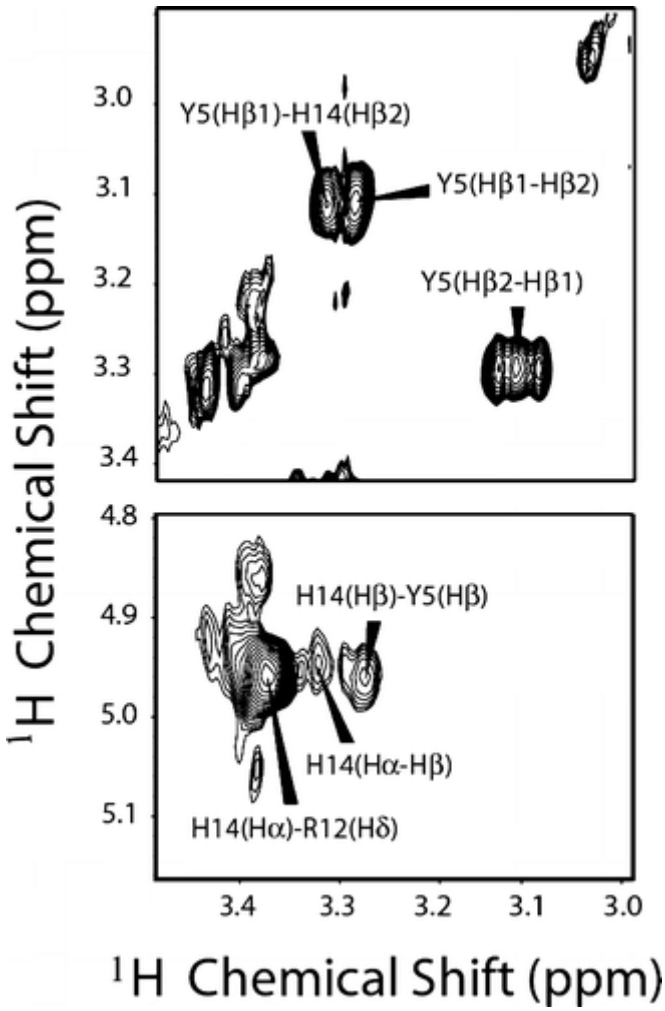


**Figure 2.2**. Portions of the $^{1}H/^{1}H$ ROESY spectrum acquired at 600 MHz showing the inter-strand contacts between Y5 and H14 in peptide A. Dipolar correlations between β-protons (top panel) and between α- and β-protons (bottom panel) of Y5 and H14. See Materials and Methods for experimental conditions.

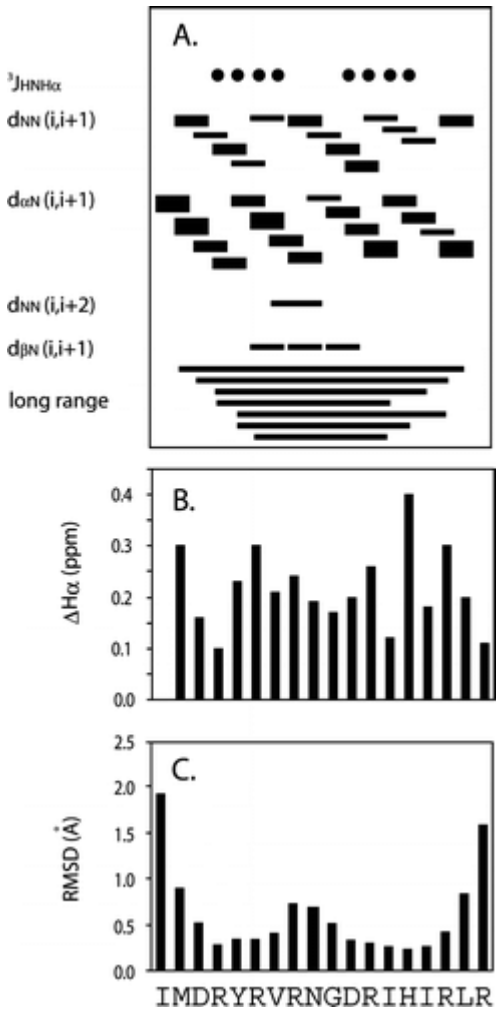


**Figure 2.3.** Summary of the NMR data: **A.** short- and long-range ROEs, **B.** the $H_\alpha$ chemical shift index, and **C.**the root-mean-square deviations of the backbone atoms ($C_\alpha$, NH, C‘) for the conformational ensemble calculated using simulated annealing procedures. See Materials and Methods for more information.

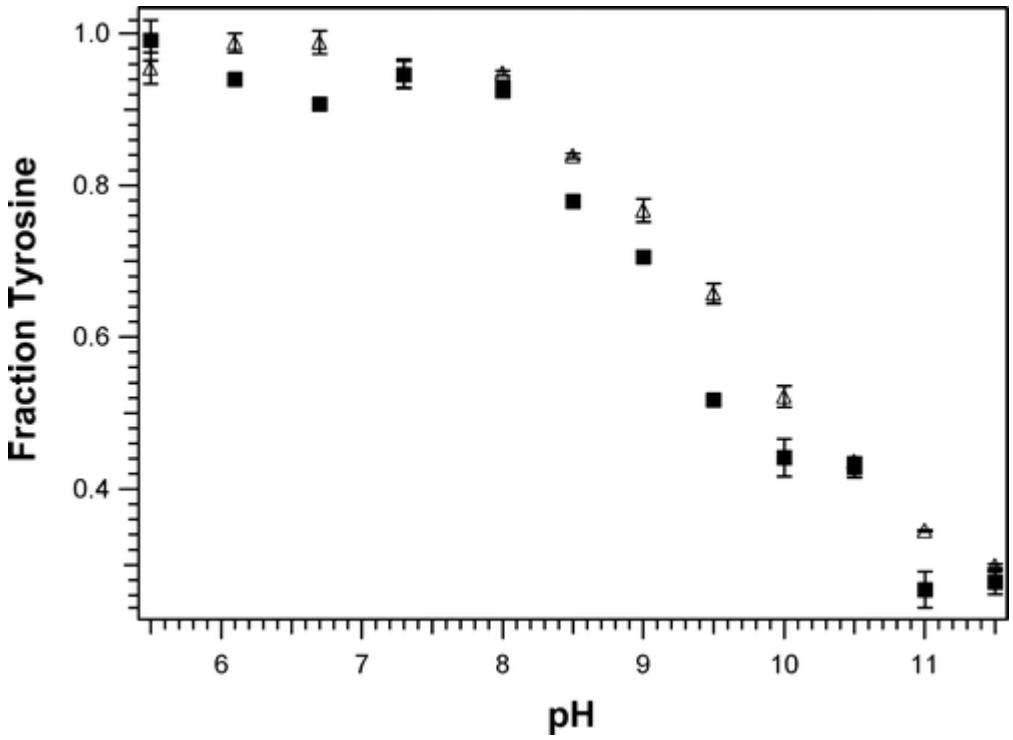


**Figure 2.4.** Optical titration of the peptide A (Δ) and tyrosine solutions (■). Fraction tyrosine is defined as [Tyr]/{[Tyr] + [$TyrO^-$]}. See Materials and Methods for experimental condtions.

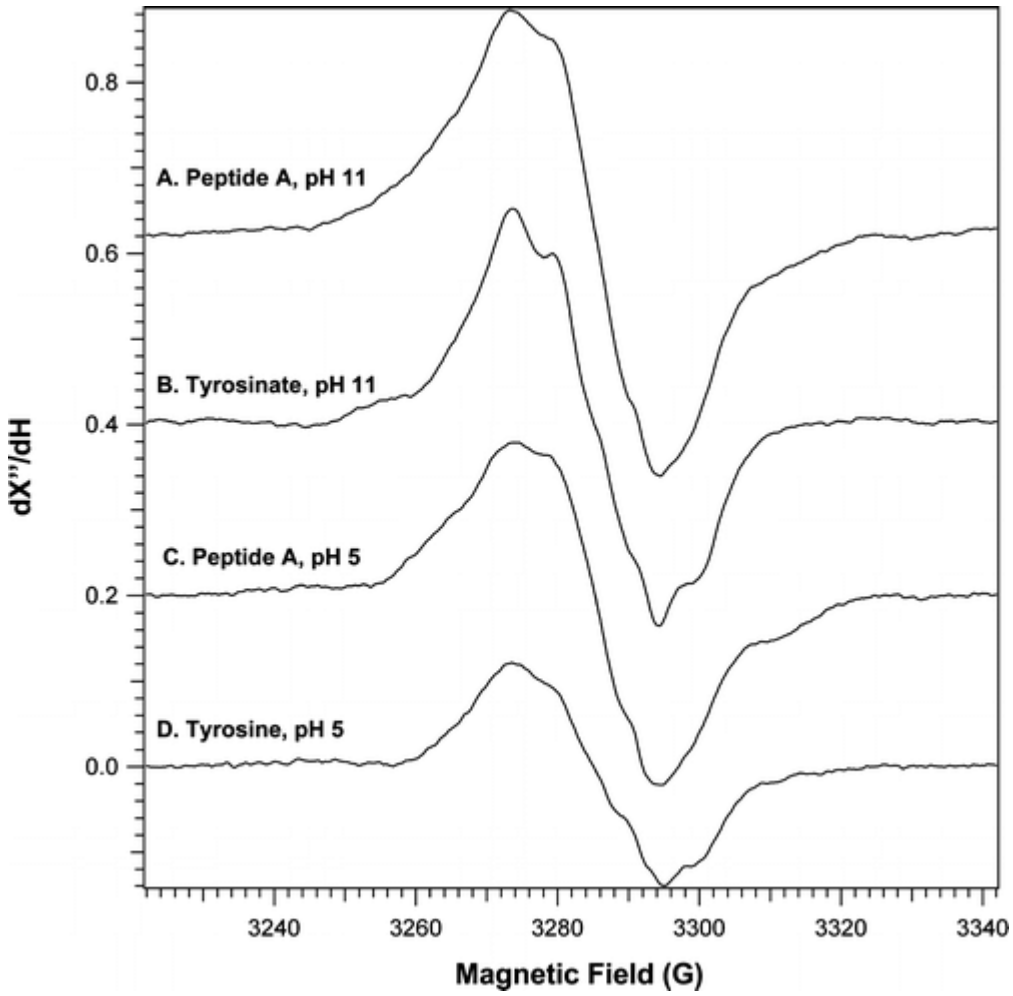


**Figure 2.5.** EPR spectra of tyrosyl radical, generated by UV photolysis, in peptide A at pH 11 **A.** and pH 5 **C.** For comparison, spectra generated from tyrosinate at pH 11 **B.** and from tyrosine at pH 5 **D.** are also shown. Spectral conditions were as follows: microwave frequency, 9.21 GHz; power, 200 μW; modulation amplitude, 3 G; modulation frequency, 100 kHz; time constant, 655.36 ms; conversion time, 163.84 ms; number of scans, 4; temperature, 103 K. See Materials and Methods for experimental conditions.

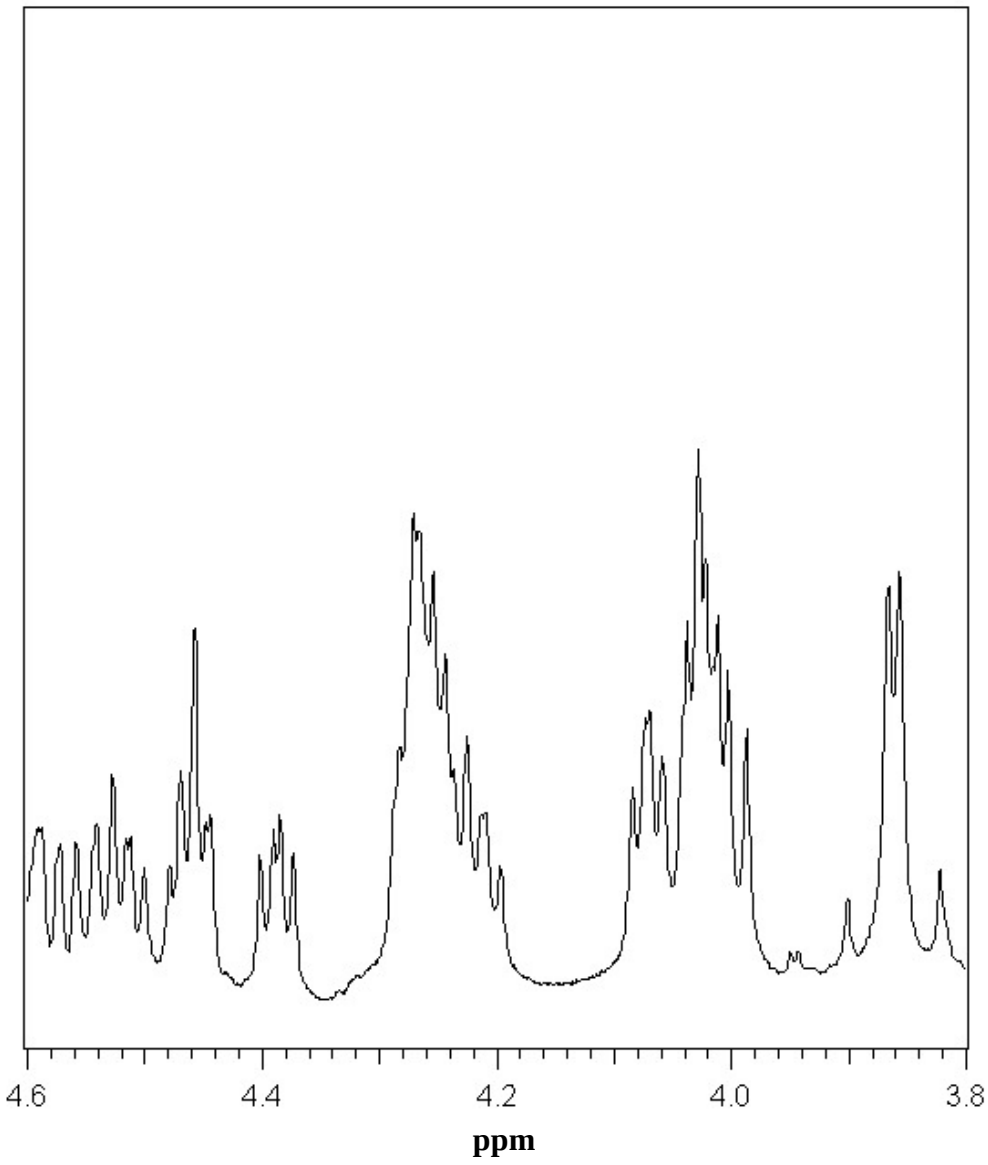


**Figure 2.6.** One-dimensional NMR spectrum of Peptide A at pH 11. The $C_{H\alpha}$ region of the spectrum is shown. The chemical shift dispersion of the 1-D NMR spectrum suggests that peptide A folds at pH 11.

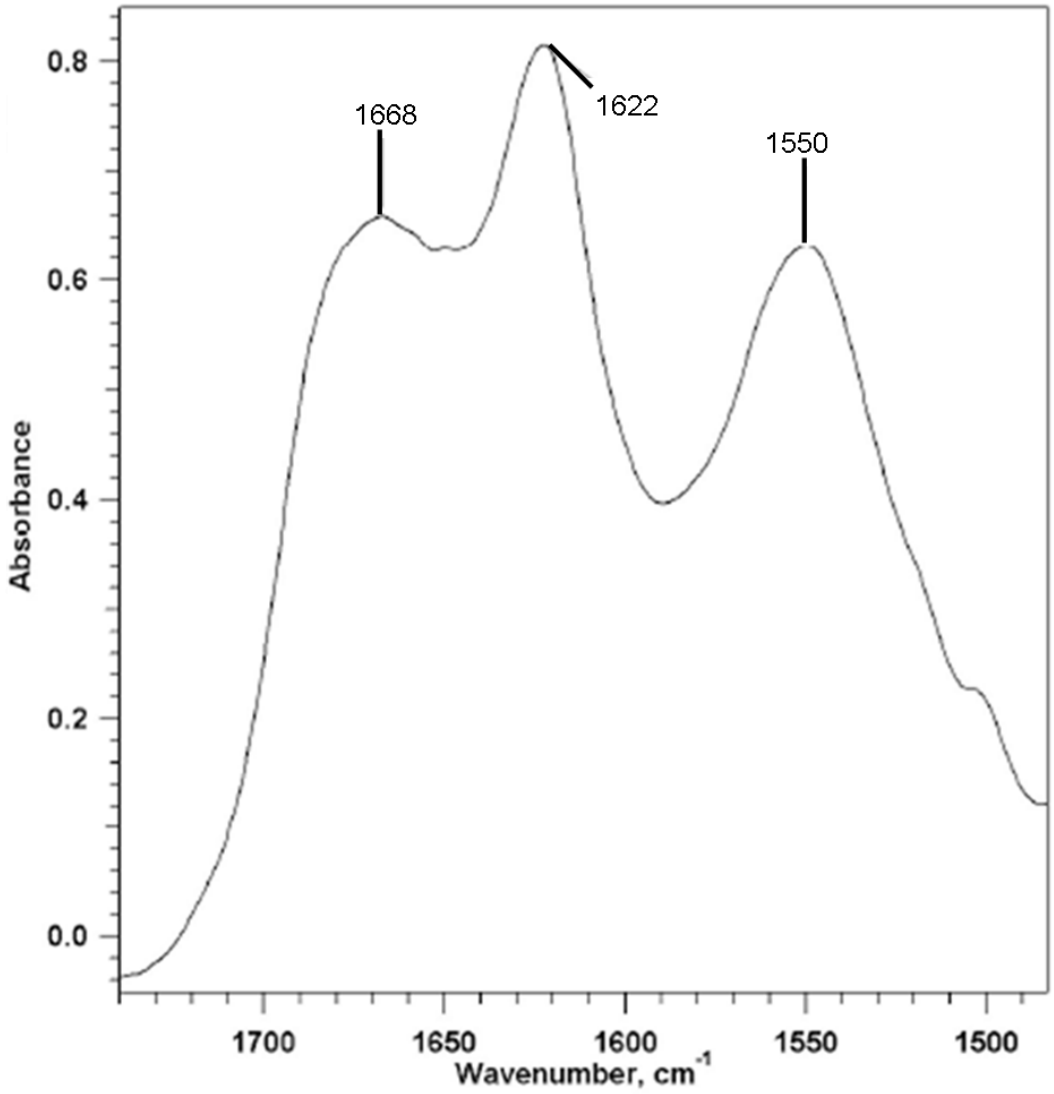


**Figure 2.7.** FT-IR spectrum of peptide A at pH 11. Observation of two bands at 1622 and 1668 $cm^{-1}$ is consistent with significant beta sheet content in the peptide at this pH. See Materials and Methods for experimental conditions.

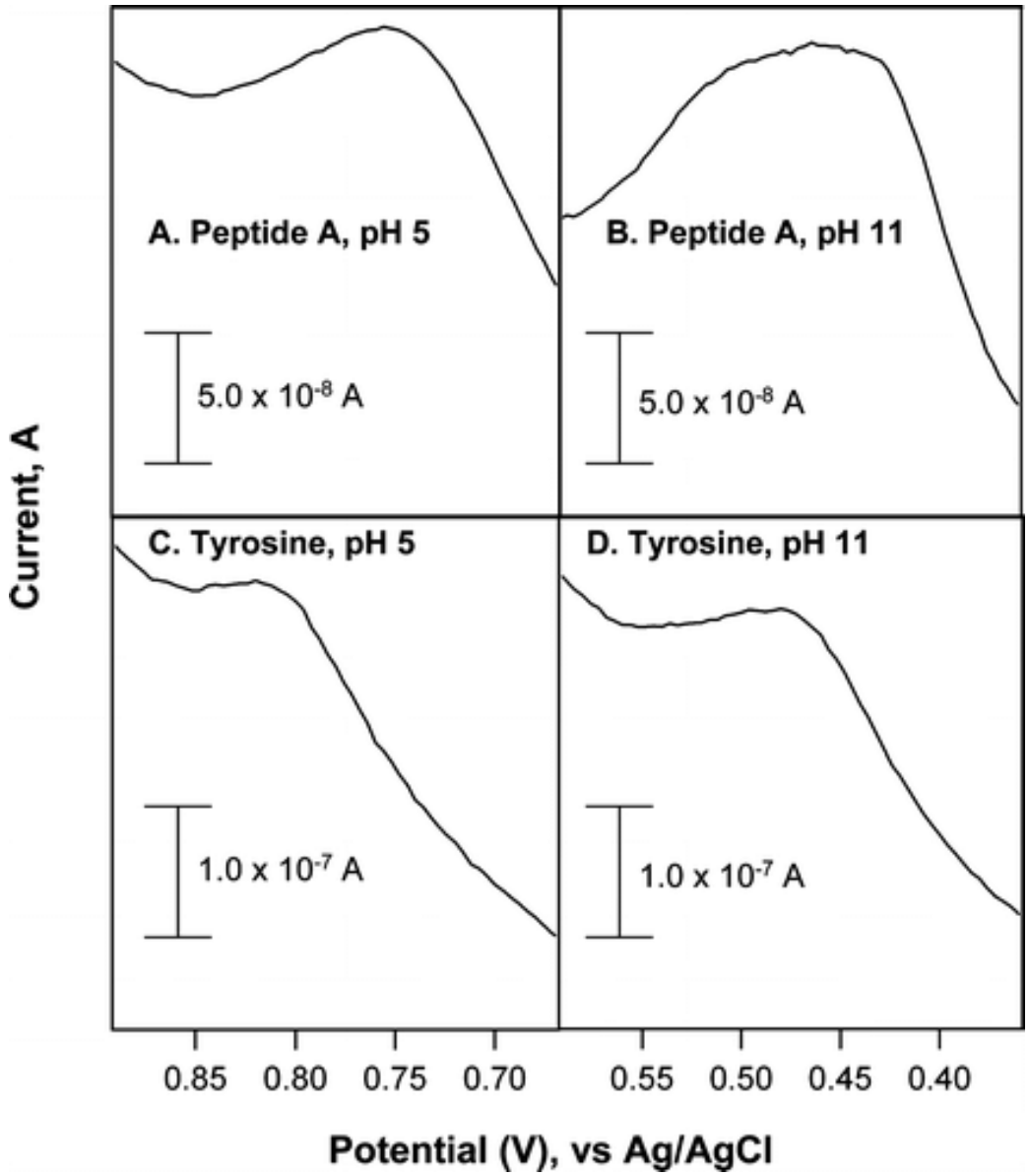


**Figure 2.8.** Square wave voltammetry of tyrosine and peptide A solutions. The anodic current versus applied potential are plotted for tyrosine at pH 5 **C.** and pH 11 **D.** and for peptide A at pH 5 **A.**and pH 11 **B.** For the assignment of peak potentials, see Table 2.1. See Materials and Methods for experimental conditions.

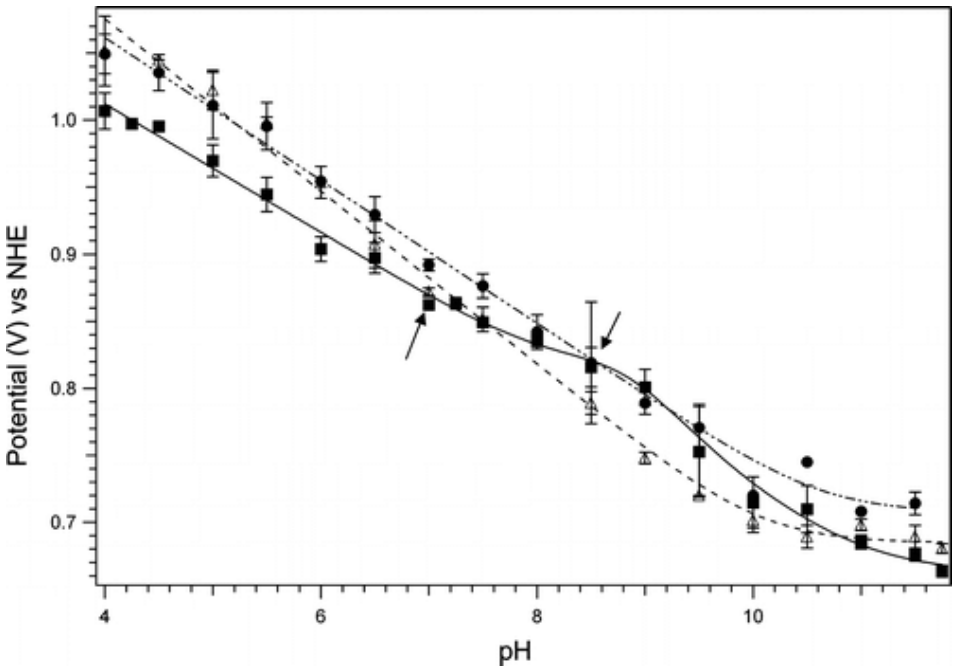


**Figure 2.9.** Effect of pH on the peak potential of the anodic waves, as assessed by square wave voltammetry, for peptide A (■), peptide C (●), and tyrosine solutions (Δ). In some cases, the error bars are smaller than the symbols used to represent the points. Data were fit with equations describing a model in which oxidation is coupled to protonation of one (peptide C, dot-dashed line and tyrosine, dashed line) or three (peptide A, solid line) ionizable groups.[40,41] See the Materials and Methods section for details concerning the fits. As expected, the tyrosine and peptide C data (Δ and ●, respectively) were fit well with a model in which protonation of the tyrosine phenolic oxygen (pK= 0, oxidized state and 10, reduced state) influences the potential (dashed and dot-dashed lines). Peptide A data were fit best with a model in which three ionizable groups influence the potential (solid line). In peptide A (solid line), pK values of 0 (oxidized state) and 10 (reduced state) were attributed to tyr, pK values of 8.0 (oxidized state) and 7.0 (reduced state) were attributed to his, and pK values of 4.5 (oxidized state) and 4.0 (reduced state) were attributed to an aspartic acid. The arrows show inflection points assigned to histidine in peptide A.

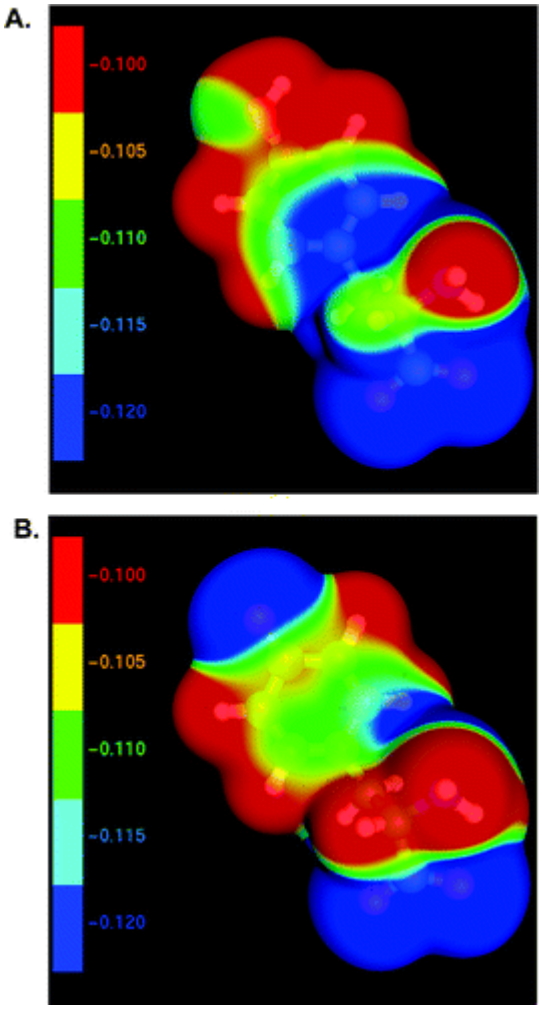


**Figure 2.10.** Electrostatic maps of tyrosine **A.** and the tyrosyl radical **B.** in their anionic forms. The molecules are anionic due to the negative charge on the carboxylate group. The colors correspond to the value of the electrostatic potential in atomic units; red colors are more positive, and blue colors are more negative.

## 2.8 References


1. Barry, B. A.; Einarsdottir, O. *Journal of Physical Chemistry B* **2005**, *109*, 6972-6981.

2. Britt, R. D. In *Oxygenic Photosynthesis: The Light Reactions*; Ort, D. R., Yocum, C. F., Eds.; Kluwer Academic Publisher: Dordrecht, 1996; Vol. 4, pp 137-164.

3. Pujols-Ayala, I.; Barry, B. A. *Biochim. Biophys. Acta* **2004**, *1655*, 205-216.

4. Malkowski, M. G. G., S. L.; Smith, W. L.; Garavito, R. M. *Science* **2000**, *289*, 1933-1937.

5. Stubbe, J.; van Der Donk, W. A. *Chem. Rev.* **1998**, *98*, 705-762.

6. Whittaker, M. M.; Whittaker, J. W. *J. Biol. Chem.* **1990**, *265*, 9610-9613.

7. Barry, B. A.; El-Deeb, M. K.; Sandusky, P. O.; Babcock, G. T. *Journal of Biological Chemistry* **1990**, *265*, 20139-20143.

8. Hulsebosch, R. J.; van der Brink, J. S.; Niewenhuis, S. A. M.; Gast, P.; Raap, J.; Lugtenburg, J.; Hoff, A. J. *Journal of the American Chemical Society* **1997**, *119*, 8685-8694.

9. Vassiliev, I. R.; Offenbacher, A. R.; Barry, B. A. *Journal of Physical Chemistry B* **2005**, *109*, 23077-23085.

10. Dixon, W. T.; Murphy, D. *Journal of the Chemical Society, Faraday Trans. 2* **1976**, *72*, 1221-1229.

11. Rhile, I. J.; Markle, T. F.; Nagao, H.; DiPasquale, A. G.; Lam, O. P.; Lockwood, M. A.; Rotter, K.; Mayer, J. M. *Journal of the American Chemical Society* **2006**, *128*, 6075-6088.

12. Chang, C. J.; Chang, M. C. Y.; Damrauer, N. H.; Nocera, D. G. *Biochimica et Biophysica Acta* **2004**, *1655*, 13-28.

13. Marcus, R. A. *Pure Appl. Chem.* **1997**, *69*, 13-29.

14. Tommos, C. S., J.; Pilloud, D. L.; Wand, A. J.; Dutton, L. P. *Biochemistry* **1999**, *38*, 9495-9507.

15. Di Bilio, A. J.; Crane, B. R.; Wehbi, W. A.; Kiser, C. N.; Abu-Omar, M. M.; Carlos, R. M.; Richards, J. H.; Winkler, J. R.; Gray, H. B. *Journal of the American Chemical Society* **2001**, *123*, 3181-3182.
16. Shifman, J. M.; Moser, C. C.; Kalsbeck, W. A.; Bocian, D. F.; Dutton, P. L. *Biochemistry* **1998**, *37*, 16815-16827.

17. Jones, G., II; Vullev, V.; Braswell, E. H.; Zhu, D. *Journal of the American Chemical Society* **2000**, 1*22*, 388-389.

18. Lombardi, A.; Nastri, F.; Pavone, V. *Chemical Reviews.* **2001**, *101*, 3165-3190.

19. Gibney, B. R.; Huang, S. S.; Skalicky, J. J.; Fuentes, E. J.; Wand, A. J.; Dutton, P. L. *Biochemistry* **2001**, *40*, 10550-10561.

20. Kennedy, M. L.; Gibney, *Journal of the American Chemical Society.* **2002**, *124*, 6826-6827.

21. Discher, B. M.; Noy, D.; Strzalka, J.; Ye, S.; Moser, C. C.; Lear, J. D.; Blasie, J. K.; Dutton, P. L. *Biochemistry* **2005**, *44*, 12329-12343.

22. Cochran, F. V.; Wu, S. P.; Wang, W.; Nanda, V.; Saven, J. G.; Therien, M. J.; DeGrado, W. F. *Journal of the American Chemical Society* **2005**, *127*, 1346-1347.

23. Shearer, J.; Long, L. M. *Inorganic Chemistry.* **2006**, *45*, 2358-2360.

24. Zhuang, J.; Amoroso, J. H.; Kinloch, R.; Dawson, J. H.; Baldwin, M. J.; Gibney, B. R. *Inorganic Chemistry* **2006**, *45*, 4685-4694.

25. Syud, F. A.; Stanger, H. E.; Gelman, S. H. *Journal of the American Chemical Society* **2001**, *123*, 8667-8677.

26. Tatko, C.; Waters, M. L. *Protein Science* **2003**, *12*, 2443-2452.

27. Kumar, A.; Ernst, R. R.; Wuthrich, K. *Biochemical and Biophysical Research Communications* **1980**, *95*, 1-6.

28. Piotto, M.; Saudek, V.; Sklenar, V. *Biomolecular NMR* **1992**, *2*, 661-665.

29. Bax, A.; David, D. G. *J. Magn. Reson.* **1985**, *65*, 355-360.

30. Shaka, A. J.; Lee, C. J.; Pines, A. *Journal of Magnetic Resonance* **1998**, *77*, 274-293.

31. Piantini, U.; Sorensen, O. W.; Ernst, R. R. *Journal of the American Chemical Society* **1982**, *124*, 6800-6801.

32. Rance, M.; Sorensen, O. W.; Bodenhausen, G.; Wagner, G.; Ernst, R. R.; Wuthrich, K. *Biochemical and Biophysical Research Communications* **1983**, *117*, 479-485.

33. Delaglio, F.; Grzesiek, S.; Vuister, G. W.; Zhu, G.; Pheifer, J.; Bax, A. *Journal of Biomolecular NMR* **1995**, *6*, 277-293.

34. Goddard, T. D.; Kneller, D. G. *SPARKY 3*; 1999.

35. Roberts, G. C. K. *NMR of macromolecules: a practical approach*; Oxford University Press: New York, 1993.

36. Brunger, A. T.; Adams, P. D.; Clore, G. M.; DeLano, W. L.; Gros, P.; Grosse-Kunstleve, R. W.; Jiang, J. S.; Kuszewski, J.; Nilges, M.; Pannu, N. S.; Read, R. J.; Rice, L. M.; Simonson, T.; Warren, G. L. *Acta Crystallography, Section D* **1998**, *54*, 905-921.

37. Schwieters, C. D.; Kuszewski, J. J.; Tjandra, N.; Clore, G. M. *Journal of Magnetic Resonance* **2003**, *160*, 65-73.

38. Nilges, M.; Gronenborn, A. M.; Brunger, A. T.; Clore, G. M. *Protein Engineering* **1988**, *2*, 27-38.

39. Laskowski, R. A.; MacArthur, M. W.; Thornton, J. M. *Current Opinion in Structural Biology* **1998**, *8*, 631-639.

40. Clark, W. M. *Oxidation reduction potentials of organic systems*; The Williams and Wilkins Company: Baltimore, MD, 1960.

41. Moore, G. R.; Pettigrew, G. W. *Cytochromes c. Evolutionary, Structural, and Physiochemical Aspects*; Springer-Verlag: Berlin, 1990.

42. Becke, A. D. *Journal of Chemical Physics* **1993**, *98*, 5648-5652.

43. Becke, A. D. *Physical Reviews A* **1988**, *38*, 3098-3100.

44. Lee, C.; Yang, W.; Parr, R. G. *Physical Reviews B* **1988**, *37*, 785-789.

45. Frisch, et al. *Gaussian03*; Gaussian, Inc.: Wallingord, CT, 2004.

46. Range, K.; Ayala, I.; York, D.; Barry, B. A. *Journal of Physical Chemistry* **2006**, *110*, 10970-10981.

47. Frisch, M. J.; Pople, J. A.; Binkley, J. S. *Journal of Chemical Physics* **1984**, *80*, 3265-3269.

48. Frisch, A.; Frisch, M.; Trucks, G. W. *Gaussian03 User's Reference*; Gaussian, Inc.: Wallinford, CT, 2003.

49. Peng, C.; Ayala, P. Y.; Schlegel, H. B.; Frisch, M. J. *Journal of Computational Chemistry* **1996**, *17*, 49-56.

50. Laaksonen, L. *gOpenMol 3.00* (htpp://222/cac.fi/gopenmol/); 2005.

51. Smith, C. K. W. J. M.; Regan, L. *Biochemistry* **1994**, *33*, 5510-5517.

52. Griffiths-Jones, S. R. M. A. J.; Searle, M. S. *Journal of Molecular Biology* **1999**, *292*, 1051-1069.

53. Ciani, B. J. M.; Searle, M. *Journal of the American Chemical Society* **2003**, *125*, 9038-9047.

54. Kiehna, S. E.; Waters, M. L. *Protein Science* **2003**, *12*, 2657-2667.

55. Waters, M. L. *Current Opinions in Chemical Biology* **2002**, *6*, 736-741.

56. Brabec, V.; Mornstein, V. *Biophysical Chemistry* **1980**, *12*, 159-165.

57. Harriman, A. *Journal of Physical Chemistry* **1987**, *91*, 6102-6104.

58. Dean, J. A. *Lange's Handbook of Chemistry*; Mcgraw-Hill Inc.: New York, 1999.

# CHAPTER 3

# CONTROL OF PROTON AND ELECTRON TRANSFER IN DE NOVO DESIGNED, BIOMIMETIC BETA HAIRPINS

[1,2]Robin S. Sibert, [1]Mira Josowicz, and [1,2]Bridgette A. Barry

*[1]Department of Chemistry and Biochemistry and the [2]Petit Institute for Bioengineering and Bioscience, Georgia Institute of Technology, Atlanta, Georgia 30332*

### 3.1 Abstract

Tyrosine side chains are involved in proton coupled electron transfer reactions (PCET) in many complex proteins, including photosystem II (PSII) and ribonucleotide reductase. In particular, PSII contains two redox active tyrosines, which have different protein environments, midpoint potentials, and roles in catalysis. Designed biomimetic peptides provide a tractable system, which can be used to investigate how the protein matrix controls these PCET reactions. In a previous report, PCET reactions were shown to occur between a tyrosine (Tyr 5) and a cross-strand histidine (His 14) in a designed, 18 amino acid beta hairpin peptide. In this peptide, the single tyrosine is hydrogen bonded to an arginine residue, Arg 16, and a second arginine, Arg 12, has a pi-cation interaction with the tyrosine. The effect of these interactions was to lower the midpoint potential of Tyr 5 at low pH values and to cause redox changes in the pK of His14. In this report, four additional peptides are used to characterize the effect of hydrogen bonding and electrostatic interactions on these PCET reactions. Circular dichroism shows that all the sequences form stable beta hairpin peptides, and electron paramagnetic resonance spectroscopy shows that the structural environment of the tyrosyl radical is not significantly altered by most substitutions. Optical titration of the peptides reveals that the pK of tyrosine is not significantly altered by removal of His14 or Arg12. However, substitution at the hydrogen bonding Arg16 decreases the pK of Tyr5 from 9.3$\pm$0.1 to 8.3$\pm$0.1. Electrochemical titration measurements confirm that histidine substitutions eliminate PCET reactions. Removal of Arg 16 or Arg 12 has no effect on PCET, but increases the midpoint potential for tyrosine oxidation by approximately 50 mV at all tested pH values. The effects of arginine substitution are consistent with the change in

midpoint potential, which is observed for the PSII redox-active tyrosine residues. Taken together, the results show that a pi cation interaction, hydrogen bond, and PCET between tyrosine and histidine alter the functional properties of redox active tyrosine residues. In particular, these interactions can contribute equally to the control of midpoint potential and, thereby, reaction rate.

## 3.2 Introduction

Beta hairpins are common secondary structural motifs found in proteins.[1-3] Since the discovery of the first autonomously folding beta hairpin[4] monomeric hairpins have proven to be useful systems in which to quantify the non-covalent interactions involved in protein folding.[5-19] Specifically, NMR studies on model peptides have revealed that aromatic interactions[17,20,21], cation-pi interactions[5,19], and salt bridges[6,20] play significant roles in stabilizing the hairpin structure. Simultaneous incorporation of salt bridges into beta hairpins have been shown to stabilize the hairpin structure by 3.6 kJ/mol.[6] Individual salt bridges contribute 1.2-1.3 kJ/mol to hairpin stability.[6] Aromatic interactions provide 0.2-0.3 kcal/mol (0.8-1.3 kJ/mol) of stabilization to beta hairpins.[20] Elucidation of structural elements, which facilitate beta hairpin formation, has enabled de novo design of biomimetic peptides.[22] These peptides can then serve as simple and functional models of more complex native proteins.[22]

Here, we employ de novo designed beta hairpins to investigate how the protein environment controls tyrosine oxidation in enzymes. A similar approach has been used previously to explore the effect of non-covalent interactions on the redox potential of hemes, iron sulfur clusters, and other metal centers in peptide models.[23-31] Our previous work used a beta hairpin peptide to study electron transfer reactions involving a redox active tyrosine (Figure 3.1A).[32]

Redox active tyrosines are found in several enzymes, including photosystem II[33-39] ribonucleotide reductase,[40-44] prostaglandin synthase[45-48], and galactose oxidase.[46,47,49] In electron transfer in these proteins, the tyrosine side chain is transiently oxidized to form a neutral tyrosyl radical, Tyr●. Because the pK of the phenolic oxygen is

dramatically altered by oxidation[50], redox active tyrosines can participate in proton coupled electron transfer (PCET) reactions in proteins.[51]

Photosystem II (PSII) contains two redox-active tyrosine residues, Tyr 161D1 (TyrZ) and Tyr 160D2 (TyrD).[52,53] Tyr 161D1 (Tyr Z) is located in the D1 polypeptide of PSII (Figure 3.1B). This redox active tyrosine participates in water oxidation by reducing $P_{680}^{+}$ and oxidizing the manganese cluster.[54-57] Tyr 160D2 (TyrD) (Figure 3.1C) is located in the D2 polypeptide of PSII and is not required for oxygen evolution.[55,56,58,59] Tyr 160D2 (TyrD) redox reactions may be involved in the assembly of the manganese cluster.[58,60] Tyr 161D1 (TyrZ) and Tyr 160D2 (TyrD) have midpoint potentials that differ by ~200 mV.[57,61] The radicals have dramatically different decay times. Tyr 161D1● (TyrZ●) has a μs to ms lifetime[62-64], while Tyr 160D2● (TyrD●) has a lifetime on the order of minutes to hours.[65,66] The protein environmental interactions, which give rise to these energetic and kinetic differences, are still not understood.

X-ray crystal structures of PSII have been reported.[67-72] The 2.9 Å crystal structure of cyanobacterial photosystem II shows that the environments of Tyr 161D1 (TyrZ) and Tyr 160D2 (TyrD) differ in the detailed placement of histidine, arginine, and aspartic acid side chains (Figure 3.1B and 3.1C) near the redox active tyrosine. Tyr 161D1 (TyrZ) is predicted to hydrogen bond with His 190D1 and is 5.08 Å from an Asp 170D1-Arg 357CP43 salt bridge. Tyr 161D1 (TyrZ) also may interact electrostatically with a second histidine and aspartic acid residue (Figure 1B). Tyr 160D2 (TyrD) is predicted to form a hydrogen bond with His 189D2 and is 6.95 Å from an Asp 333D2-Arg 180D2 salt bridge. In addition, Tyr 160D2 (TyrD) has a potential pi-cation interaction with a second arginine, Arg 272 of the CP47 subunit at 7.81 Å, and an

electrostatic interaction with a third arginine, Arg 294D2 at 6.48 Å, which are not found in the environment of Tyr 161D1 (TyrZ). Although pi-cation interactions typically occur between amino acids separated by 6 Å or less, some pi-cation interactions occur over distances up to 10 Å.[73]

The electron transfer rate in proteins is responsive to changes in distance and midpoint potential.[74-76] A number of redox active tyrosine model systems have been used to examine how function is controlled by the responsive protein matrix. Studies involving phenol derivatives with pendant bases have shown that hydrogen bonding alters the reduction potential of tyrosine.[77] Tyrosine and tryptophan residues have been linked to ruthenium photosensitizers, which resulted in model complexes for proton-coupled electron transfer from amino acids.[78] In designed helical proteins, the redox potential of tyrosine was found to be modulated by placement in a non-polar environment and by shielding from proton acceptors.[79,80]

In a recent study, we described a beta hairpin peptide, IMDRYRVRNGDRIHRILR (peptide A), in which PCET reactions between Tyr5 and His14 modified the midpoint potential of the single tyrosine residue.[32] In peptide A, Tyr5 is hydrogen bonded to an arginine residue, Arg16, and a second arginine, Arg12, has a possible pi-cation interaction with the tyrosine. Here, we report results obtained from studies of four additional beta hairpin peptides, in which substitutions were made at His14, Arg12, and Arg16. The results show that hydrogen bonding, pi-cation, and PCET interactions alter the midpoint potential of redox active tyrosines. In addition, hydrogen bonding and pi-cation interactions with tyrosine alter the pH range over which PCET reactions occur.

## 3.3 Materials and Methods

*3.3.1 Peptide synthesis.* Peptide A (IMDRYRVRNGDRIHIRLR), peptide B (IMDRYRVRNGDVIRIRLR), peptide C (His14Cha) (IMDRYRVRNGDRI[Cha]IRLR), peptide D (His14Val; Arg12Ala) (IMDRYRVRNGDAIVIRLR), peptide E (Arg16Ile) (IMDRYRVRNGDRIHIILR), and peptide F (Arg12Ile) (IMDRYRVRNGDIIHIRLR) were synthesized by Sigma Genosys (The Woodlands, TX). The peptides were purified to 95% homogeneity by the manufacturer. Mass spectrometry was used to verify the sequence, and the purity was determined by analysis of the reverse phase HPLC chromatogram. The peptides were used without further purification.

*3.3.2 Circular dichroism.* A JASCO J-810 CD spectropolarimeter equipped with a thermostated cell holder was employed. CD samples were prepared to concentrations between 0.1 mM and 0.2 mM in 5 mM acetate buffer at pH 5.0 or 5 mM borate buffer at pH 11.0, and were filtered using Acrodisc® 25 mm syringe filters with 0.45 µm HT Tuffryn membrane prior to data collection. The spectra were collected between 186 nm and 250 nm in 1 mm quartz cells at a scan speed of 50 nm/min.[81,82] Four to twelve scans were averaged to generate each spectrum, and three to five spectra were collected and averaged for each peptide. A baseline was recorded using 5 mM acetate buffer or 5 mM borate buffer, and the baseline was subtracted manually. Spectral conditions were as follows: sensitivity, 100 mdeg; data pitch, 1 nm; scanning mode, continuous; scan speed, 50 nm/min; response time, 1 sec; bandwidth, 1 nm.

*3.3.4 pK determination.* A Hitachi U-3000 spectrophotometer equipped with 1 cm path length cuvettes was employed. The samples were prepared to a concentration of 50

μM and buffered using 10 mM MES-NaOH (pH 5.5), 10 mM HEPES-NaOH (pH 6.0-8.0), 10mM boric acid-NaOH (pH 8.5-9.5) or 10 mM CAPS-NaOH (pH 10.0-11.5). The solutions were filtered using Acrodisc® 25 mm syringe filters with 0.45 μm HT Tuffryn membrane. Backgrounds were recorded at each pH using the appropriate buffer. The optical spectrum was recorded between 200 nm and 350 nm, as a function of pH. Spectral conditions were as follows: slit width, 2.0 nm; scan speed, 120 nm/min. Deprotonation of tyrosine was monitored by measuring the change in absorbance at 295 nm, at which $TyrO^-$ contributes.[83] The 295 nm absorption was corrected for baseline instabilities by subtracting out the absorbance at 330 nm. Data were obtained for two to six different samples and were averaged. Extinction coefficients were calculated for tyrosinate by substituting the pathlength of the cuvettes, the measured absorbance of each sample at pH 11.0, and the sample concentration into Beer's law.

*3.3.5 Electrochemistry.* Square wave voltammetry measurements were performed on a computer-controlled CH instruments, Inc. (Austin, TX) workstation. The experiments were conducted in a three-electrode cell, equipped with a 3 mm glassy carbon working electrode from Bioanalytical Systems, Inc. (West Lafayette, IN), a platinum counter electrode, and a reference electrode (Ag/AgCl in 1 M KCl, E = 0.22 V (NHE)). The sample concentrations were 0.05 mM in 0.2 M KCl and 10 mM sodium acetate-NaOH (pH 4.5-5.5), 10 mM sodium phosphate-NaOH (pH 6.0-7.5), 10 mM boric acid-NaOH (pH 8.0-9.5) or 10 mM CAPS (pH 10.0-11.5). The sample was purged with nitrogen gas during data collection. Oxidation was initiated with a holding time of 2 s at 0.1 V and then scanned up to 1.1 V. Data were collected in increments of $\Delta E = 0.004$ V. The square wave frequency, f, was 5 Hz, and the amplitude, A, of the applied pulse was

0.025 V (scan rate ν = f*A = 125 mV/s). The data were fit to a baseline manually, and the centroid was used to derive the peak potential. Three trials were performed and averaged for each peptide.

*3.3.6 EPR Spectroscopy.* EPR spectra were collected on a Bruker EMX spectrometer equipped with a standard TE cavity (Billerica, MA).[37,84] Spectra were recorded at 108 K using a Wilmad (Buena, NJ) flow-through liquid nitrogen dewar. The samples were prepared to a concentration of 1 mM at pH 5.0 and pH 11.0 in 5 mM sodium phosphate-NaOH (pH 5.0) buffer or 5 mM boric acid-NaOH (pH 11.0) buffer. The radical was generated with a 266 nm photolysis pulse.[37,84] Baseline correction of the spectra was performed using Igor Pro software (Wavemetrics, Lake Oswego, OR). The samples were flashed in the EPR cavity with fifty laser flashes with a pulse energy of 50-60 mJ. Spectral conditions were as follows: microwave frequency, 9.2 GHz; microwave power, 200 μW; modulation amplitude, 3 G; modulation frequency, 100 kHz; scan time, 168 s; number of scans, 4; time constant, 655 ms. Data were obtained for two different samples and were averaged**.** At pH 5.0, the g values for the radicals were, 2.0042 for tyrosine solution, 2.0037 for peptide A, 2.0041 for peptide C (His14Cha), 2.0043 for peptide D (Arg12Ala; His14Val), 2.0037 for peptide E (Arg16Ile), and 2.0043 for peptide F (Arg12Ile). At pH 11.0, the g values for the radicals were, 2.0042 for tyrosine solution, 2.0042 for peptide A, 2.0041 for peptide C (His14Cha), 2.0043 for peptide D (Arg12Ala; His14Val), 2.0043 for peptide E (Arg16Ile), and 2.0044 for peptide F (Arg12Ile). These values are indistinguishable.

## 3.4 Results

*3.4.1 Peptide design.* Figure 3.2 shows the amino acid sequence and predicted cross-strand interactions for peptides A through F. The ProtParam tool was used to compute the physico-chemical properties of the peptides.[85] Sequences were predicted to be stable and soluble in water. The peptides were designed with a net charge of +1 or +2 to ensure solubility and a pI of greater or equal to 11. Each peptide contains a single tyrosine residue, at least one salt bridge,[6,20] a type I' Asn-Gly turn,[8,9] and several amino acids with high propensities for forming beta sheets.[13,14] Peptide A, peptide E (Arg16Ile), and peptide F (Arg12Ile) also contain an aromatic interaction[17,20,21] between Tyr 5 and His 14.

In the NMR structure of peptide A[32], Tyr 5 accepts a hydrogen bond from the ε-NH of Arg 16. The structure also showed a pi-stacked aromatic interaction between Tyr5 and His14 and a possible pi-cation interaction between Tyr5 and Arg 12, which are 7.81 Å apart**.** In peptides C and D, His 14 is replaced by cyclohexylalanine and valine, respectively. This replacement is expected to disrupt PCET. In peptide D, Arg 12 is substituted with Ala. In peptides E and F, Arg 16 and Arg 12 are substituted with Ile to assess the role of the hydrogen bond and pi-cation interaction.

*3.4.2 Peptides A-F form beta hairpin structures*. Circular dichroism (CD) spectropolarimetry was used to verify that peptides C, D, E, and F form beta hairpins in aqueous solution. The CD spectrum of RNase A (Figure 3.3), which contains beta sheet[86] was used as a control. At 20$^{o}$C, the RNase A spectrum exhibits a minimum at 210 nm, which shifts to 200 nm when the temperature is increased to 80$^{o}$C. The minimum shifts

back to 210 nm upon cooling RNase A back to 20$^{o}$C. These results are in agreement with results in the literature.[86]

Figure 4 presents the CD spectra of peptide A (Figure 3.4A), peptide B (R12V; H14R) (Figure 3.4B), peptide C (His14Cha) (Figure 3.4C), peptide D (His14Val; Arg12Ala) (Figure 3.4D), peptide E (Arg16Ile) (Figure 3.4E), and peptide F (Arg12Ile) (Figure 3.4F). These experiments were conducted at pH 5.0, and thermal denaturation experiments were performed on each peptide. Peptide A (Figure 3.4A) served as a folded control, because previous NMR experiments have shown that the peptide is folded at this pH.[32] NMR spectra of peptide B (Figure 3.4B) indicate that it is a random coil; therefore, peptide B served as an unfolded control.

At 20$^{o}$C, the CD spectrum of peptide A (Figure 3.4A) exhibits a minimum at 197 nm. At 80$^{o}$C, the amplitude of the minimum decreases by 7 mdeg and its location shifts slightly to 200 nm. Additionally, a second broad minimum appears at 221 nm when peptide A is heated. The original amplitude and location of the CD minimum of peptide A is regained by cooling the sample back to 20$^{o}$C. The spectra of peptide A also contain an isodichroic point at 207 nm. Thus, peptide A experiences reversible thermal denaturation at pH 5.0. Therefore, the CD data indicate that, as expected, peptide A forms a beta hairpin at pH 5.0.

The CD spectrum of peptide B (Figure 3.4B) displays a shallow minimum at 200 nm at 20$^{o}$C. At 80$^{o}$C, the spectrum exhibits minima at 201 nm and 221 nm. Unlike peptide A, the amplitude of the minimum at 200 nm at 20$^{o}$C is only 2 mdeg larger than the amplitude of the 201 nm minimum at 80$^{o}$C. These results suggest that, as expected, peptide B does not form a beta hairpin at pH 5.0.

At pH 5.0 and 20$^{o}$C, the CD spectra of peptide C (His14Cha) (Figure 3.4C), peptide D (His14Val; Arg12Ala) (Figure 3.4D), peptide E (Arg16Ile) (Figure 3.4E), and peptide F (Arg12Ile) (Figure 3.4F) all display 197 nm minima, which shift to 200 nm upon heating, like peptide A. Also, like peptide A, the spectra of peptides C through F each contain a broad minimum at 221 nm at 80$^{o}$C, and undergo reversible thermal denaturation between 20$^{o}$C and 80$^{o}$C. Thus, the data support the conclusion that peptides C through F form beta hairpin structures at pH 5.0.

CD spectra were also collected for the peptides A, C (His14Cha), D (Arg12Ala; His14Val), E (Arg16Ile), and F (Arg12Ile) at pH 11.0 (Figure 3.5). Peptides A (Figure 3.5A), peptide C (His14Cha) (Figure 3.5B), and peptide D (Arg12Ala; His14Val) (Figure 3.5C) display reversible thermal denaturation between 20$^{o}$C and 80$^{o}$C. These data support the conclusion that peptides A, C (His14Cha), and D (Arg12Ala; His14Val) are stably folded at pH 11.0.

At pH 11.0 and 20$^{o}$C, peptide E (Arg16Ile) displayed a shallow minimum at 199 nm. (Figure 3.5D). Increasing the temperature to 80$^{o}$C decreased the amplitude of the minimum and shifted the minimum to 201 nm. Cooling peptide E (Arg16Ile) back to 20$^{o}$C (post-melt) shifted the minimum back to 199 nm. The spectrum collected at 80$^{o}$C has an isodichroic point with the 20$^{o}$C pre-melt spectrum at 203 nm. This isodichroic point shifts to 208 nm when compared with the 20$^{o}$C post-melt spectrum. These data support the conclusion that peptide E (Arg16Ile) forms a stable beta hairpin structure at pH 11.0.

At 20$^{o}$C, peptide F (Arg12Ile) displayed a shallow minimum at 198 nm at pH 11.0 (Figure 3.5E). Increasing the temperature to 80$^{o}$C increased the amplitude of the

minimum and shifted it to 201 nm. Cooling peptide F (Arg12Ile) back to 20°C (post-melt) shifted the minimum back to 198 nm. However the amplitude of the 20°C post-melt minimum is larger than the amplitude of the 20°C pre-melt minimum. These data support the interpretation that peptide F can adopt a beta hairpin structure at pH 11.0 under some conditions.

*3.4.3 pK determination.* Optical titration curves were used to assess the effect of substitutions on the pK of Tyr 5 in peptides A, C (His14Cha), D (Arg12Ala; His14Val), E (Arg16Ile), and F (Arg12Ile) (Figures 3.6 and Figure 3.7). Tyrosinate and tyrosine are distinguishable in the UV region by the deprotonation-induced red shift of the 270 nm absorption band (Figure 3.6). The deprotonation can be monitored at 295 nm in a titration experiment (Figures 3.6 and 3.7). Table 3.1 gives tyrosinate wavelength maxima and extinction coefficients for the peptides (Table 3.1). To determine the pK of tyrosine in solution and in peptides, we performed a least square fit of the optical titration curves to the Henderson-Hasselbach equation. The data for tyrosine in solution, peptide A, and peptide D (Arg12Ala; His14Val) were fit between pH 4.0 and pH 10.5. Because the concentration of tyrosinate was independent of pH between pH 4.0 and pH 8.0 for these samples, the lowest pH used for peptides C (His14Cha), E (Arg16Ile), and F (Arg12Ile) was pH 5.5 in order to conserve the samples. The data for peptide C (His14Cha) and peptide F (Arg12Ile) were fit between pH 5.5 and 10.5. The data for peptide E (Arg16Ile) was fit between pH 5.5 and pH 10.0. In the titration curve for peptide F (Arg12Ile), the concentration of tyrosinate decreases sharply as the pH increases above pH 10.5. This may be explained by hydrolysis of the peptide above pH 10.5. Therefore, for tyrosine in solution and for peptides A, C (His14Cha), D (Arg12Ala, His14Val), and F (Arg12Ile),

data collected beyond pH 10.5 were not included. For peptide E (Arg16Ile), we included data up to pH 11.0 to show its unique second equivalence point, which is present between pH 10.0 and pH 11.0. The circular dichroism spectra for peptide E (Arg16Ile) at pH 11.0 (Figure 3.5D) indicate an intact beta hairpin at pH 11.0.

**Table 3.1.** Extinction coefficients, wavelength maxima, and pK values for tyrosinate in solution and in beta hairpin peptides[†]

| Sample[a] | $\lambda_{maxTyrO^-}$ (nm) | $\varepsilon_{TyrO^- 295}$ (L mol$^{-1}$cm$^{-1}$) | $pK_D$ | Chi$^2$ |
|---|---|---|---|---|
| Tyrosine | 291.6 | 1664 | 9.8 ± 0.1 | 1.11 x 10$^{-10}$ |
| Peptide A | 295.8 | 1300 | 9.3 ± 0.1 | 1.22 x 10$^{-10}$ |
| Peptide C (H14Cha) | 293.6 | 2146 | 9.4 ± 0.1 | 1.81 x 10$^{-10}$ |
| Peptide D (R12A;H14V) | 293.6 | 1400 | 9.4 ± 0.1 | 5.04 x 10$^{-10}$ |
| Peptide E (R16I) | 293.0 | 3776 | 8.3 ± 0.1 | 3.99 x10$^{-10}$ |
| Peptide F (R12I) | 293.0 | 2911 | 9.6 ± 0.1 | 8.45 x 10$^{-10}$ |

[†]pK values were derived from a least squares fit to the data in Figure 3.7, using the Henderson-Hasselbach equation, $[Tyr\text{-}O^-] = [(10^{pH-pK})*(\text{Total Concentration})]/[1+10^{pH-pK}]$ and Igor Pro software (Wavemetrics, Osewego, OR) The chi$^2$ values were used to evaluate the quality of the fit. The data were fit between pH 5 and 11, except for peptide E, which was fit between pH 5 an 10.

[a]Sequence variations are shown in parentheses.

As a control, the pK of tyrosine in solution was determined and found to be 9.8 ± 0.1 (Table 3.1), which is close to the value of 10.17 ± 0.02 reported in the literature.[83,87] The pK of Tyr 5 in peptide A is 9.3 ± 0.1. The pK values of tyrosine in peptides C (His14Cha), D (Arg12Ala; His14Val), and F (Arg12Ile) are 9.4 ± 0.1, 9.4 ± 0.3, and 9.6 ± 0.1, respectively. These data support our previous conclusion that His14 does not influence the dissociation constant of Tyr 5.[32] They also show that Arg12 does not influence the dissociation constant of Tyr 5. However, the titration curve for peptide E (Arg16Ile), in which the hydrogen bond to Arg 16 is eliminated, (Figure 3.7E) appears to contain two equivalence points. Fitting the low pH transition gave a pK of 8.3 ± 0.1 for the first equivalence point. These data support the conclusion that the hydrogen bond to Arg 16 does alter the proton affinity of the phenolic oxygen. The presence of two pK values in peptide E (Arg16Ile) suggests that high pH values alter non-covalent interactions with Tyr 5.

*3.4.5 Electrochemical titrations.* To analyze the effects of non-covalent interactions on tyrosine oxidation, we performed electrochemical titrations of peptides C through F using square wave voltammetry. The potential for tyrosyl radical formation was plotted versus pH for each sample (Figure 3.8). The side chains of aspartic acid, tyrosine, and histidine have pK values within the pH range of the electrochemical titration. The electrochemical data from the peptides (Figure 3.8) were fit with a Nernst equation in which one or more ionizable groups influence the potential[32], and $chi^2$ values were used to evaluate the quality of the least square fits (Table 3.2). As an example of this procedure, Figure 3.9 and Table 3.3 show the results of fitting peptide F (Arg12Ile) data with one, two, or three ionizable groups. The $chi^2$ value decreases with the inclusion

of more inflection points (Table 3.3). The quality of the fit (Figure 3.9, solid line) improves with the inclusion of three ionizable groups, which are present in the peptide. While the fit illustrated in Figure 3.9C adequately represent the data, the simulation cannot be regarded as a unique fit.

The data for peptide A were fit with the Nernst equation in which three ionizable groups, Asp 3, Tyr 5, and His 14, influence the potential (Figure 3.8, solid lines). In fitting the data from each peptide, the $pK_{red}$ of Tyr was fixed at either 9.8 (tyrosine in solution), 9.4 (peptide A, peptide C (His14Cha), and peptide D (Arg12Ala; His14Val)), 8.3 (peptide E (Arg16Ile)), or 9.6 (peptide F (Arg12Ile)), depending on the pK derived for the corresponding sample by optical titration experiments (Table 3.1). The $pK_{ox}$ of Tyr was fixed at 0.[32,50] The fit to the peptide A data (Figure 3.8, solid lines) predicts inflection points at pH 3.1, 5.6, 6.0, and pH 8.9 (Table 3.3). The inflection points at pH 3.1 and 5.6 are attributed to Asp 3 in the $Tyr^{red}$ and $Tyr^{ox}$ forms of the peptide, respectively (Table 3.3). This result is consistent with a tyrosine-oxidation induced electrostatic perturbation of this amino acid. The inflection points at pH 6.0 and 8.9 are attributed to redox-induced changes in the proton affinity of His 14 in the $Tyr^{red}$ and $Tyr^{ox}$ forms of the peptide, respectively.[32]

**Table 3.2.** Parameters used to fit the electrochemical titration data (Figure 3.8)[†]

| Sample | $E^*$ (V) | S (V/pH) | $Tyr^{ox}$ | $Asp^{ox}$ | $His^{ox}$ | $Tyr^{red}$ | $Asp^{red}$ | $His^{red}$ | $Chi^2$ |
|---|---|---|---|---|---|---|---|---|---|
| Tyrosine[a] | 1.35 | 0.07 | 0.0 | - | - | 9.8 | - | - | $2.25 \times 10^{-3}$ |
| Peptide A[b] | 1.69 | 0.20 | 0.0 | 5.6 | 8.9 | 9.4 | 3.1 | 6.0 | $2.15 \times 10^{-3}$ |
| Peptide C[c] (H14Cha) | 1.29 | 0.06 | 0.0 | 5.8 | - | 9.4 | 4.8 | - | $5.28 \times 10^{-3}$ |
| Peptide D[c] (R12A;H14V) | 1.31 | 0.06 | 0.0 | 6.3 | - | 9.4 | 5.2 | - | $6.57 \times 10^{-3}$ |
| Peptide E[b] (R16I) | 2.05 | 0.24 | 0.0 | 5.2 | 7.3 | 8.3 | 3.5 | 5.8 | $2.96 \times 10^{-3}$ |
| Peptide F[b] (R12I) | 1.91 | 0.19 | 0.0 | 6.7 | 8.9 | 9.6 | 4.6 | 7.1 | $4.59 \times 10^{-3}$ |

[†]Parameters were derived by performing a least squares fit of the data to the Nernst equation using Igor Pro software. The $chi^2$ values were used to evaluate the fits. The pK values reported for $Tyr_{red}$ and $Tyr_{ox}$ were determined from the optical titration data ($Tyr_{red}$) (Figure 3.7 and Table 3.1) and from the literature ($Tyr_{ox}$).[83,87]

[a]The data were fit to the Nernst equation: $E_m = E^* - S \log[\{10^{-pKox} + 10^{-pH}\}/\{10^{-pKred} + 10^{-pH}\}]$, which describes the influence of one ionizable group on the midpoint potential of tyrosine.

[b]The data were fit to the modified Nernst equation: $E_m = E^* - S \log[[(\{10^{-pH}\}^3 + \{10^{-pH}\}^2 * \{10^{-pKox1}\}) + (\{10^{-pH}\} * \{10^{-pKox1}\} *\{10^{-pKox2}\}) + (\{10^{-pKox1}\} * (10^{-pKox2}) * \{10^{-pKox3}\})]/[(\{10^{-pH}\}^3 + \{10^{-pH}\}^2 * \{10^{-pKred1}\}) + (\{10^{-pH}\} * \{10^{-pKred1}\} * \{10^{-pKred2}\}) + (\{10^{-pKred1}\} * (10^{-pKred2}) * \{10^{-pKred3}\})]]$, which describes the influence of three ionizable groups on the midpoint potential of tyrosine.

[c]The data were fit to the modified Nernst equation: $E_m = E^* - S \log[[(\{10^{-pH}\}^2)+(\{10^{-pH}\} * \{10^{-pKox1}\})+(\{10^{-pKox1}\} * \{10^{-pKox2}\})]/[(\{10^{-pH}\}^2)+(\{10^{-pH}\} * \{10^{-pKred1}\})+(\{10^{-pKred1}\} * \{10^{-pKred2}\})]]$, which describes the influence of two ionizable groups on the midpoint potential of tyrosine.

[d]pK values of ionizable groups associated with oxidized tyrosine.

[e]pK values ionizable groups associated with singlet reduced tyrosine.

**Table 3.3.** Parameters used to evaluate fits to the electrochemical data, recorded on peptide F (Arg12Ile) (Figure 3.9)[†]

| # of Ionizable Groups | $E^*$ (V) | S (V/pH) | $Tyr^{ox}$ | $Asp^{ox}$ | $His^{ox}$ | $Tyr^{red}$ | $Asp^{red}$ | $His^{red}$ | $Chi^2$ |
|---|---|---|---|---|---|---|---|---|---|
| One[a] | 1.35 | 0.07 | 0.0 | - | - | 9.6 | - | - | $1.10 \times 10^{-2}$ |
| Two[b] | 1.69 | 0.20 | 0.0 | - | 7.6 | 9.6 | - | 5.6 | $6.15 \times 10^{-3}$ |
| Three[c] | 1.29 | 0.06 | 0.0 | 6.7 | 8.9 | 9.6 | 4.6 | 7.1 | $4.59 \times 10^{-3}$ |

[†]Parameters were derived by performing a least squares fit of the data to the Nernst Equation using Igor software. The $chi^2$ values were used to evaluate the fits. The pK values reported for $Tyr_{red}$ and $Tyr_{ox}$ were determined from the optical titration data) ($Tyr_{red}$) (Figure 3.7 and Table 3.1) and from the literature ($Tyr_{ox}$).[83,87]

[a]The data were fit to the Nernst equation: $E_m = E^* - S \log[\{10^{-pKox} + 10^{-pH}\}/\{10^{-pKred} + 10^{-pH}\}]$, which describes the influence of one ionizable group on the midpoint potential of tyrosine.

[b]The data were fit to the modified Nernst equation: $E_m = E^* - S \log[[(\{10^{-pH}\}^2)+(\{10^{-pH}\} * \{10^{-pKox1}\})+(\{10^{-pKox1}\} * \{10^{-pKox2}\})]/[(\{10^{-pH}\}^2)+(\{10^{-pH}\} * \{10^{-pKred1}\})+(\{10^{-pKred1}\} * \{10^{-pKred2}\})]]$, which describes the influence of two ionizable groups on the midpoint potential of tyrosine.

[c]The data were fit to the modified Nernst equation: $E_m = E^* - S \log[[(\{10^{-pH}\}^3 + \{10^{-pH}\}^2 * \{10^{-pKox1}\}) + (\{10^{-pH}\} * \{10^{-pKox1}\} *\{10^{-pKox2}\}) + (\{10^{-pKox1}\} * (10^{-pKox2}) * \{10^{-pKox3}\})]/[(\{10^{-pH}\}^3 + \{10^{-pH}\}^2 * \{10^{-pKred1}\}) + (\{10^{-pH}\} * \{10^{-pKred1}\} * \{10^{-pKred2}\}) + (\{10^{-pKred1}\} * (10^{-pKred2}) * \{10^{-pKred3}\})]]$, which describes the influence of three ionizable groups on the midpoint potential of tyrosine.

[d]pK values of ionizable groups associated with oxidized tyrosine.

[e]pK values ionizable groups associated with singlet reduced tyrosine.

Previously, we predicted pK values of Tyr 5, Asp 3, and His 14 by fitting the data to linear segments between pH 4.0 and 4.5, pH 4.5 and 7.0, pH 7.0 and 8.0, pH 8.0 and 10.0, and pH 10.0 and pH 11.8.[32] Using that method, the pKs were predicted from the intersections of the linear segments, yielding $pK_{ox}$ values of 0, 4.5, and 8.0 for Tyr 5, Asp 3, and His 14, respectively and $pK_{red}$ values of 10.0, 4.0, and 7.0 for Tyr 5, Asp 3, and His 14, respectively.[32] These results were also consistent with oxidation-induced changes in the pK values of Asp 3 and His 14.[32]

Figure 3.8 presents electrochemical data, acquired from peptide C (His14Cha) (Figure 3.8A), peptide D (Arg12Ala; His14Val) (Figure 3.8B), peptide E (Figure 3.8C), and peptide F (Figure 3.8D). Fits to the data are shown superimposed as the dotted line (Table 3.2). For comparison, electrochemical data derived from peptide A are also shown in each Figure 3.8 panel, with a fit superimposed as a solid line (Table 3.2). As expected, substitution at His 14 in peptide C (His14Cha) (Figure 3.8A) and peptide D (Arg12Ala; His14Val) (Figure 3.8B) eliminates the His 14 inflection points at pH 6.0 and 8.9 (Table 3.2), which are observed in peptide A. Also as expected, the His 14 inflection points are still present in the titration curves for peptide E (Arg16Ile) and peptide F (Arg12Ile), although the range over which the inflection points occur is altered (this alteration is discussed below). This result is consistent with our previous work[32] , which showed that the PCET reactions in peptide A involve His 14 as the proton acceptor. Moreover, removal of His 14 in peptides C (His14Cha) and D (Arg12Ala; His14Val) increases the redox potential at low pH values.

Peptide C (His14Cha) (Figure 3.8A) contains a single amino acid substitution at His 14. Peptide D (Arg12Ala; His14Val) (Figure 3.8B) contains two amino acid

substitutions, one at His 14 and one at Arg 12. In addition to eliminating the PCET reaction, these substitutions in peptide C (His14Cha) and peptide D (Arg12Ala; His14Val) also alter the pK values of Asp 3. The single substitution at His 14 in peptide C (Figure 3.8A) increases the pK of Asp 3 in the $Tyr^{red}$ form (pK change=1.7) (Table 3.2). These two alterations increase the pK of Asp 3 in the $Tyr^{ox}$ (pK change=0.7) and $Tyr^{red}$ (pK change=2.1) forms of the peptide (Table 3.2).

Figure 3.8C presents electrochemical titration data acquired from peptide E (Arg16Ile), in which the hydrogen bond between Arg 16 and Tyr 5 is eliminated. In peptide E (Arg16Ile) (dotted line), a ~50 mV change in midpoint potential is observed at all pH values, when the data are compared to peptide A (solid line). Fits to the data show that the pK of His 14 in the $Tyr^{ox}$ form of peptide E (Arg16Ile) decreases from 8.9 to 7.3 due to the substitution at Arg 16 (Table 3.2). The fits also show that removal of the Arg-Tyr hydrogen bond lowers the pK of His 14 by only 0.2 pK units in the $Tyr^{red}$ form of the peptide (Table 3.2). These modifications are consistent with a decrease in the strength of the Tyr 5-His 14 interaction, perhaps due to a change in the distance between Tyr 5 and His 14. Table 3.2 also shows that the pK values for Asp 3 in the $Tyr^{ox}$ and $Tyr^{red}$ forms are not significantly altered (pK change is less than 0.5) by substitution at Arg 16. In peptide A, Asp 3 accepts a hydrogen bond from Arg 16. Insensitivity of the Asp 3 pK to Arg 16 substitution in peptide E indicates that Asp 3 accepts a hydrogen bond from Tyr 5 when Arg 16 is removed.

Figure 3.8D presents electrochemical titration data of peptide F (Arg12Ile) (dotted line), in which the putative pi-cation interaction between Arg 12 and Tyr 5 has been eliminated. The data show inflection points similar to those observed in peptide A (solid

line). In peptide F (Arg12Ile) (dotted line), a ~50 mV change in midpoint potential is observed at all pH values, when the data are compared to peptide A (solid line). Substitution at Arg 12 significantly increases the pK of Asp in the $Tyr^{ox}$ and $Tyr^{red}$ forms of the peptide (Table 3.2). This result is consistent with a change in the strength of the Asp 3-Arg 12 hydrogen bond upon removal of the Tyr 5-Arg 12 pi-cation interaction. The pK of histidine in the $Tyr^{red}$ form is also increased, but the pK of His in the $Tyr^{ox}$ form is not affected.

*3.4.6 EPR spectroscopy.* A tyrosyl radical can be generated in tyrosine solutions and in the beta hairpin peptides by UV photolysis.[34-36] The resulting neutral radical has electron spin density on the 1', 3', and 5' carbon atoms of the aromatic ring and on the phenolic oxygen.[34,89,90] Changes in the electron spin density distribution and in the conformation at the Cβ-C1' dihedral angle can also be detected as changes in EPR lineshape.[34,89]

Figures 3.10A and 3.11A presents the EPR spectrum of the tyrosyl radical in tyrosine solution (black) and peptide A (red spectrum) at pH 5.0 and 11.0, respectively. As expected, tyrosine solutions exhibit an EPR spectrum with a g value of 2.0042, an overall splitting of ~20 G, and partially resolved hyperfine splittings.[89] Small changes in EPR lineshape, when peptide A and tyrosine solution are compared, are most likely due to the different tyrosyl radical conformation in the peptide.[32,89] In tyrosine solution the EPR spectrum of the tyrosyl radical exhibits small pH-induced changes (Figure 3.12A). In peptide A, however, no significant alterations in the radical spectrum is observed between pH 5.0 and pH 11.0 (Figure 3.12B). This result is consistent with the conclusion that the immediate environment of the tyrosyl radical is not modified by pH changes.

Peptide C (His14Cha) (Figures 3.10B and 3.11B, black), peptide D (Arg12Ala; His14Val) (Figures 3.10C and 3.11C, black), and peptide F (Arg12Ile) (Figures 3.10E and 3.11E, black) exhibit tyrosyl radical spectra, which are similar to peptide A (each panel, red) both at pH 5.0 (Figure 3.10) and at pH 11.0 (Figure 3.11). Again, no significant changes in EPR lineshape are observed with pH change (Figure 3.12C, D, and F), suggesting that the structure of the peptide near the tyrosyl radical is pH independent. This result demonstrates that His 14 and Arg 12 substitutions have no significant influence on the conformation of the peptide tyrosyl radical or its spin density distribution at either pH value.

Figure 3.10D (black) and 3.11D (black) present the EPR spectrum of tyrosyl radical in peptide E (Arg16Ile), in which the hydrogen bond between the tyrosyl radical and Arg 16 is eliminated. This substitution slightly alters the EPR lineshape, compared to peptide A (red), at pH 5.0 (Figure 3.10D, black), but has no significant impact at pH 11.0 (Figure 3.11D, black). The spectral change can be observed in a comparison of the EPR data at the two pH values (Figure 3.12E), in which increased amplitude is observed at g=2 at pH 5.0 (red). This result suggests that tyrosyl radical conformation may be slightly pH dependent in this peptide[91], perhaps because the stabilizing hydrogen bond has been eliminated, and a new hydrogen bond has been formed.

## 3.5 Discussion

*3.5.1 Structural characterization of beta hairpin peptides.* We have designed four 18-mer polypeptides, in which we have investigated the effect of non-covalent interactions on tyrosine redox properties. Circular dichroism was used to verify that the

peptides form beta hairpins in aqueous solution at pH 5.0. CD data of peptides C through F exhibited a minimum at 197 nm at pH 5.0 and 20°C. This is unusual because beta sheets in proteins commonly exhibit a CD minimum at 210 nm[92-94], while random coils yield a minimum near 200 nm.[92] However, it is common for monomeric beta hairpins to exhibit atypical CD spectral features.[93] In fact, circular dichroism of beta hairpins is known to be complicated by factors including the presence of aromatic amino acids in the peptide sequence and twisting of the hairpin structure.[92-94] Indeed, peptides C through F all contain one or two aromatic amino acids. To determine if twisting of the beta hairpins may contribute to the CD spectra of peptides C through F, we compared their CD spectra with the spectrum generated by peptide A. The NMR structure of peptide A confirms that this peptide adopts a twisted beta hairpin conformation at pH 5.0.[32] The CD spectrum of peptide A also exhibits a well defined minimum at 197 nm, suggesting that peptides C through F form twisted beta hairpins at pH 5.0.

Thermal denaturation experiments were performed to gain additional support for folding of peptides C through F. As expected, peptides A, all exhibited reversible thermal denaturation between 20°C and 80°C at pH 5.0. This result is unlikely to occur in un-ordered or random coil peptides. Moreover, the CD spectra of peptides A, C (His14Cha), D (Arg12Ala; His14Val), E (Arg16Ile), and F (Arg12Ile) between 20°C and 80°C each contained an isodichroic point at 207 nm. An isodichroic point is indicative of a two-state folding transition.[95,96]

To determine the pH dependence of beta hairpin formation in peptides A through F, CD spectra were also collected at pH 11.0. Similar to the results at pH 5.0, all of the peptides displayed a CD minimum at 198 nm or at 199 nm at pH 11.0 and 20°C. Peptides

A, C (His14Cha), D (Arg12Ala; His14Val), and E (Arg16Ile) also exhibited reversible thermal denaturation with isodichroic points at 203 nm or 208 nm. Conversely, for peptide F (Arg12Ile) the amplitude of the 20$^{o}$C post-melt spectrum was larger than the amplitude of the 20$^{o}$C pre-melt spectrum.

Taken together, the CD data support the conclusion that peptides A, C (His14Cha), D (Arg12Ala; His14Val) and E (Arg16Ile) form stable beta hairpin structures at pH 5.0 and at pH 11.0. Peptide F (Arg16Ile) also forms a stable beta hairpin at pH 5.0. However, because alterations in the data are observed after thermal denaturation, we conclude that peptide F (Arg16Ile) can form a beta hairpin at pH 11.0 under some conditions. The fact that electrochemical and EPR data from this peptide are well behaved at pH 11.0 also supports this conclusion. This conclusion may also explain why the optical data for peptide F (Arg12Ile) show a dramatic decrease in the concentration of tyrosinate at pH 11.0, since the light source may cause temperature-dependent changes in the conformation of peptide F (Arg12Ile).

*3.5.2 Substitutions at His14 eliminate PCET reactions.* Peptides in which substitutions are made at His 14 eliminate inflection points in the electrochemical titration data. This observation is consistent with our previous conclusion that oxidation of Tyr 5 in peptide A is thermodynamically coupled with PCET to this histidine.[32] Because the pK of His 14 increases with tyrosine oxidation, protonation of histidine will occur between pH 6 and 9 when the tyrosine is oxidized. This oxidation-induced protonation of His 14 is an example of a PCET reaction, in which the electron goes to one acceptor (solvent) and the proton goes to a second acceptor, the imidazole ring.

Our electrochemical data show that the effect of histidine protonation is to decrease the midpoint potential of the tyrosine at low pH values. This has been previously attributed to electrostatic stabilization of electron density on the phenolic oxygen[32] in the tyrosyl radical. Because Tyr 5 and His 14 are not hydrogen bonded, the PCET reaction likely occurs through a network of water molecules between Tyr 5 and His 14.

*3.5.3 Hydrogen bonding controls the conformation of Tyr 5.* The NMR structure of peptide A shows that Tyr 5 accepts a hydrogen bond from Arg 16.[32] The effect of the Tyr 5-Arg 16 hydrogen bond on the structure of the tyrosyl radical was examined by comparing the optical titration and EPR data for peptide E (Arg16Ile) with the data for peptides A, C (His14Cha), D (Arg12Ala; His14Val), and F (Arg12Ile). Similarities between the optical titration data and the EPR spectra of peptides A, C (His14Cha), D (Arg12Ala; His14Val), and F (Arg12Ile) suggest that the Tyr 5-Arg 16 hydrogen bond persists in these peptides, despite removal of His 14 (peptide C and peptide D) or Arg 12 (peptide D and peptide F). When the Tyr 5-Arg 16 hydrogen bond is eliminated in peptide E, however, the optical titration curve displays two equivalence points which indicate pK values of 8.3 and ~10.5 for Tyr 5. Moreover, the EPR spectrum of peptide E (Arg16Ile) is similar to the spectrum of peptide A at pH 11.0, but displays an increase in amplitude at g=2 at pH 5.0. The similarities between the spectra of peptide E and peptide A at pH 11.0 are explained by the fact that Tyr 5 accepts a hydrogen bond from Arg 16 in peptide A and can still accept a hydrogen bond from an arginine residue (Arg 12) in peptide E (Arg16Ile). The increased amplitude of the EPR spectrum at g=2 (pH 5.0) for peptide E (Arg16Ile) is attributed to formation of a new hydrogen bond upon removal of

Arg 16. In fact, Tyr 5 can donate a hydrogen bond to Asp 3 in peptide E (Arg16Ile). The fit for the electrochemical titration curve of peptide E (Arg16Ile) predicted that the pK of Asp 3 in the $Tyr^{ox}$ and the $Tyr^{red}$ form of peptide E (Arg16Ile) is unperturbed by removal of Arg 16. Because Asp 3 accepts a hydrogen bond from Arg 16 in peptide A, this result suggests that Asp 3 still accepts a hydrogen bond from a nearby amino acid in peptide E (Arg16Ile). This nearby amino acid is most likely Tyr 5. Thus, in peptide A, the hydrogen bond with Arg 16 restricts the conformation of Tyr 5. Removal of the Tyr 5-Arg 16 hydrogen bond releases this restriction so that Tyr 5 can donate a hydrogen bond to Asp 3 at pH 5.0 and accept a hydrogen bond from Arg12 at pH 11.0 via pH dependent rotation about its Cα-Cβ bond.

*3.5.4 Substitutions at Arg16 increase tyrosine midpoint potential and alter the pH range over which PCET reactions occur.* Elimination of the hydrogen bond between Arg 16 and Tyr 5 gives a 50 mV increase in potential at all examined pH values. The NMR structure of peptide A shows that Tyr 5 is hydrogen bonded as the proton acceptor. The observed increase in potential can be rationalized because oxidation of tyrosine has been shown to result in the migration of electron density to the phenolic oxygen of the radical. The effect on midpoint potential in peptide E (Arg16Ile) is consistent with stabilization of electron density on the tyrosyl radical phenolic oxygen through the Arg 16-Tyr 5 hydrogen bond.[32] These data suggest that hydrogen bonds to redox active tyrosines can decrease the tyrosine midpoint potential, as predicted from model compound studies.[77] As previously stated, substitution at Arg 16 does not alter the pK of Asp 3 in the oxidized or reduced state of peptide E (Arg16Ile), probably because in peptide E (Arg16Ile) Asp 3 accepts a hydrogen bond from Tyr 5 at low pH values. Therefore, another explanation for

the increased midpoint potential is that interaction with the negatively charged Asp 3 destabilizes the electron density on the tyrosyl radical. At high pH values the EPR data suggest that Tyr 5 accepts a hydrogen bond from Asp 12 in peptide E (Arg16Ile), yet the midpoint potential of Tyr 5 is still ~50 mV higher in peptide E (Arg16Ile) than in peptide A. This increased midpoint potential is thus attributed to a decrease in the strength of the Tyr 5-His 14 aromatic interaction that results from rotation of Tyr 5 about its Cα-Cβ bond. Indeed, the pK of His 14 in the $Tyr^{ox}$ form of peptide E (Arg16Ile) decreases by 1.6 units compared to peptide A.

*3.5.5 Substitutions at Arg12 increase tyrosine midpoint potential and alter the pH range over which PCET reactions occur*. The NMR structure of peptide A suggests that Arg12 and Tyr 5 have a pi-cation interaction. Elimination of the putative electrostatic interaction between Arg12 and Tyr 5 (peptide F (Arg12Ile)) gave a 50 mV increase in potential at all examined pH values. The observed increase in potential can be rationalized as destabilization of electron density on the tyrosyl radical phenolic oxygen by removal of the pi-cation interaction. These data suggest that pi-cation interactions with redox active tyrosines can decrease tyrosine midpoint potential in enzymes.

Peptide F (Arg12Ile) also exhibited increases in the pK of Asp in both the $Tyr^{ox}$ and $Tyr^{red}$ forms. The pK of histidine in the $Tyr^{red}$ form increased, but there was no effect on His pK in the $Tyr^{ox}$ form. The effect on the His 14 pK in the $Tyr^{red}$ form suggests that a pi-cation interaction with tyrosine can alter the pH range over which PCET reactions occur in enzymes. The alterations in Asp 3 pK values may be due to small changes in the Arg 16/Asp 3 salt bridge distance when a substitution is made at Arg 12. Peptide D (Arg12Ala; His14Val), which contains two amino acid substitutions, one at His14 and

one at Arg 12, also showed increases in the pK of Asp 3 in both the $Tyr^{ox}$ and $Tyr^{red}$ form. These alterations in Asp 3 pK values may also be due to small changes in the Arg 16/Asp 3 salt bridge distance.

*3.5.6 Comparison with PSII tyrosyl radicals.* PSII contains two redox active tyrosines, Tyr 161D1 (TyrZ) (Figure 3.1B) and Tyr 160D2 (Tyr D) (Figure 3.1C). The midpoint potential of TyrZ[57] is ~200 mV higher than the potential of TyrD.[57] Both tyrosines are predicted to hydrogen bond to histidine.[67-69,71,72] Therefore, the detailed placement of other amino acids in the protein environment must account for the observed potential difference. Figure 3.1B and C show that the placement of arginine residues may contribute to functional differences between the two redox active tyrosines. For TyrZ (Figure 3.1B) Arg 357 in the CP43 subunit is 7.58 Å away. For TyrD (Figure 3.1C), Arg180 in the D2 polypeptide is 6.95 Å away, a second arginine, Arg 272 in the CP47 subunit, is located 7.81 Å away, and a third arginine, Arg 294 in the D2 polypeptide is located at 6.48 Å. Near TyrZ, Arg 357 has a salt bridge interaction with Asp 170 in the D1 polypeptide, and, near TyrD, Arg 180 has a salt bridge interaction with Asp 333 in the D1 polypeptide. However, the arginine from the CP47 subunit (Arg 272), located near TyrD, may have a pi-cation interaction with the tyrosyl radical. The distance between TyrD and Arg 272 is 7.81 Å. In other proteins, pi-cation interactions occur over distances as long as 10 Å with most pi-cation pairs separated by 6 Å or less.[73] Such a pi cation interaction would be expected to contribute ~13 mV[33] to the decrease in potential observed when TyrD and TyrZ are compared, though calculations from one study suggest that the pi-cation interaction increases the midpoint potential of a tryptophanyl radical

cation.[97] The effect of pi-cation interactions on the midpoint potential of aromatic radicals may thus be context dependent.

### 3.6 Summary

Our studies of beta hairpin peptides provide a model for PCET reactions in proteins. In beta hairpin peptide A, proton transfer occurs to a cross strand histidine when tyrosine is oxidized. The tyrosine and histidine are not directly hydrogen bonded, but PCET can occur through bridging solvent. A hydrogen bond to tyrosine or a pi-cation interaction with tyrosine cause pH-independent decreases in midpoint potential. Pi-cation and hydrogen bonding interactions also alter the pH range over which PCET reactions occur. Moreover, hydrogen bonding controls the conformation of tyrosine. Protonation of the histidine, the pi-cation interaction, and the hydrogen bond contribute approximately equally to the alteration in midpoint potential.

### 3.7 Acknowledgments

The authors thank Dr. Nicholas Hud and the members of his lab for use of the circular dichroism spectropolarimeter, and NIH GM 43273 (B.A.B).

### 3.8 Figures

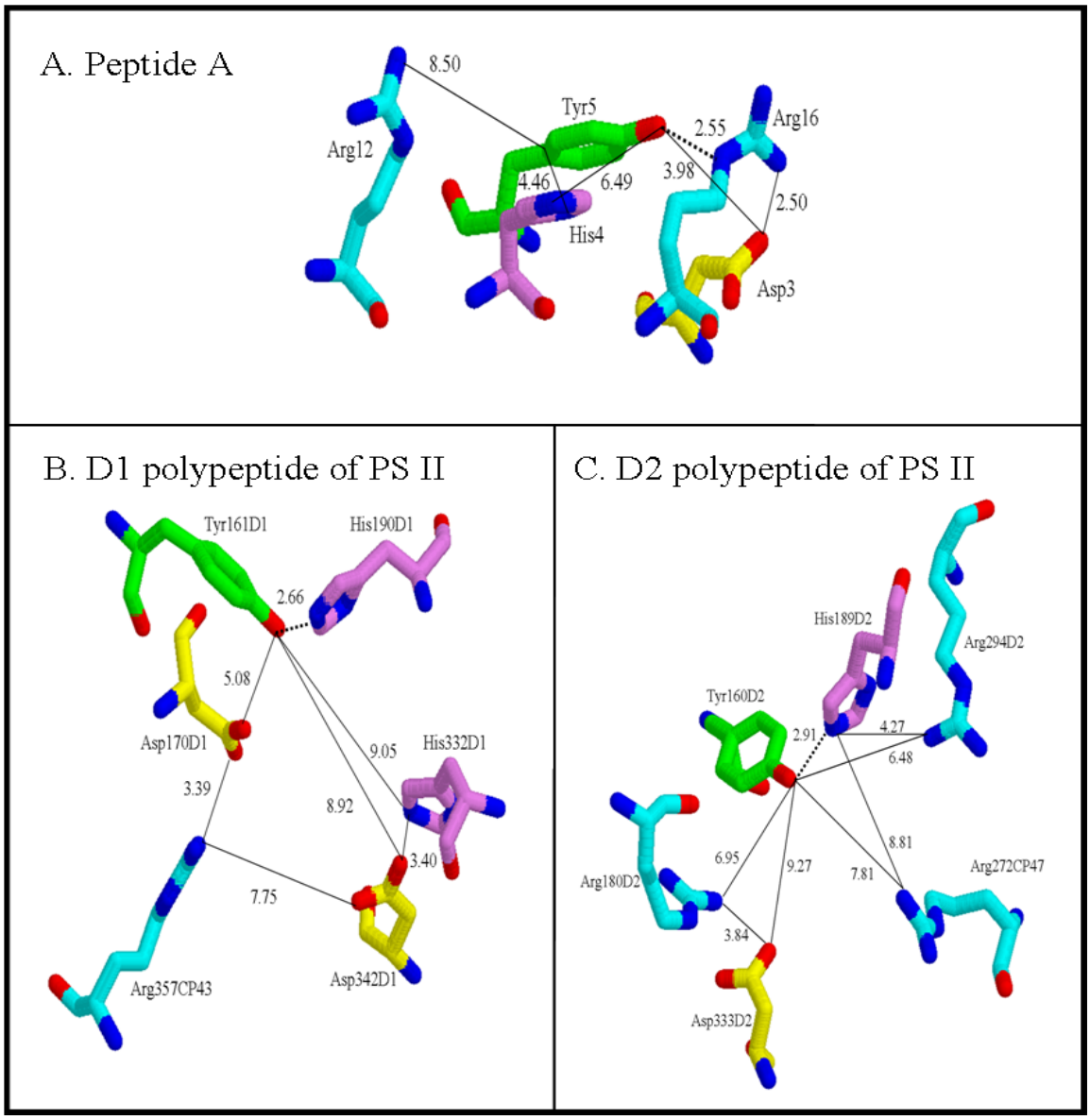


**Figure 3.1.** Environment of redox-active tyrosines in peptide A and in PSII. **A.** shows Tyr 5 in peptide A[32], **B.** shows Tyr 161D1 (TyrZ) in PSII[68], PDB ID 3BZ1 and **C.** shows Tyr 160D2 (TyrD) in PSII47, PDB ID 3BZ1. The solid lines indicate distances between tyrosine and neighboring amino acids, and the dotted lines represent hydrogen bonds. The RasMol molecular visualization tool was used to depict histidine (violet), arginine (cyan), and aspartic acid (yellow) residues within 10.0 Å of the tyrosine (green).

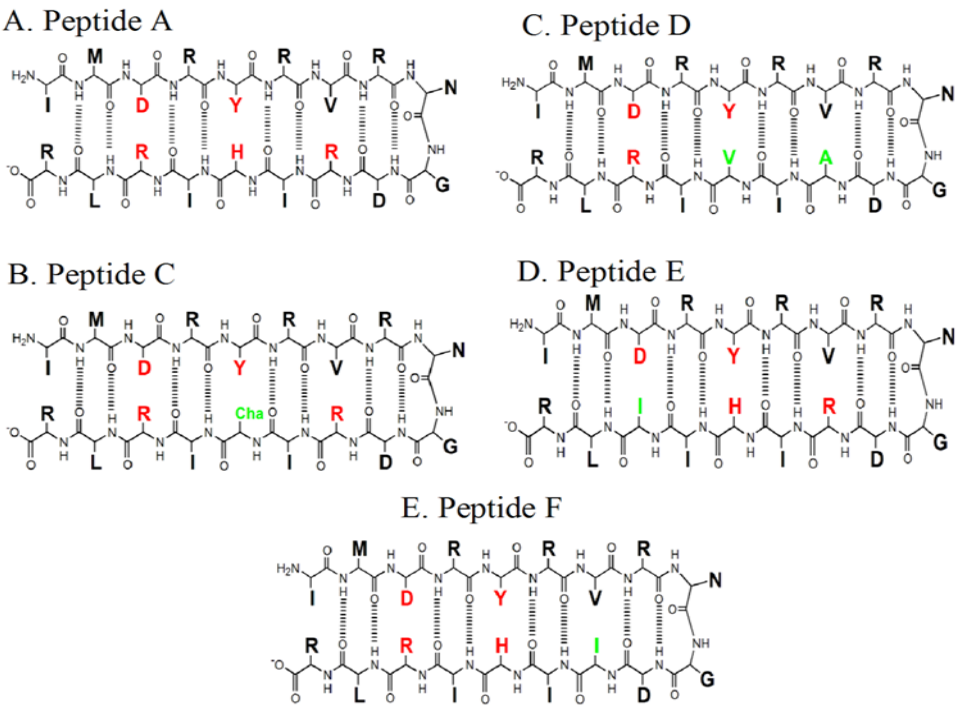


**Figure 3.2.** Predicted structures and cross strand interactions for beta hairpin peptides. In peptide A, tyrosine and interacting residues are shown in red. Sequence alterations are shown in green in peptides C through F. The sequence of peptide B (IMDRYRVRNGDRIVIRLR) is not shown because it is an unfolded control sequence.

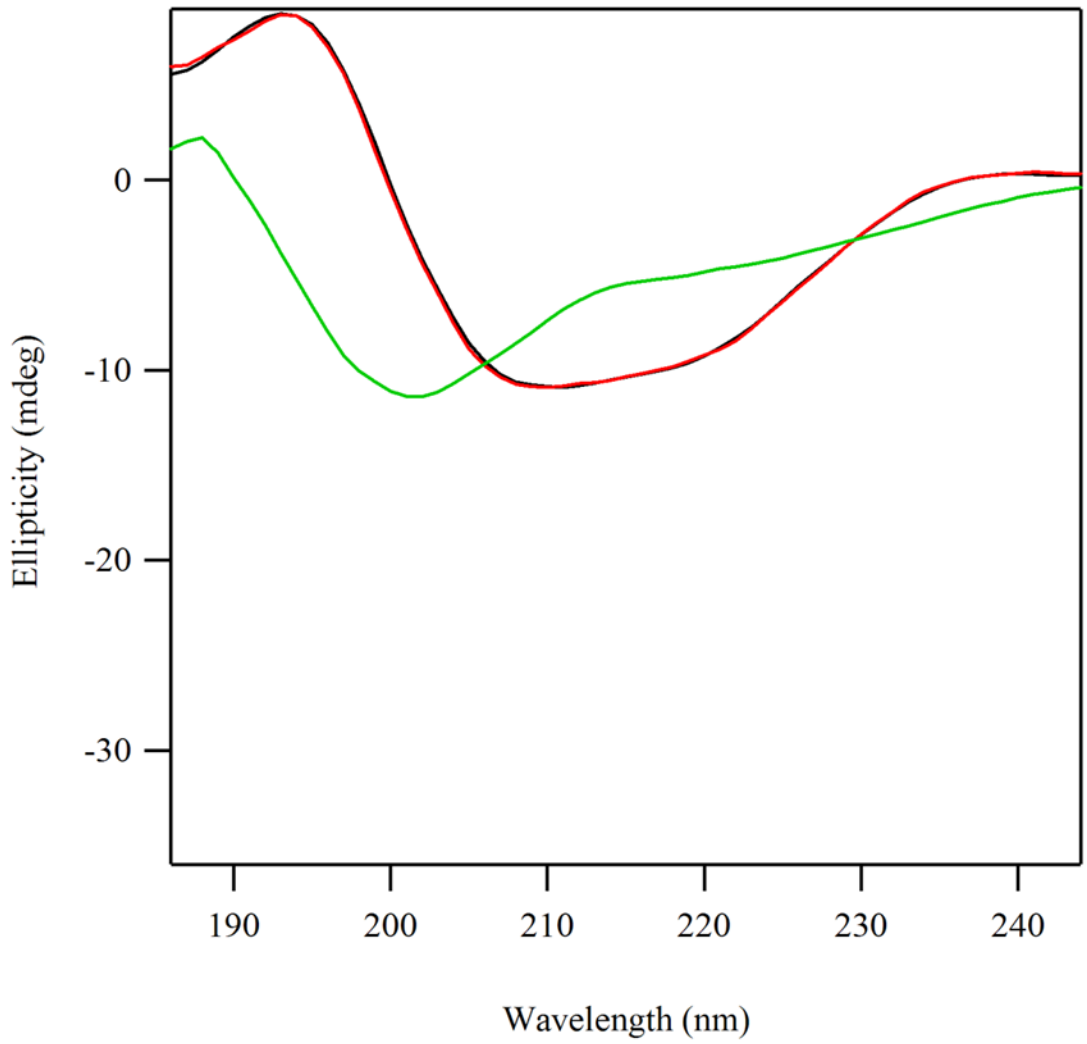


**Figure 3.3.** Circular dichroism of RNase A at pH 5.0. The spectra were collected at 20°C (-, pre-melt), 80°C (-), and 20°C (**-,** post-melt). See Materials and Methods for spectral conditions.

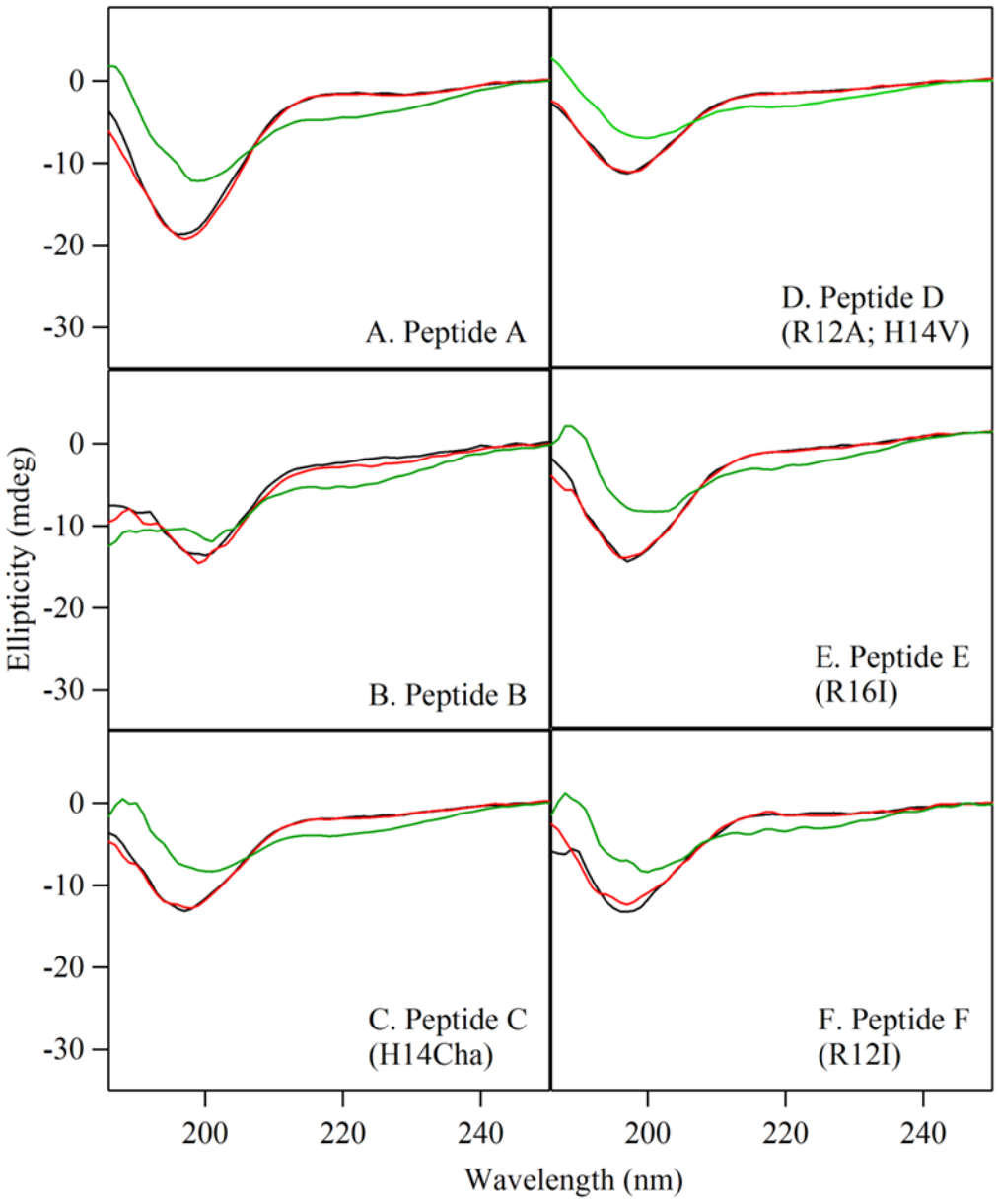


**Figure 3.4.** Circular dichroism of beta hairpin peptides at pH 5.0. The panels show data acquired from **A.** peptide A, **B.** peptide C (His14Cha), **C.** peptide D (H14V; R12A), **D.** peptide E (R16I), and **E.** peptide F (R12I). The spectra were collected at 20°C (-, pre-melt), 80°C (-), and 20°C (**-,** post-melt). See Materials and Methods for spectral conditions.

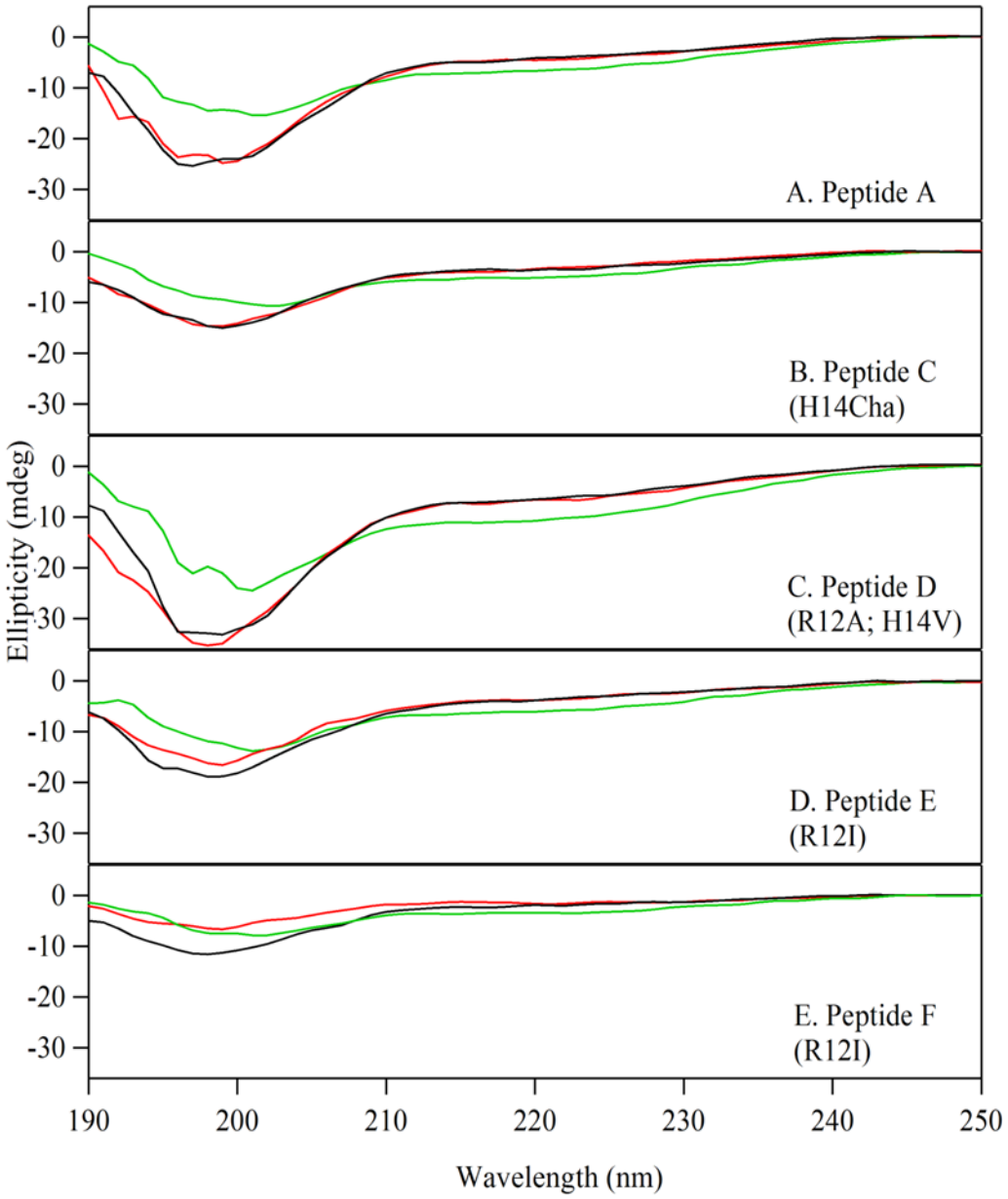


**Figure 3.5.** Circular dichroism of beta hairpin peptides at pH 11. The panels show data acquired from **A.** peptide A, **B.** peptide C (H14Cha), **C.** peptide D (H14V; R12A), **D.** peptide E (R16I), and **E.** peptide F (R12I). The spectra were collected at 20°C (-, pre-melt), 80°C (-), and 20°C (-, post-melt). See Materials and Methods for spectral conditions.

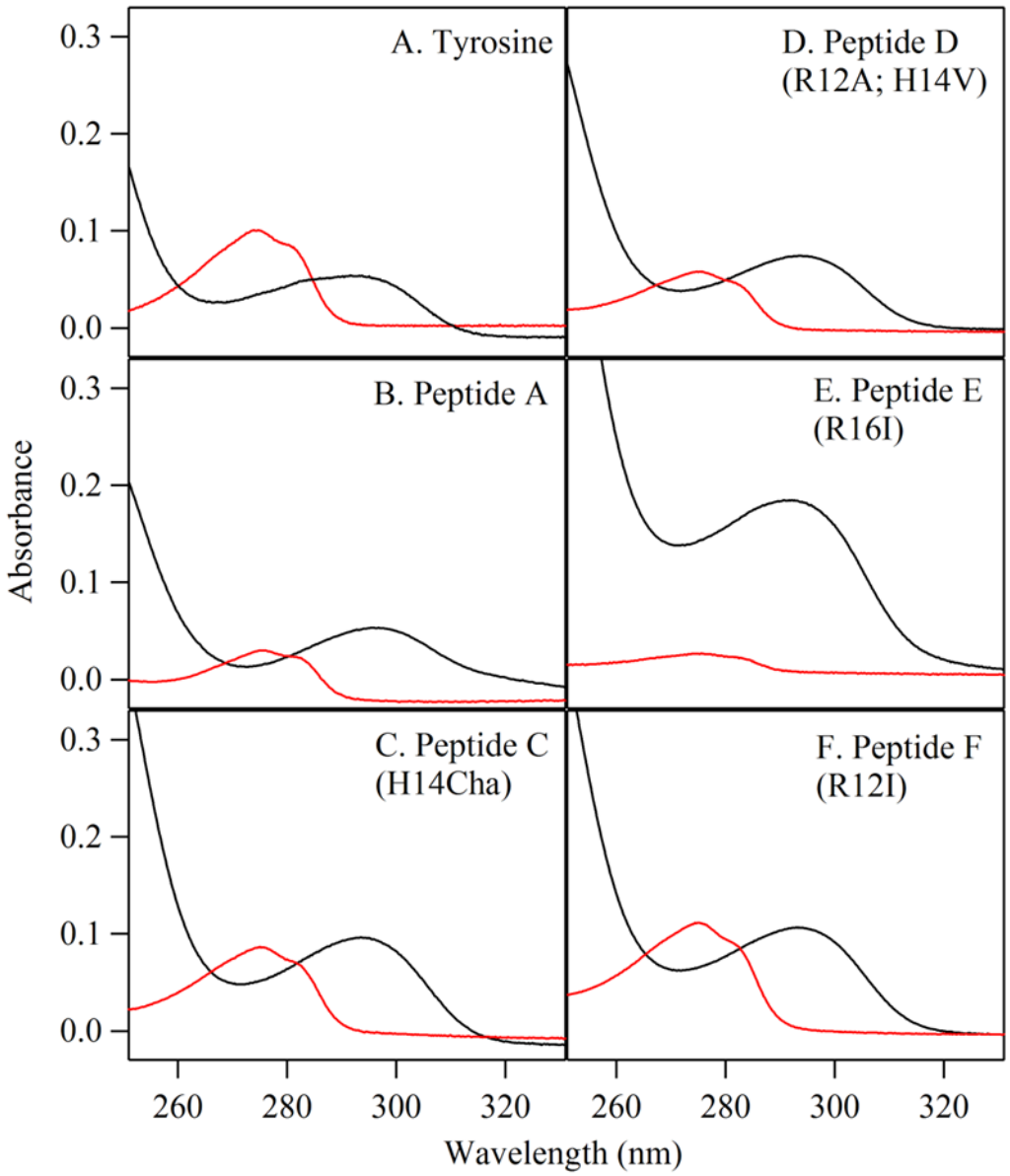


**Figure 3.6.** Absorption spectra of tyrosine in solution and beta hairpin peptides at pH 5 (red) and 11 (black). The panels show data acquired from **A.** tyrosine, **B.** peptide A, **C.** peptide C (H14Cha), **D.** peptide D (H14V; R12A), **E.** peptide E (R16I), and **F.** peptide F (R12I). See Table 3.1 for spectral parameters and Materials and Methods for spectral conditions.

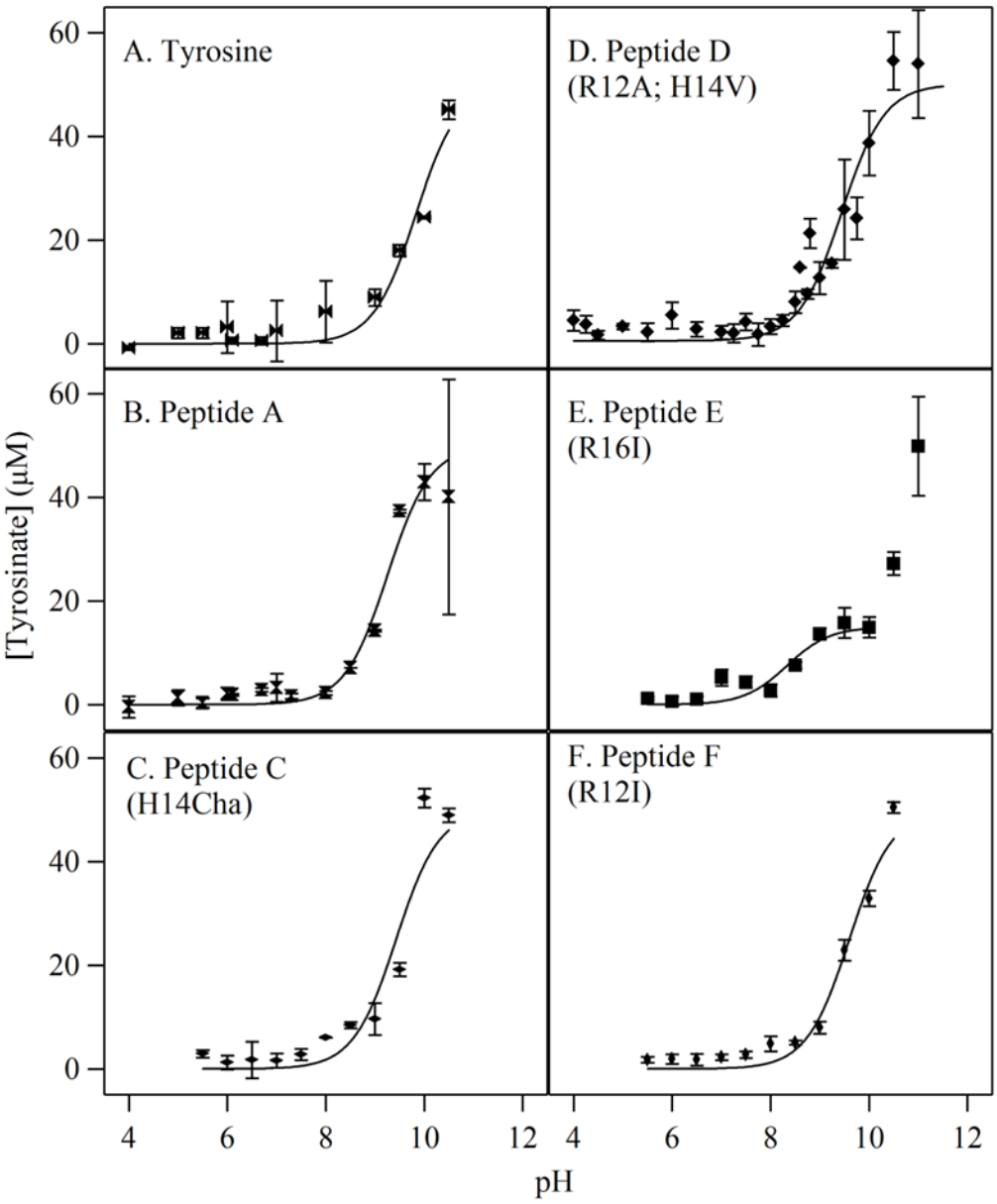


**Figure 3.7.** Optical titration of tyrosine in solution and in beta hairpin peptides, monitoring tyrosinate absorbance at 295 nm. The panels show data acquired from **A.** tyrosine, **B.** peptide A, **C.** peptide C (H14Cha), **D.** peptide D (H14V; R12A), **E.** peptide E (R16I), and **F.** peptide F (R12I). The error bars represent one standard deviation. See Table 3.1 for the pK values and the Materials and Methods for spectral conditions.

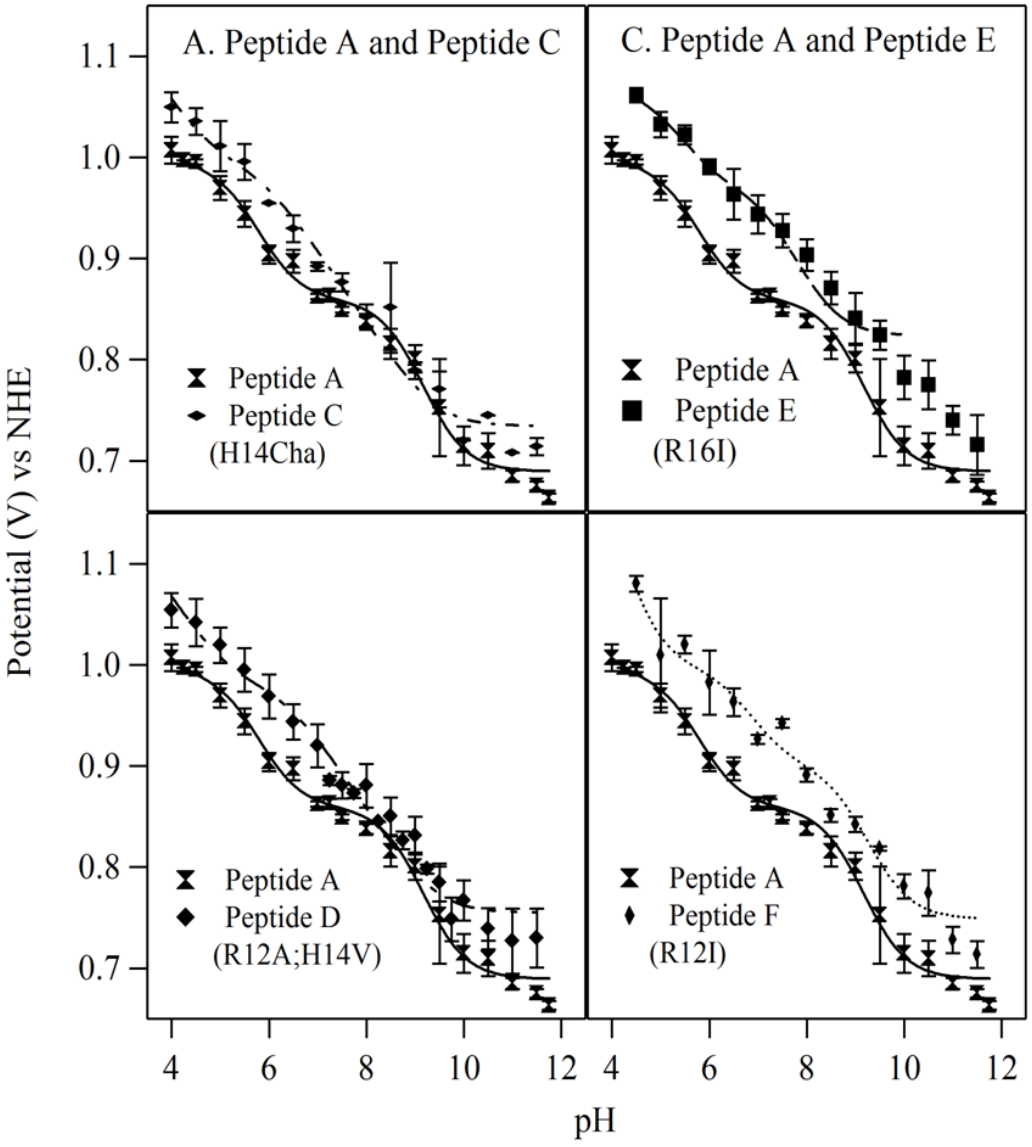


**Figure 3.8.** Electrochemical titrations of beta hairpin peptides. The titration curve of peptide A is shown in each panel. The panels also show data acquired from **A.** peptide C (H14Cha), **B.** peptide D (H14V; R12A), **C.** peptide E (R16I), and **D.** peptide F (R12I). The solid lines show the results of fitting the data to the Nernst equation. The error bars represent one standard deviation. See Table 3.2 for fit parameters and Materials and Methods for spectral conditions.

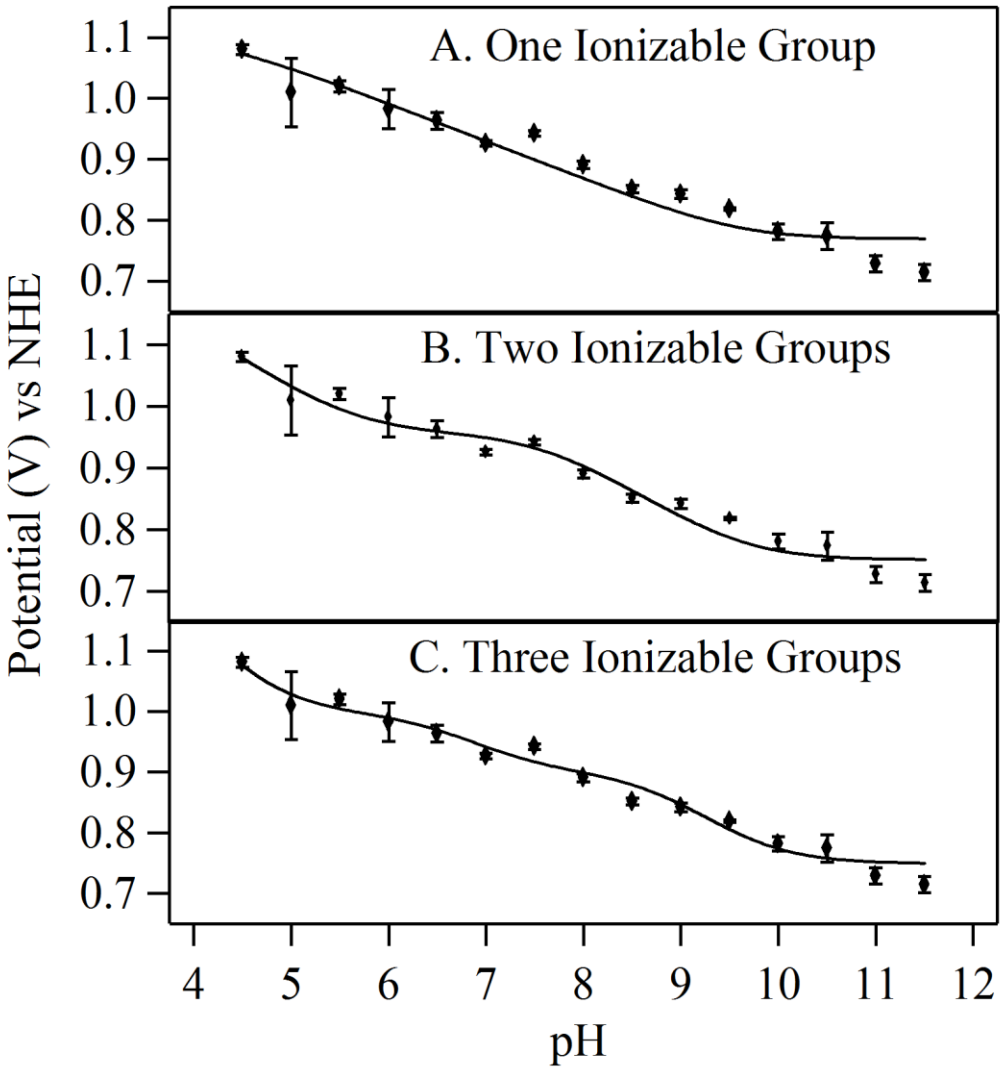


**Figure 3.9.** Electrochemical titration of peptide F (R12I). The data are repeated from Figure 3.8D. The solid lines show the results of fitting to Nernst equations, involving the influence of **A.** one, **B**. two, or **C.** three ionizable groups. The error bars represent one standard deviation. See Table 3.3 for fit parameters and Materials and Methods for spectral conditions.

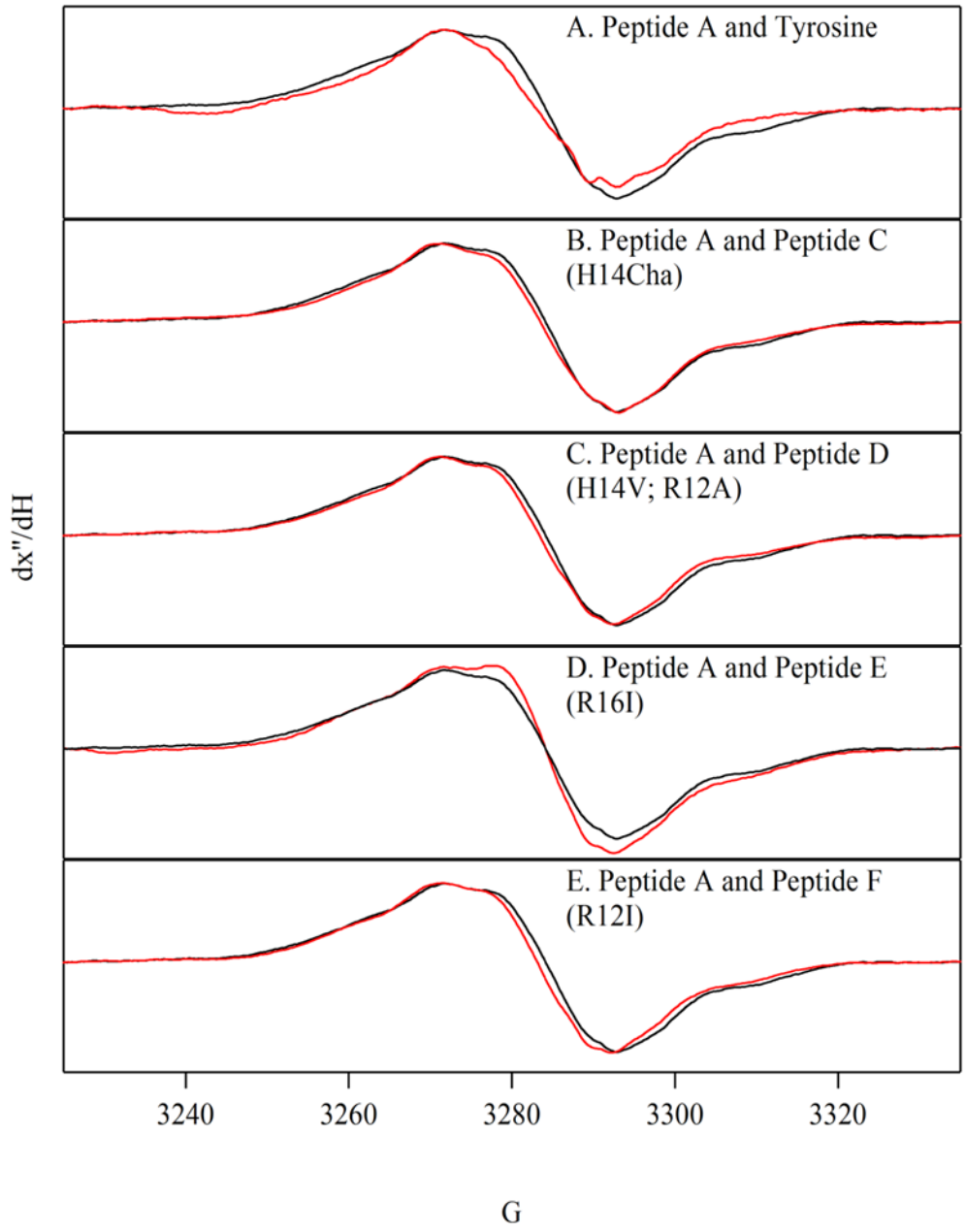


**Figure 3.10.** EPR spectra of tyrosyl radicals in solution and in beta hairpin peptides at pH 5.0 and 108 K. The radicals were generated by UV photolysis. The spectrum of peptide A (red) is shown in each panel. The panels also show spectra (black) acquired from **A.** tyrosine, **B.** peptide C (H14Cha), **C**. peptide D (H14V; R12A), **D.** peptide E (R16I), and **E.** peptide F (R12I). To compare spectral linewidth, the spectra were normalized for amplitude differences. See Materials and Methods for spectral conditions.

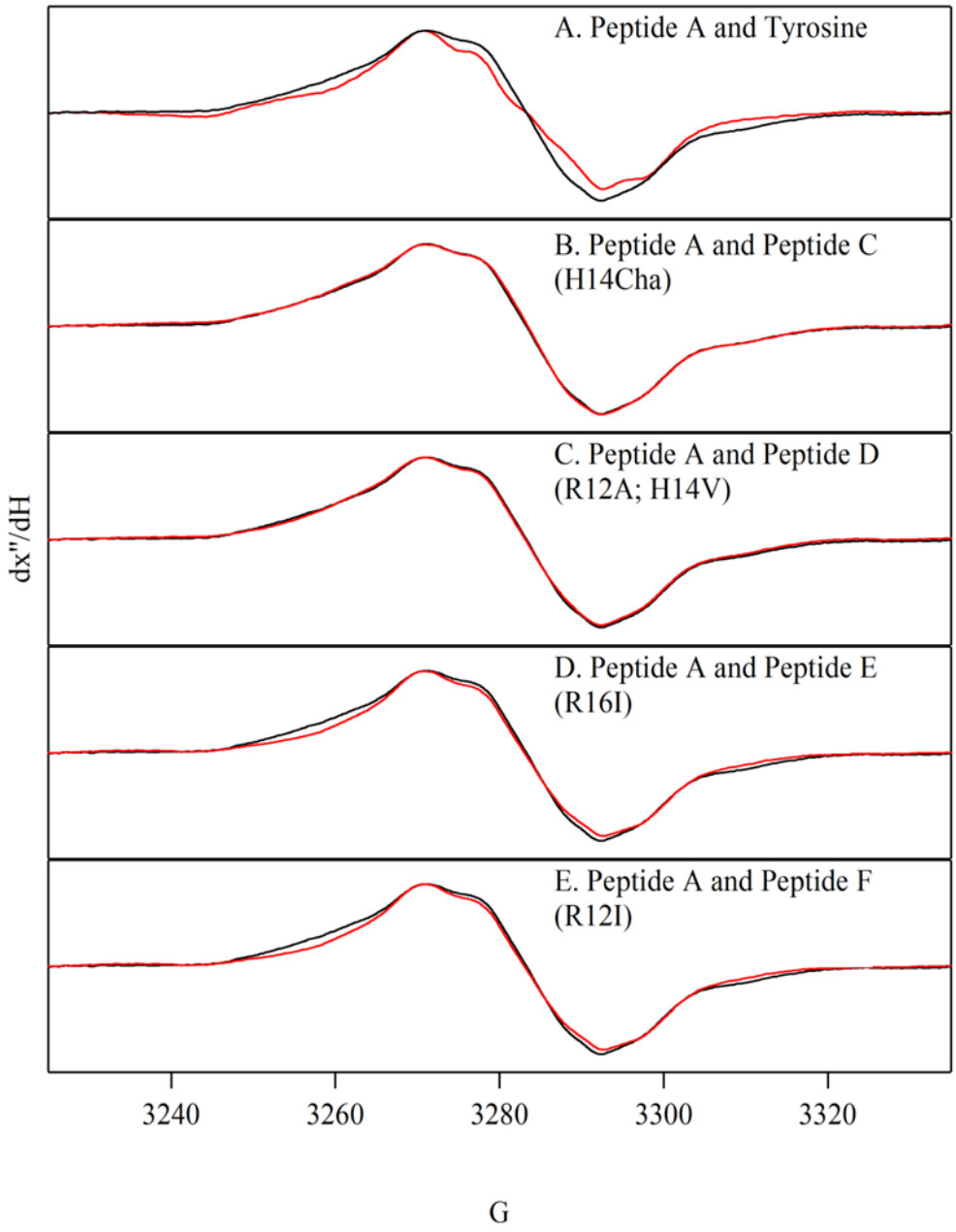


**Figure 3.11.** EPR spectra of tyrosyl radicals in solution and in beta hairpin peptides at pH 11.0 and 108 K. The radicals were generated by UV photolysis. The spectrum of peptide A (red) is shown in each panel. The panels also show spectra (black) acquired from **A.** tyrosine, **B.** peptide C (H14Cha), **C**. peptide D (H14V; R12A), **D.** peptide E (R16I), and **E.** peptide F (R12I). To compare spectral linewidth, the spectra were normalized for amplitude differences. See Materials and Methods for spectral conditions.

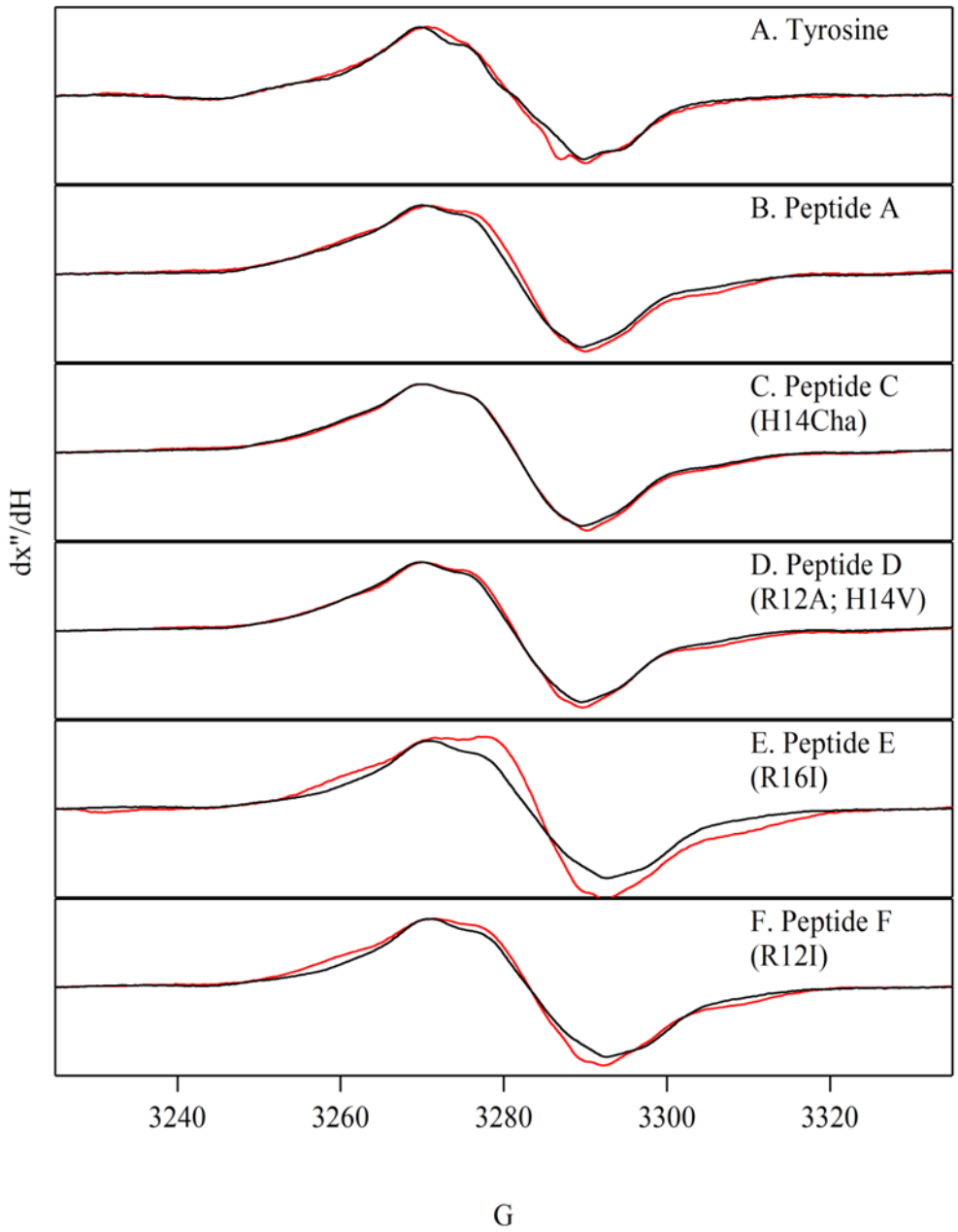


**Figure 3.12.** EPR spectra of tyrosyl radicals in beta hairpin peptides at pH 5.0 (red) and 11.0 (black) and 108 K. The radicals were generated by UV photolysis. The panels show spectra acquired from **A.** tyrosine, **B.** peptide A, **C.** peptide C (H14Cha), **D**. peptide D (H14Val; R12A), **E.** peptide E (R16I), and **F.** peptide F (R12I). To compare spectral linewidth, the spectra were normalized for amplitude differences. See Materials and Methods for spectral conditions.

## 3.9 References


**1.** Kabsch, W.; Sander, C. *Biopolymers* 1983, *22*, 2577-2637.

**2.** Milner-White, E. J.; Poet, R. *Biochemical Journal* 1986, *240*, 289-292.

**3.** Sibanda, B. L.; Thornton, J. M. *Nature* 1985, *316*, 170-176.

**4.** Blanco, F. J.; Jimenez, M. A.; Herranz, J.; Rico, M.; Santoro, J.; Nieto, J. L. *Journal of American Chemical Society* 1993, *115*, 5887-5888.

**5.** Burghardt, T. P.; Juranic, N.; Macura, S.; Ajtai, K. *Biopolymers* 2002, *63*, 261-272.

**6.** Ciani, B.; Jourdan, M.; Searle, M. S. *Journal of the American Chemical Society* 2003, *125*, 9038-9047.

**7.** De Alba, E.; Rico, M.; Jimenez, M. A. *Protein Science* 1997, *6*, 2548-2560.

**8.** Griffiths-Jones, S. R.; Maynard, A., J.; Searle, M. S. *Journal of Molecular Biology* 1999, *292*, 1051-1069.

**9.** Griffiths-Jones, S. R.; Maynard, A. J.; Sharman, G. J. *Chemical Communications* 1998, 789-790.

**10.** Hutchinson, G. E.; Thornton, J. M. *Protein Science* 1994, *3*, 2207-2216.

**11.** Phillips, S. T.; Piersanti, G.; Bartlett, P. A. *Proceedings of the National Academy of Sciences* 2005, *102*, 13737-13742.

**12.** Ramirez-Alvarado, M.; Blanco, F. J.; Serrano, L. *Protein Science* 2001, *10*, 1381-1392.

**13.** Smith, C. K.; Regan, L. *Science* 1995, *270*, 980-982.

**14.** Smith, C. K.; Withka, J. M.; Regan, L. *Biochemistry* 1994, *33*, 5510-5517.

**15.** Stanger, H. E.; Gellman, S. H. *Journal of the American Chemical Society* 1998, *120*, 4236-4237.

**16.** Syud, F. A.; Stanger, H. E.; Gellman, S. H. *Journal of the American Chemical Society* 2001, *123*, 8667-8677.

**17.** Tatko, C. D.; Waters, M. L. *Journal of the American Chemical Society* 2002, *124*, 9372-9373.

**18.** Tatko, C. D.; Waters, M. L. *Journal of the American Chemical Society* 2004, *126*, 2028-2034.

**19.** Tatko, C. D.; Waters, M. L. *Protein Science* 2004, *12*, 2443-2452.

**20.** Kiehna, S. E.; Waters, M. L. *Protein Science* 2003, *12*, 2657-2667.

**21.** Waters, M. L. *Biopolymers* 2004, *76*, 435-445.

**22.** Stotz, C. E.; Topp, E. M. *Journal of Pharmaceutical Sciences* 2004, *93*, 2881-2894.

**23.** Cochran, F. V.; Wu, S. P.; Wang, W.; Nanda, V.; Saven, J. G.; Therien, M. J.; DeGrado, W. F. *Journal of the American Chemical Society* 2005, *127*, 1346-1347.

**24.** Discher, B. M.; Noy, D.; Strzalka, J.; Ye, S.; Moser, C. C.; Lear, J. D.; Blasie, J. K.; Dutton, L. P. *Biochemistry* 2005, *44*, 12344-54.

**25.** Gibney, B. R.; Huang, S. S.; Skalicky, J. J.; Fuentes, E. J.; Wand, J. A.; Dutton, L. P. *Biochemistry* 2001, *40*, 10550-10561.

**26.** Jones, G. I.; Vullev, V.; Braswell, E. H.; Zhu, D. *Journal of the American Chemical Society* 2000, *122*, 388-389.

**27.** Kennedy, M. L.; Gibney, B. R. *Journal of the American Chemical Society* 2002, *124*, 6826-6827.

**28.** Lombardi, A.; Nastri, F.; Pavone, V. *Chemical Reviews* 2001, *101*, 3165-3189.

**29.** Shearer, J.; Long, L. M. *Inorganic Chemistry* 2006, *45*, 2358-2360.

**30.** Shifman, J. M.; Moser, C. C.; Kalsbeck, W. A.; Bocian, D. F.; Dutton, P. L. *Biochemistry* 1998, *37*, 16815-16827.

**31.** Zhuang, J.; Amoroso, J.; Kinloch, R.; Dawson, J.; Baldwin, M.; Gibney, B. R. *Inorganic Chemistry* 2006, *45*, 4685-4685.

**32.** Sibert, R.; Josowicz, M.; Porcelli, F.; Veglia, G.; Range, K.; Barry, B. A. *Journal of the American Chemical Society* 2007, *129*, 4393-4400.

**33.** Barry, B. A.; Pujols-Ayala, I. *Biochimica et Biophysica Acta* 2004, *1655*, 205-216.

**34.** Barry, B.; Babcock, G. T. *Proceedings of the National Academy of Sciences* 1987, *84*, 7099-7103.

**35.** Barry, B. A.; El-Deeb, M. K.; Sandusky, P. O.; Babcock, G. T. *The Journal of Biological Chemistry* 1990, *265*, 20139-20143.

**36.** Boerner, R. J.; Barry, B. A. *Journal of Biological Chemistry* 1993, *268*, 17151-17154.

**37.** Vassiliev, I. R.; Offenbacher, A. R.; Barry, B. A. *Journal of Physical Chemistry B* 2005, *109*, 23077-23085.

**38.** Kouglougliotis, D.; Tang, X. S.; Diner, B.; Brudvig, G. W. *Biochemistry* 1995, *34*, 2850-2856.

**39.** MacDonald, G. M.; Bixby, K.; Barry, B. A. *Proceedings of the National Academy of Sciences* 1993, *90*, 11024-11028.

**40.** Seyedsayamdost, M. R.; Chan, C. T. Y.; Mugnaini, V.; Stubbe, J.; Bennati, M. *Journal of the American Chemical Society* 2007, *129*, 15748-15749.

**41.** Barry, B. A.; Einarsdottir, O. *Journal of Physical Chemistry B* 2005, *109*, 6972-6981.

**42.** Chang, M. C. Y.; Yee, C. S.; Nocer, D. G.; Stubbe, J. *Journal of American Chemical Society* 2004, *126*, 16702-16703.

**43.** Larsson, A.; Sjoeberg, B. M. *EMBO Journal* 1986, *5*, 2037-2040.

**44.** Seyedsayamdost, M. R.; Yee, C. S.; Reece, S. Y.; G, N. D.; Stubbe, J. *Journal of the American Chemical Society* 2006, *128*, 1562-1568.

**45.** Wu, G.; Kulmacz, R. J.; Tsai, A. *Biochemistry* 2003, *42*, 13772-13777.

**46.** Kulmacz, R. J.; Palmer, G.; Tsai, A. L. *Molecular Pharmacology* 1991, *40*, 833-837.

**47.** Malkowski, M.; Ginell, S.; Smith, W.; Garavito, R. *Science* 2000, *289*, 1933-1938.

**48.** Smith, W. L.; Eling, T. E.; Kulmacz, R. J.; Marnett, L. J.; Tsai, A. L. *Biochemistry* 1992, *31*, 3-7.

**49.** Whittaker, M.; Whittaker, J. *The Journal of Biological Chemistry* 1990, *265*, 9610-9613.

**50.** Dixon, W. T.; Murphy, D. *J. Chem. Soc. London, Faraday Trans. II* 1976, *72*, 1221-1230.

**51.** Stubbe, J.; Nocera, D. G.; Yee, C. S.; Chang, M. C. Y. *Chem. Rev.* 2003, *103*, 2167-2201.

**52.** Barry, B. A.; Babcock, G. T. *Proceedings of the National Academy of Sciences* 1987, *84*, 7099-7103.

**53.** Boerner, R. J.; Barry, B. A. *The Journal of Biological Chemistry* 1993, *268*, 17151-17154.

**54.** Babcock, G. T.; Blankenship, R. E.; Sauer, K. *FEBS Letters* 1976, *61*, 286-289.

**55.** Debus, R.; Barry, B.; Sithole, I.; Babcock, G.; McIntosh, L. *Biochemistry* 1988, *27*, 9072-9074.

**56.** Gerken, S.; Brettel, K.; Schlodder, E.; Witt, H. T. *FEBS Letters* 1988, *237*, 69-75.

**57.** Metz, J. G.; Nixon, P. J.; Rögner, M.; Brudvig, G. W.; Diner, B. A. *Biochemistry* 1989, *28*, 6960-6969.

**58.** Rutherford, A. W.; Boussac, A.; Faller, P. *Biochimica et Biophysica Acta* 2004, *1655*, 222-230.

**59.** Vermaas, W. F. J.; Rutherford, A. W.; Hansson, O. *Proceedings of the National Academy of Sciences* 1988, *85*, 8477-8481.

**60.** Ananyev, G.; Sakiyan, I.; Diner, B. A.; Dismukes, G. *Biochemistry* 2002, *41*, 974-980.

**61.** Boussac, A.; Etienne, A. L. *Biochimica et Biophysica Acta* 1984, *766*, 576-581.

**62.** Dekker, J. P.; Gorkom, H. J. V.; Brok, M.; Ouwehand, L. *Biochimica et Biophysica Acta* 1984, *764*, 301-309.

**63.** Hoganson, C. W.; Babcock, G. T. *Biochemistry* 1988, *27*, 5848-5855.

**64.** Rappaport, F.; Blanchard-Desce, M.; Lavergne, J. *Biochimica et Biophysica Acta* 1994, *1184*, 178-192.

**65.** Styring, S.; Rutherford, A. W. *Biochemistry* 1987, *26*, 2401-2405.

**66.** Vass, I.; Styring, S. *Biochemistry* 1991, *30*, 830-839.

**67.** Ferreira, K. N.; Iverson, T. M.; Maghlaoui, K.; Barber, J.; Iwata, S. *Science* 2004, *303*, 1831-1838.

**68.** Guskov, A.; Kern, J.; Gabdulkhakov, A.; Boser, M.; Zouni, A.; Saenger, W. *Nature Structural and Molecular Biology* 2009, *16*, 334-342.

**69.** Shen, J. R.; Kamiya, N. *Biochemistry* 2000, *39*, 14739-14744.

**70.** Shen, J. R.; Kamiya, N. *Advances in Photosynthesis and Respiration* 2005, *22*, 449-467.

**71.** Zouni, A.; Kern, J.; Loll, B.; Fromme, P.; Orth, P.; Krauss, N.; Saenger, W.; Biesiadka, J. In *Proceedings of the 12th International Congress on Photosynthesis*; Luttge, U., Osmond, B., Voesenek, R., Eds.; Thieme: Stuttgart, 2002; Vol. In press., p S05-003.

**72.** Zouni, A.; Witt, H. T.; Kern, J.; Fromme, P.; Krauß, N.; Saenger, W.; Orth, P. *Nature* 2001, *409*, 739-743.

**73.** Gallivan, J. P.; Dougherty, D. A. *Proceedings of the National Academy of Sciences* 1999, *96*, 9459-9464.

**74.** Gray, H. B.; Winkler, J. R. *Proceedings of the National Academy of Science USA* 2005, *102*, 3534-3539.

**75.** Moser, C.; Page, C.; Farid, R.; Dutton, P. *Journal of Bioenergetics and Biomembranes* 1995, *27*, :263-274.

**76.** Moser, C. C.; Page, C. C.; Dutton, P. L. *Photochemical and Photobiological Sciences* 2005, *4*, 933-939.

**77.** Rhile, I. J.; Markle, T. F.; Nagao, H.; G, D. A.; Lam, O. P.; Lockwood, M. A.; Rotter, K.; Mayer, J. *Journal of the American Chemical Society* 2006, *128*, 6075-6088.

**78.** Lomoth, R.; Magnuson, A.; Sjodin, M.; Huang, P.; Styring, S.; Hammarstrom, L. *Photsynthesis Research* 2006, *87*, 25-40.

**79.** Di Bilio, A. J.; Crane, B. R.; Wehbi, W. A.; Kiser, C. N.; Abu-Omar, M. M.; Carlos, R. M.; Ruchards, J. H.; Winkler, J. R.; Gray, H. B. *Journal of the American Chemical Society* 2001, *123*, 3181-3182.

**80.** Tommos, C. S.; Skalicky, J. J.; Pilloud, D. L.; Wand, J.; Dutton, L. *Biochemistry* 1999, *38*, 9495-9507.

**81.** Hilario, J.; Kubelka, J.; Keiderling, T. A. *Journal of the American Chemical Society* 2003, *125*, 7562-7574.

**82.** Moraes, L. G. M.; Fazio, M. A.; Vieira, R., F.F.; Nakaie, C., R.; Miranda, M. T. M.; Schreier, S.; Daffre, S.; Miranda, A. *Biochimica et Biophysica Acta* 2007, *1768*, 52-58.

**83.** Ishimitsu, T.; Hirose, S.; Sakurai, H. *Chemical and Pharmaceutical Bulletin* 1976, *24*, 3195-3198.

**84.** Ayala, I.; Range, K.; York, D.; Barry, B. A. *Journal of the American Chemical Society* 2002, *124*, 5496-5505.

**85.** Gasteiger, E.; Gattiker, A.; Hoogland, C.; Ivanyi, I.; Appel, R. D.; Bairoch, A. *Nucleic Acids Research* 2003, *31*, 3784-3788.

**86.** Navon, A.; Ittah, V.; Laity, J. H.; Scheraga, H. A.; Haas, E.; Gussakovsky, E. E. *Biochemistry* 2001, *40*, 93-104.

**87.** Ishimitsu, T. *Talanta* 1983, *30*, 879-883.

**88.** Range, K.; Ayala, I.; York, D.; Barry, B. A. *Journal of Physical Chemistry* 2006, *110*, 10970-10981.

**89.** Barry, B. A.; El-Deeb, M. K.; Sandusky, P. O.; Babcock, G. T. *The Journal of Biological Chemistry* 1990, *265*, 20139-20143.

**90.** Evelo, R. G.; Hoff, A. J.; Dikanov, S. A.; Tyryshkin, A. M. *Chemical Physics Letters* 1989, *161*, 479-484.

**91.** Hulsebosch, R. J.; Brink, J. S. v. d.; Niewenhuis, S. A. M.; Gast, P.; Raap, J.; Lugtenburg, J.; Hoff, A. J. *Journal of the American Chemical Society* 1997, *119*, 8685-8694.

**92.** Johnson, C. W. *Annual Review of Biophysics and Biophysical Chemistry* 1988, *17*, 145-166.

**93.** Ovchinnikova, T. V.; Shenkarev, Z. O.; Nadezhdin, K. D.; Balandin, S. V.; Zhmak, M. N.; Kudelina, I. A.; Finkina, E. I.; Kokryakov, V. N.; Arseniev, A. A. *Biochemical and Biophysical Research Communications* 2007, *360*, 156-162.

**94.** Searle, M. *Journal of the Chemical Society, Perkins Transactions 2* 2001, *2*, 1011-1020.

**95.** Jarvet, J.; Dambert, P.; Bodell, K.; Eriksson, L. G.; Grslund, A. *Journal of American Chemical Society* 2000, *122*, 4261-4268.

**96.** Maynard, A. J.; Sharman, G. J.; Searle, M. *Journal of the American Chemical Society* 1998, *120*, 1996-2007.

**97.** Hoganson, C. W.; Tommos, C. *Biochimica et Biophysica Acta* 2004, *1655*, 116-122.

## CONCLUSIONS

Tyrosine is a key cofactor involved in electron transfer in photosystem II (PSII),[1,2] prostaglandin H synthase[3], galactose oxidase[4], and ribonucleotide reductase.[5] In particular, photosystem II provides an excellent example of how the redox properties of tyrosine can be altered by the enzymatic environment. PSII contains two redox active tyrosine residues, Tyr 161D1 (Tyr Z) and Tyr 160D2 (Tyr D), located in the D1 and D2 polypeptides, respectively.[6-10] Although both tyrosine residues are redox active, Tyr 161D1 (Tyr Z) is responsible for reduction of the primary donor, $P_{680}^{+}$,[37] while Tyr160D2 (Tyr D) is associated with assembly of the manganese cluster.[11] Both Tyr 161D1 (Tyr Z) and Tyr 160D2 (Tyr D) are hydrogen bonded to histidine residues. Tyr161D1 (Tyr Z) hydrogen bonds to His 190, while Tyr 160D2 (Tyr D) hydrogen bonds to His 189.[6-10] However, the radical formed by Tyr 160D2 (Tyr D) has a lower midpoint potential and a longer lifetime than the radical formed by Tyr 161D1 (Tyr Z).[1,13-14] The 2.9 Å crystal structure of the D2 polypeptide of PSII shows a potential pi-cation interaction between Tyr 160D2 (Tyr D) and Arg 272 of the CP47 subunit[7] that may explain why the redox properties of Tyr 160D2 (Tyr D) are different from Tyr 161D1 (Tyr Z).

Being inspired by photosystem II, we have designed five beta hairpins, peptides A, C, D, E, and F, which each contain a single tyrosine residue. These beta hairpins were used as tractable models for studying how the redox properties of tyrosine are controlled by hydrogen bonding, pi-cation interactions, and proton coupled electron transfer reactions with neighboring amino acids. The NMR structure of peptide A confirmed that it forms a beta hairpin at pH 5.0. The NMR structure also showed that tyrosine participates in a hydrogen bond with arginine, an aromatic interaction with histidine, and

a possible pi-cation interaction with a second arginine. Circular dichroism spectropolarimetry confirmed that the peptides A, C, D, E, and F form beta hairpins at pH 5.0 and pH 11.0.

Electrochemical titration was performed on the designed peptides. A least squares fit to the Nernst equation showed that the pK of His14 increases from 6.2 to 8.9 with oxidation of tyrosine in peptide A. We concluded that this oxidation-induced increase in the pK of His14 is consistent with a proton coupled electron transfer reaction between Tyr5 and His14. Replacement of His 14 by cyclohexylalanine (peptide C) or by valine (peptide D) confirmed this conclusion by eliminating the PCET reaction.

Electrochemical data also showed that protonated histidine decreases the midpoint potential of tyrosine at low pH values in peptide A. To explain this result, electrostatic maps of tyrosine and of the tyrosyl radical were calculated. The electrostatic maps showed oxidation-induced movement of electron density from the aromatic ring to the phenolic oxygen. Therefore, we concluded that protonated histidine stabilizes electron density on the phenolic oxygen.

The electrochemical titration curve of peptide E showed that substitution of the hydrogen bonded arginine increases the midpoint potential of tyrosine by 50 mV at all examined pH values. Since electrostatic maps of tyrosine and the tyrosyl radical showed migration of electron density from the aromatic ring to the phenolic oxygen upon oxidation of tyrosine, we concluded that the Tyr5-Arg16 hydrogen bond stabilizes the electron density on the phenolic oxygen of tyrosine as the radical is formed.

The electrochemical titration curve of peptide F showed that substitution of Arg 12, which forms a pi-cation interaction with Tyr 5, increases the midpoint potential of

Tyr 5 at all examined pH values. This result was also attributed to stabilization of electron density on the phenolic oxygen of tyrosine as the radical is formed.

Taken together, our studies of beta hairpin peptides provide a model for PCET reactions in proteins. The data also show that a hydrogen bonding or a pi-cation interaction with tyrosine lowers the midpoint potential of tyrosine by stabilizing electron density on the phenolic oxygen. As an explanation for differences in the redox properties of Tyr 161D1 (TyrZ) and Tyr 160D2 (TyrD), the data presented in these studies show that protonation of histidine, hydrogen bonding, and the pi-cation interaction contribute equally to the midpoint potential of tyrosine.

**References**


**1.** Barry, B.; Babcock, G. T. *Proceedings of the National Academy of Sciences* **1987**, *84*, 7099-7103.

**2.** Debus, R.; Barry, B.; Sithole, I.; Babcock, G.; McIntosh, L. *Biochemistry* **1988**, *27*, 9072-9074.

**3.** Malkowski, M.; Ginell, S.; Smith, W.; Garavito, R. *Science* **2000**, *289*, 1933-1938.

**4.** Baron, A. J.; Stevens, C.; Wilmot, C.; Seneviratne, K. D.; Blakeley, V.; Dooley, D. M.; Phillips, S. E.; Knowles, P. F.; McPherson, M. J. *Journal of Biological Chemistry* **1994**, *269*, 25095-25105.

**5.** Seyedsayamdost, M. R.; Yee, C.; Reece, S. Y.; Nocera, D.; Stubbe, J. *Journal of the American Chemical Society* **2006**, *128*, 1562-1568.

**6.** Ferreira, K. N.; Iverson, T. M.; Maghlaoui, K.; Barber, J.; Iwata, S. *Science* **2004**, *303*, 1831-1838.

**7.** Guskov, A.; Kern, J.; Gabdulkhakov, A.; Boser, M.; Zouni, A.; Saenger, W. *Nature Structural and Molecular Biology* **2009**, *19*, 334-342.

**8.** Shen, J.; Kamiya, N. *Biochemistry* **2000**, *39*, 14739-14744.

**9.** Shen, J.; Kamiya, N. *Advances in Photosynthesis and Respiration* **2005**, *22*, 449-467.

**10.** Zouni, A.; Witt, H. T.; Kern, J.; Fromme, P.; Kraub, N.; Saenger, W.; Orth, P. *Nature* **2001**, *409*, 739-743.

**11.** Ananyev, G.; Sakiyan, I.; Diner, B. A.; Dismukes, G. *Biochemistry* **2002**, *41*, 974-980.

**12.** Babcock, G. T.; Blankenship, R. E.; Sauer, K. *FEBS Letters* **1976**, *61*, 286-289.

**13.** Boussac, A.; Etienne, A. L. *Biochimica et Biophysica Acta* **1984**, *766*, 576-581.

**14.** Metz, J. G.; Nixon, P. J.; Rögner, M.; Brudvig, G. W.; Diner, B. A. *Biochemistry* **1989**, *28*, 6960-6969.